

On Voltage and Frequency Control in Multi-Area Power Systems Security

THÈSE N° 6053 (2014)

PRÉSENTÉE LE 21 MARS 2014

À LA FACULTÉ DES SCIENCES ET TECHNIQUES DE L'INGÉNIEUR
GROUPE DE SCIENTIFIQUES STI
PROGRAMME DOCTORAL EN GÉNIE ÉLECTRIQUE

ÉCOLE POLYTECHNIQUE FÉDÉRALE DE LAUSANNE

POUR L'OBTENTION DU GRADE DE DOCTEUR ÈS SCIENCES

PAR

Omid ALIZADEH MOUSAVI

acceptée sur proposition du jury:

Prof. F. Rachidi-Haeri, président du jury
Dr S.-R. Cherkaoui, directeur de thèse
Prof. M. Paolone, rapporteur
Dr W. Sattinger, rapporteur
Prof. T. Van Cutsem, rapporteur



ÉCOLE POLYTECHNIQUE
FÉDÉRALE DE LAUSANNE

Suisse
2014

To whom it may concern.

Abstract

The electric power networks are complex infrastructures which are continuously evolving worldwide to provide reliable and affordable energy supply to the consumers. The significant evidences of these evolutions are (i) the increase of the interconnection of several power networks with independent Transmission System Operators (TSOs) and (ii) the economic utilization of resources under liberalized electricity market rules. Furthermore, different sources of uncertainties, like load and renewable energy production forecast deviations and equipment outages, have increased the complexity of the management of power systems. Several blackouts in the last two decades have demonstrated that the reliability and security of power systems are jeopardized by elevated risk levels. These challenges emphasize the revision and update of security analysis methods of interconnected power systems in accordance with current challenges and new requirements.

In the liberalized electricity market environment, the concept of ancillary services is introduced to guarantee stable and secure operation of the system. The voltage and frequency control are among the most prominent ancillary services. The appropriate provision of these control services is essential for secure operation of the system. This issue becomes even more important in the interconnected networks with independent TSOs where these control actions can be shared or exchanged between controlled areas. Therefore, this thesis addresses the security of Multi-Area Power Systems (MAPS) from the voltage and frequency control perspectives.

Firstly, the voltage and reactive power control practices in several TSOs are reviewed. Then, the fundamental preliminaries for optimization and analysis of voltage stability margin are investigated based on PV and VQ methods. Regarding these two approaches, two formulations for the maximization of loading factor and the maximization of effective reactive power reserve are studied. Both of them can be considered as preventive actions for improving voltage stability margins. Other formulations are presented for the contingency analysis and the evaluation of the required corrective actions. The proposed formulations benefit from: (i) the detailed modeling of generators reactive power limits, (ii) the generators mode switch between

constant terminal voltage and constant reactive power output according to complementarity constraints and (iii) the distributed slack bus model for the compensation of active power imbalances.

Afterwards, we focus on the inter-area optimization of the voltage and reactive power. Different aspects of the mathematical formulation of the optimization problem for interconnected power system, including objective function, constraints and appropriate modeling of neighboring areas, are revisited in depth. Various implementations of solution approaches, including centralized and decentralized implementations, as well as coordinated and non-coordinated solution approaches in the context of collaborative and non-collaborative environments are proposed and illustrated.

In the case of Single Area Power System (SAPS), an original optimization model based on the criteria of the effective reactive power reserve is developed. It aims at effectively managing the voltage and reactive power resources in a coordinated manner. The criteria of the effective reactive power reserve takes into account the voltage stability margin of system. In addition, this particular objective function requires the appropriate selection of pilot nodes. In this respect, an optimization based on genetic algorithm is developed to identify these pilot nodes.

The aforementioned optimization model is extended to MAPS using centralized/decentralized implementations. It is demonstrated that the consideration of the complementarity constraints at border buses asks for particular attention in the case of decentralized implementation. In this respect, the required modifications in the mathematical formulation of the decentralized optimization of each area are presented and discussed in depth.

The results and conclusions about the voltage and reactive power control are based on the application of the proposed methods to networks such as New England 39-bus and IEEE 57-bus.

Regarding the contribution of this thesis on the frequency control, the blackouts data of the interconnected network of continental Europe is firstly investigated for identifying possible power law distribution. This particular distribution implies that the short- and long-term dynamics of blackouts can be associated with the complex systems with self-organized criticality. In the context of short-term dynamics, a Monte Carlo simulation based approach is proposed to evaluate the effect of the frequency control reserves on the risk of cascading outages and blackouts. This method takes into account the cascading outages due to the transmission overloading and the hidden failure of protection systems. It also considers the automatic and manual response of frequency control reserves and under-frequency load shedding. These investigations obviously demonstrate that there is a trade-off between the probability of small and large blackouts with respect to the value of frequency control reserves, particularly for interconnected power systems. In order to illustrate the developed methodology and discuss the obtained results and conclusions, the IEEE 118-bus network is used.

Keywords: multi-area power system, voltage control, voltage stability margin, effective reactive power reserve, complementarity constraints, centralized/decentralized optimization, frequency control, cascading outages, large blackouts, risk assessment.

Résumé

Les réseaux électriques sont des infrastructures complexes qui sont en continuelle évolution à travers le monde pour assurer un approvisionnement en énergie qui soit sûr, fiable et à un prix abordable pour les consommateurs. Les preuves significatives de cette évolution sont (i) l'augmentation de l'interconnexion de plusieurs réseaux électriques supervisés par des gestionnaires indépendants (GRT) (ii) la gestion à caractère commerciale des ressources en vertu des règles de la libéralisation du marché de l'électricité. Par ailleurs, différentes causes d'incertitudes, notamment celles liées à la prévision des charges et la production d'énergies renouvelables et les défaillances d'équipement, ont augmenté la complexité de la gestion des réseaux électriques. Plusieurs blackouts durant les deux dernières décennies ont démontré que la fiabilité et la sécurité des réseaux électriques sont mises en cause de par des niveaux de risque élevés. Ces défis soulignent la nécessité de réviser et mettre à jour les méthodes d'analyse de la sécurité des réseaux électriques interconnectés conformément aux défis actuels et aux nouvelles exigences.

Dans l'environnement d'un marché d'électricité ouvert, le concept de service auxiliaire est introduit pour garantir une exploitation stable et sécurisée du réseau. Le contrôle de la fréquence et de la tension sont parmi les services auxiliaires les plus importants. Un niveau de provision approprié de ces services est indispensable pour une exploitation viable du réseau. Ce sujet devient de nos jours de plus en plus important dans les réseaux interconnectés avec des GRTs indépendants où ces actions peuvent être soit partagés soit échangées entre différentes zones de contrôle. Par conséquent, ce travail de thèse traite de la sécurité des réseaux électriques multizone (MAPS) du point de vue du contrôle de la tension et de la fréquence.

Tout d'abord, les approches actuelles du contrôle de la tension et de la puissance réactive au sein de différents GRTs sont recensées et analysées. Ensuite, les éléments fondamentaux pour l'optimisation et l'analyse de la marge de stabilité de la tension sont étudiées selon des méthodes PV et VQ . Concernant ces deux approches, deux formulations pour la maximisation du facteur de la charge et la maximisation de la réserve de puissance réactive effective sont étudiées. Toutes deux peuvent être considérées comme des mesures préventives pour améliorer la marge

de stabilité de la tension. D'autres formulations sont présentées pour l'analyse des contingences et l'évaluation des actions correctives nécessaires. Les formulations proposées s'appuient sur: (i) une modélisation détaillée des limites de puissance réactive des générateurs, (ii) une commutation des générateurs entre les modes à tension constante et à puissance réactive constante selon des contraintes de complémentarité et (iii) un modèle de nœud bilan distribué pour la compensation des déséquilibres de puissance active.

Ensuite, nous nous concentrons sur l'optimisation interzone de la tension et de la puissance réactive. Différents aspects de la formulation mathématique du problème d'optimisation pour un réseau électrique interconnecté, incluant notamment la fonction objectif, les contraintes et la modélisation appropriée des régions voisines, sont revisités de manière approfondie. Différentes implémentations d'approches de solution originales sont proposées et illustrés. Il s'agit d'implémentations centralisées ou décentralisées et d'approches de solution coordonnées ou non coordonnées dans des contextes d'exploitation collaboratifs ou non collaboratifs.

Dans le cas d'un réseau à zone unique, un modèle d'optimisation original s'appuyant sur le critère de la réserve de puissance réactive effective est développé. Il vise à gérer efficacement et de manière coordonnée les ressources contrôlant les tensions ou les puissances réactives. Le critère de la réserve de puissance réactive effective tient compte de la marge de stabilité des tensions aux nœuds. En outre, il nécessite un choix judicieux des nœuds pilotes. À cet égard, une optimisation utilisant un algorithme génétique est développée pour identifier ces nœuds pilotes.

Le modèle d'optimisation précité est ensuite étendu au cas d'un réseau multizone (MAPS) notamment dans le cas d'une implémentation décentralisée. Il est démontré que la prise en compte des contraintes de complémentarité aux nœuds frontières demande une attention particulière dans le cas de cette implémentation. À ce sujet, les modifications requises dans la formulation mathématique de l'optimisation décentralisée de chaque zone sont présentées et discutées en détail.

Les résultats et les conclusions au sujet du contrôle des tensions et des puissances réactives s'appuient sur l'application des méthodes proposées à des réseaux tels que le New England 39 nœuds ou l'IEEE 57 nœuds.

Concernant la contribution de cette thèse au sujet du contrôle de la fréquence, les données relatives aux blackouts du réseau interconnecté de l'Europe continentale sont tout d'abord étudiées pour identifier une éventuelle distribution en loi de puissance. Cette distribution particulière implique notamment que les dynamiques à court et long terme des blackouts peuvent être associées à des systèmes complexes dotés d'une criticité auto-organisée. Dans le contexte de la dynamique à court terme, une approche originale basée sur la simulation de Monte Carlo est proposée pour évaluer l'effet des réserves de contrôle de fréquence sur le risque de blackouts et des déclenchements en cascade. Cette méthode tient compte des déclenchements en cascade en raison de surcharges et de défaillances cachées de systèmes de protection. Elle tient compte également de la réponse automatique et manuel des moyens de contrôle de la fréquence et du délestage de charges sous-fréquence. Il découle de ces investigations que manifestement il existe un compromis entre la probabilité de petits et grands blackouts par rapport à la valeur des réserves de contrôle de fréquence, particulièrement pour les réseaux

électriques interconnectés. Afin d'illustrer la méthodologie développée et discuter les résultats et les conclusions obtenus, le réseau IEEE 118 nœuds est utilisé.

Mots-clés: réseau électrique multizone, réglage de tension, marge de stabilité de tension, réserve de la puissance réactive effective, contraintes de complémentarité, optimisation centralisée/décentralisée, contrôle de fréquence, déclenchements en cascade, larges blackouts, évaluation des risques.

Acknowledgment

I would like to acknowledge everybody who supported me during these years and made the accomplishment of this work possible.

First of all, I would like to express my special appreciation to my director of thesis Dr. Rachid Cherkaoui for giving me the opportunity to work in power systems group at EPFL. The accomplishment of this thesis was possible only with his scientific and kind supports. He is not only an extraordinary mentor for making understandable the complicated problems but also an intimate friend.

I would like to express many thanks to the president of jury Prof. Farhad Rachidi. He is one of the main sources for providing a convivial atmosphere in ELL building. His generosity, friendship, and responsible feeling for everyone drive me to the point that I can say he is the god father of ELL.

I would like to express my gratitude to the member of jury Prof. Mario Paolone. He was not my supervisor but discussion with him about any scientific subject is always fruitful and strongly recommended to researchers. His unstoppable driving force for evolving engineering and science is kept in my mind as the symbol of human intelligence and hard working.

I would like to express my sincere acknowledgement to the member of jury Prof. Thierry Van Cutsem for his precious comments, intelligent advices and valuable discussions on the voltage control subject before, during and after the Ph.D. exam. I would like to equally thank the member of jury Dr. Walter Sattinger for his technical and realistic comments on my work.

I gratefully acknowledge the Swiss Electric Research as this Ph.D. work has been carried out within the frame-work of the research project “Security of Multi-Area Power Systems (MARS)”.

A warm thank to my officemate and close friend Carlos Alberto Romero Romero and his wife Nora Kronig for being my good friends. He has encouraged and helped me in learning French and improving it.

My time at EPFL was made enjoyable by amicable environment in the laboratory. I am grateful for the time I spent with friendly people in ELL building (in order of appearance for me): Hamid Shoory, Andrée Moinat, Alexander Smorgonskiy, Abbas Mosaddeghi, Felix Vega, Nicolas Mora, Jean-Michel Buemi, Lazar Bizumic, Anna Arestova, Mokhtar Bozorg, Gaspar Lugrin, Reza Razzaghi, Maryam Bahramipanah, Mostafa Nick, Mathilde Brocard, Darius Farman, Paolo Romano, Stela Sarri, Konstantina Christakou, Dimitri Torregrossa, Daniel Lopez, Uzair Javaid, Negin Sohrabkhani, Marco Pignati, Lorenzo Reyes, Lorenzo Zanni, Sophie Flynn and Mohammad Azadifar.

I would like to highly thank Marya Tipton for kindly proof reading this thesis and also my uncle Reza Jalal for his continues and kindly supports.

And finally, fundamental thanks go to my family. To my brother Behrouz Alizadeh Mousavi who is always my hope and I can absolutely count on him. To my mother Nayereh Jalal who is the one that always encouraged me to pursue my studies with her infinite patience and compassion. To my wise father Naser Alizadeh Mousavi, the best friend that I ever had, who I am always learning from him about life and thinking during our endless and pleasant discussions. To my wife Mahboube Rahnama for accepting to be next to me in the road of life with her immense kindness and empathy, whether I am walking or jogging or running in the road.

Contents

Abstract	i
Résumé	iii
Acknowledgment	vii
Contents	ix
List of Figures	xi
List of Tables	xv
List of Acronyms	xvii
1 Introduction.....	1
1.1 Security of Multi-Area Power System	2
1.1.1 Voltage Control.....	4
1.1.2 Frequency Control.....	5
1.2 Objectives and Contributions of the Thesis	5
1.3 Thesis Outline	7
2 Voltage and Reactive Power Control.....	9
2.1 Fundamentals of Voltage and Reactive Power Control	10
2.1.1 Classifications of Voltage and Reactive Power Control Studies	11
2.1.2 Voltage Stability Analysis and Optimization.....	13
2.1.3 Provision of the Voltage and Reactive Power Control.....	15
2.2 Current Practices on Voltage Control	18
2.3 Security of Voltage Control in SAPS.....	21
2.3.1 Preliminaries	22
2.3.2 Investigation of PV and VQ Curve Based Optimizations.....	23
2.3.3 Formulations	26

2.3.4	Simulation Results.....	31
2.4	Voltage and Reactive Power Scheduling for MAPS.....	42
2.4.1	Preliminaries.....	43
2.4.2	Multi-Area Voltage and Reactive Power Optimization	43
2.4.3	Various Approaches for Collaborative Optimization of Voltage and Reactive Power in MAPS.....	51
2.4.4	Case Studies and Discussions on Practical Use/Implementation of Results.....	54
2.5	Pilot Node Selection for <i>max.ERPR</i>	61
2.5.1	Preliminaries.....	61
2.5.2	Problem Formulation.....	62
2.5.3	Simulation and Results.....	64
2.6	Security Constrained Voltage and Reactive Power Scheduling in MAPS.....	66
2.6.1	Preliminaries.....	66
2.6.2	Problem Formulation.....	67
2.6.3	Simulation Results.....	71
2.7	Relation Between Voltage and Frequency Control	75
3	Frequency Control vs. Blackouts Risk.....	77
3.1	Investigation of Blackouts Data	78
3.2	Problem Definition.....	80
3.3	Proposed Risk Assessment Approach	82
3.4	Simulation Results.....	86
3.5	Discussion for Further Investigations.....	95
4	Conclusions.....	97
4.1	Highlights	97
4.2	Perspectives.....	98
	Bibliography.....	101

List of Figures

Figure 1.1. Time scales of different power system controls.	4
Figure 2.1. Single line diagram of the two bus system.	14
Figure 2.2. The PV curves of the two bus system.	14
Figure 2.3. The VQ curves of the two bus system.	14
Figure 2.4. LRPR, TGRPR, and EGRPR for the two bus system.	17
Figure 2.5. Structure of a typical hierarchical voltage regulation with SVR and TVR.	19
Figure 2.6. Structure of typical CVR.	19
Figure 2.7. One line diagram of 6-bus system.	32
Figure 2.8. One line diagram of New England 39-bus system.	33
Figure 2.9. One line diagram of IEEE 57-bus system.	33
Figure 2.10. The results of maximization of the loading factor (LF) for different loading levels for 6-bus system.	34
Figure 2.11. The results of maximization of the ERPR for different loading levels for 6-bus system.	34
Figure 2.12. The results of maximization of the loading factor (LF) for different loading levels for 39-bus system.	36
Figure 2.13. The results of maximization of the loading factor (LF) for different loading levels for 57-bus system.	36
Figure 2.14. The results of maximization of the ERPR for different loading levels for 39-bus system.	37
Figure 2.15. The results of maximization of the ERPR for different loading levels for 57-bus system.	37
Figure 2.16. Structure and time constant of the multi-area voltage regulation in comparison with different level of voltage regulation [38].	44

Figure 2.17. Classification of the MAVR based on different coordination approaches and collaborative/non-collaborative behavior of TSOs.	44
Figure 2.18. One line diagram of New England 39-bus system with 3 areas.....	54
Figure 2.19. MAVR for New England 39-bus system for high loading pattern when areas apply the same objective function.....	56
Figure 2.20. MAVR for New England 39-bus system for low loading pattern when areas apply the same objective function.....	56
Figure 2.21. MAVR for New England 39-bus system for high loading pattern when areas apply different objective functions.....	58
Figure 2.22. MAVR for New England 39-bus system for low loading pattern when areas apply different objective functions.....	58
Figure 2.23. The percentage of selection of buses as pilot node for different contingencies for New England 39-bus system.	65
Figure 2.24. The <i>max.ERPR</i> for New England 39-bus system: high loading level - centralized with CC and without CC - decentralized without CC.	72
Figure 2.25. The <i>max.ERPR</i> for New England 39-bus system: high loading level - centralized with CC - decentralized with CC regardless of the proposed modifications.....	73
Figure 2.26. The <i>max.ERPR</i> for New England 39-bus system: high loading level - centralized with CC -decentralized with CC regardless of the proposed modifications.....	73
Figure 2.27. The <i>max.ERPR</i> for New England 39-bus system: high/low loading levels - centralized with CC - decentralized with CC using the proposed modifications.	74
Figure 3.1. Cumulative distribution functions (black circles) and their maximum likelihood power law fit (gray dashed line) for ENTSOE reliability quantities from January 2002 to June 2012.....	79
Figure 3.2. Fast dynamics and external/internal forces.....	81
Figure 3.3. Flowchart and models of the proposed simulation procedure for a given scenario <i>s</i>	84
Figure 3.4. IEEE 118-bus system with three areas.....	86
Figure 3.5. CCDF of lost load for interconnected system for $PgA = 25\%$ with its confidence interval.....	88
Figure 3.6. PDF of number of transmission outages.....	89
Figure 3.7. CCDF of number of transmission outages.....	90
Figure 3.8. CCDF of lost load	91
Figure 3.9. The simulation results of all the scenarios for the interconnected system based on frequency deviation and for $PgA = 5\%$	93

Figure 3.10. The simulation results of all the scenarios for the interconnected system based on frequency deviation and for $PgA = 25\%$	93
Figure 3.11. The simulation results of all the scenarios for the interconnected system based on tie line loading and for $PgA = 5\%$	94
Figure 3.12. The simulation results of all the scenario for the interconnected system based on tie line loading and for $PgA = 25\%$	94
Figure 3.13. a) The system dynamics model for FCRs regarding cascading outages, b) The effect of different forces on PDF of blackout size measure.	95

List of Tables

Table 2.1. The list of blackouts due to voltage collapse.	9
Table 2.2. Different design stages in voltage control studies.....	11
Table 2.3. Various preventive and corrective countermeasures for different time-scales of voltage instability.....	12
Table 2.4. Summary of different practices in voltage and reactive power control.	20
Table 2.5. Summary of different provision and remuneration methods in voltage and reactive power control.	20
Table 2.6. The effect of distributed slack bus model on $max.LF$ for some loading levels (unit:-).	38
Table 2.7. The effect of distributed slack bus model on $max.ERPR$ for some loading levels (unit:MVAR).....	38
Table 2.8. The value of the control variables for 6-bus system with 3 PV generators for loading level equal to 1.	39
Table 2.9. The value of the control variables for 39-bus system for loading level equal to 1. ...	39
Table 2.10. The value of the control variables for 57-bus system for loading level equal to 1. .	39
Table 2.11. Total reactive power output of generators for studied systems in loading level equal to 1.	40
Table 2.12. The effect of active power rescheduling on the value of the objective functions for the studied systems for loading level equal to 1.....	40
Table 2.13. The active power rescheduling to improve the VSMs for 6-bus system.....	40
Table 2.14. The active power rescheduling to improve the VSMs for 39-bus system.....	40
Table 2.15. The active power rescheduling to improve the VSMs for 57-bus system.....	40
Table 2.16. Evaluation of post-contingency VSMs and required corrective actions for 6-bus system with 2 PV and 1 PQ generators for loading level equal to 1.....	41

Table 2.17. The value of control variables for New England 39-bus system for high loading pattern when areas apply the same objective function.	55
Table 2.18. The value of control variables for New England 39-bus system for low loading pattern when areas apply the same objective function.	56
Table 2.19. The value of control variables for New England 39-bus system for high loading pattern when areas apply different objective functions.	57
Table 2.20. The value of control variables for New England 39-bus system for low loading pattern when areas apply different objective functions.	58
Table 2.21. The robustness of different approaches to the strategic behavior of TSO _B	60
Table 2.22. Selected pilot nodes for SVR and TVR for New England 39-bus system.	64
Table 2.23. The value of control variables and generators reactive power output for New England 39-bus system in low loading level.	75
Table 2.24. The value of control variables and generators reactive power output for New England 39-bus system in high loading level.	75
Table 3.1. Statistics of major events in ENTSOE from January 2002 to June 2012.	79
Table 3.2. Generation and reserve of each area.	87
Table 3.3. Unbiased expected number of outages for all study cases for various amounts of reserve.	91
Table 3.4. Probability of Scenario with lost load for all study cases for various amounts of reserve.	92
Table 3.5. <i>ELNS</i> in every area and interconnected system for various amounts of reserves.	92

List of Acronyms

CC	Complementarity Constraints
CCDF	Complementary Cumulative Distribution Function
CVaR	Conditional Value at Risk
CVR	Centralized Voltage Regulation
DC OPF	Linearized Optimal Power Flow
DCLF	Linearized Load Flow
ELNS	Expected Load Not Supplied
ENM	External Network Modeling
ENO	Expected Number of Outages
ENS	Energy Not Supplied
ENTSOE	European Network of Transmission System Operators for Electricity
ERPR	Effective Reactive Power Reserve
FCR	Frequency Control Reserve
GRPR	Generator Reactive Power Reserve
LNS	Load Not Supplied
MAPS	Multi-Area Power System
MAVR	Multi-Area Voltage Regulation

MCS	Monte Carlo Simulation
NERC	North American Electric Reliability Corporation
OPF	Optimal Power Flow
PDF	Probability Distribution Function
PVR	Primary Voltage Regulation
QI	Qualitative Indices
RCCOPF	RPR-based Contingency Constrained Optimal Power Flow
RPR	Reactive Power Reserve
RT	Restoration Time
SAPS	Single Area Power System
SCOPF	Security Constraint Optimal Power Flow
SOC	Self-Organized Criticality
SVR	Secondary Voltage Regulation
TGRPR	Technical Generator Reactive Power Reserve
TSO	Transmission System Operator
TVR	Tertiary Voltage Regulation
UENO	Unbiased Expected Number of Outages
VaR	Value at Risk
VSCOPF	Voltage Stability Constrained Optimal Power Flow
VSM	Voltage Stability Margin
WECC	Western Electricity Coordinating Council

1 Introduction

The human species is able to ponder its energy resources and manage them for its survival. The profitable utilization of these resources, along with the menace of unforeseen events which jeopardize their availability, and therefore survival, are among the major challenging issues for evolution and progress. In each era, certain kinds of energy careers have been prominent according to human necessities and knowledge. Nowadays, and most likely in the future, electricity is the principal form of energy in human life. It plays an important and indisputable role in sustainable development. From the energy perspective, power stations convert different forms of energy into electricity and power grids that are responsible for conveying this energy to consumers. The planning and operation of the power grids also grapple with the twin challenges of maintaining reliable and affordable energy supplies.

The significant effect of these two challenges is quite evident in the evolution of power networks worldwide. For instance, the interconnection of several power networks with independent Transmission System Operators (TSOs) is an important initiative toward global economic operation and reduction of operational risks. The interconnections allow economic interchange of energy to decrease power generation costs and emergency interchange of power in case of contingencies. Today, the interconnected power systems are present in many geographical locations and even on a continental scale (e.g. interconnected networks in continental Europe – ENTSOE and North America – NERC). These interconnected systems are also referred to as Multi-Area Power Systems (MAPSs) such that each TSO corresponds to an area. Another footprint of these challenges in the evolution of power networks is the intention for the economic utilization of resources which has led to the idea of the electricity market. The introduction of the electricity market concepts and privatization which is addressed as market liberalization was initiated in the 80s. It has shifted the electric power industry from the corporative vertically integrated monopoly to the market based competitive environment. In the monopoly situation, the vertically integrated utilities are responsible for generation, transmission and distribution, whereas in the market environment, transmission systems serve as a framework for markets of electrical energy.

The increase of the interconnections and the rules of the liberalized electricity markets have drastically modified the role of control areas within an interconnected network as well as the responsibilities of supplying utilities and system operators. Furthermore, the power grids are continuously exposed to numerous sources of uncertainties which threaten the reliable and secure supply of electricity. These uncertainties are mainly due to the occurrence of contingencies and more recently the high penetration of intermittent renewables. As a consequence, the management of interconnected power systems has become more and more complex and consequently their reliability and security is jeopardized by elevated risk levels. The major evidences are widespread blackouts worldwide in the last two decades which have imposed high social and economic expenditures in different countries. These challenges emphasize the revision and update of security analysis methods of interconnected power systems in accordance with current challenges and new requirements.

The stable and reliable supply of electricity requires appropriate mitigation strategies to prevent the propagation of disturbances or even blackouts. In the monopoly environment and within a Single Area Power System (SAPS), the system operator is the sole entity responsible to ensure the reliability and security of supply and the delivery of electricity to consumers. However after the deregulation of the power industry it is much more difficult to satisfy these tasks with respect to the market regulations and the competitive behaviors of market players. For this purpose, the concept of ancillary services markets is introduced as a complement to guarantee the secure and efficient operation of the system.

The ancillary services are those services necessarily procured by the system operator from the system users to maintain the reliable operation of the transmission system. These services include: active power reserves (frequency control reserves), voltage support, black start capability, compensation of active power losses, etc. In general, the definitions and classifications of the ancillary services vary from one system operator to another. Nevertheless, the frequency and voltage control services have always been an essential part of operating a power system ubiquitously. In spite of different developed schemes for the voltage and frequency control by various TSOs, there are still ongoing research attempts to better define these control services even in SAPS. Within the context of MAPS, the share and exchange of the ancillary services between control areas is an important issue which has received much attention in recent literature. Therefore, it is necessary to investigate different aspects of the voltage and frequency control services and their effect on the security of SAPS and MAPS.

1.1 Security of Multi-Area Power System

In the electricity market environment, the appropriate provision of the ancillary services is among the major responsibilities of a system operator. These control services should ensure the secure operation of the system while they are provided in an economically efficient way. Although for a SAPS these control services are provided by a TSO from the resources within its own control area, in a MAPS they can be shared or exchanged with other control areas. From the market point of view, the transaction of control services will result to lower costs for the

entire interconnected system. From the technical point of view, it is expected that this interchange improves the security of MAPS. However, the interchange of control services should be accompanied with further coordination between TSOs to facilitate the safe operation of the interconnected system.

The interconnected systems might be operated in a non-coordinated situation due to the intention of each TSO to not disclose its control action to other TSOs. The lack of coordination among TSOs may lead to insecure operation of the MAPS even though TSOs find their own control areas secure [1]. This coordination can be attained in (i) a centralized approach with a higher level of control that act as the coordinator of the lower level TSOs (e.g. North America) or in (ii) a decentralized approach based on multi-lateral agreement and cooperation between TSOs with limited information exchange (e.g. Europe). In the former, the operation of MAPS under supervision of a super TSO with a higher level of control would be more expensive and require more communications. While in the latter, the limited information exchange makes the possible control interactions more complicated. The concerns for the secure operation of an interconnected system in Continental Europe have recently resulted in a launch of cooperative initiatives and organizations to improve security practices like Coordination of Electricity System Operators (CORESO) [2], TSO Security Cooperation (TSC) [3] and Security Service Center (SSC) [4]. In addition, there are ongoing efforts toward studying the security related problems and the required coordinations in MAPS.

The voltage and frequency control services are among the most prominent ancillary services since the voltage and frequency equilibrium points, respectively, correspond to the balances between the produced and consumed reactive and active power. Therefore, in this thesis we study only those control services which contribute to the voltage and frequency control. In order to be able to study power systems which are inherently complex with interactive and diverse controls, it is necessary to decompose the associated study problems into several sub-problems.

The time scale decomposition perspective can be utilized to indicate time horizon of various phenomena and system components actions taking part in the voltage and frequency controls [5]. A schematic diagram showing the timescales of different power system control schemes is depicted in Figure 1.1. This time decoupling allows to categorize the different control schemes and to perform more precise studies for different control schemes individually. The short-term and long-term control schemes correspond to the fast acting automatically and the slow acting manually controlled equipments, respectively. Hence, the response of the voltage and frequency controls is also classified according to the short-term/long-term or automatic/manual categories.

Furthermore, the frequency and voltage control issues can be decoupled into two independent problems [6]. It is due to the fact that the frequency is highly dependent on the active power while the voltage is highly dependent on the reactive power. Thus, one issue is the reactive power and voltage control while another is about the active power and frequency control. It is worth noting that the active and reactive powers have combined effects on the frequency and voltage, but this decoupling assumption is quite acceptable for power systems analysis.

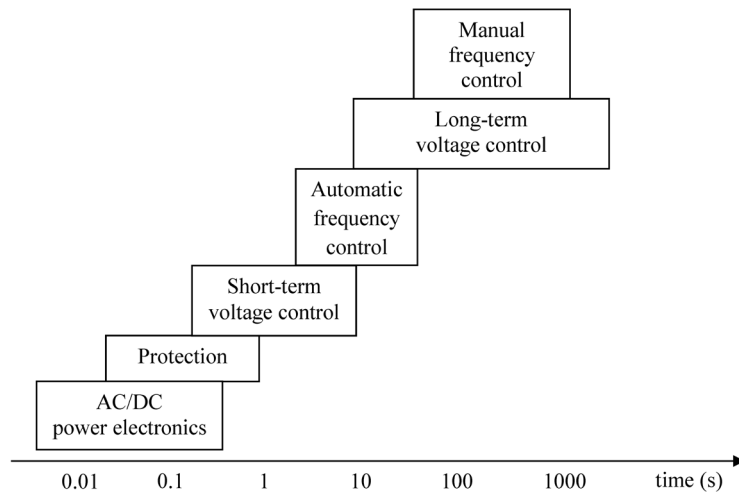


Figure 1.1. Time scales of different power system controls.

Different voltage and frequency control services are introduced by several TSOs to maintain the voltage and frequency within the acceptable operating limits required for the secure operation of the system. The control system of large and complex power systems is often hierarchically organized [5]. It consists of a number of nested control loops that lower control levels which are characterized by smaller time constants than higher control levels. Furthermore, the security controls are performed by preventive and corrective control actions [7]. The preventive control actions are provided in normal operation prior to the disturbance in order to be able to face unforeseen events. The corrective actions are required after the disturbance to eliminate the violation of operational limits and bring the system to a secure state. In the following two subsections, different classifications for the voltage and frequency control services are reviewed concisely. More details on the voltage and frequency control structures are presented in section 2.1 and section 3.2, respectively.

1.1.1 Voltage Control

The voltage and reactive power resources should be managed to keep the voltage at its target value. In normal operation, the proper reactive power generation and consumption level is required in order to reach an appropriate voltage profile. Further control actions have to be provided to maintain the voltages in an acceptable range in case of disturbances. These control actions comprise reactive power reserves and emergency countermeasures which can be considered as preventive and corrective controls, respectively. They ought to ensure the power system security with respect to the voltage control. The definitions and classifications of these control services are explained in section 2.1.

From a system point of view, the regulation of the voltage and reactive power is usually organized in three levels; primary, secondary and tertiary voltage regulation [8]. The Primary

Voltage Regulation (PVR) refers to the local automatic response of the controllers. The Secondary Voltage Regulation (SVR) is an automatic control that coordinates the actions of PVRs at a zonal level. The secondary regulation level is not implemented in all TSOs since its added cost and complication are not always justified. The Tertiary Voltage Regulation (TVR) refers to the manual optimization of the voltage and reactive power at regional or national system level (area). The regulation scheme with three levels is referred to (i) hierarchical voltage regulation, whereas the regulation scheme without SVR is referred to (ii) Centralized Voltage Regulation (CVR) [9]. The definition, the implementation and the control objective of the hierarchical and the centralized regulation vary from one TSO to another. The structure of these two regulation schemes as well as the current practices for the voltage and reactive power control is discussed more in depth in section 2.2.

1.1.2 Frequency Control

The frequency of a system is dependent on the generated and consumed active power balance. In order to control the frequency at its target value, a certain amount of active power reserves is kept available to maintain the balance between the active power generation and consumption in case of disturbance. There are many different terms, definitions and rules concerning what frequency control reserves entail [10]. The general hierarchical classifications of frequency reserve services are: (i) frequency response, regulation, contingency reserve and load following in the NERC and, (ii) primary frequency control, secondary frequency control, tertiary frequency control and time control in the ENTSOE [11]. The ENTSOE has recently classified the frequency reserve services as frequency containment reserve, frequency restoration reserve and replacement reserve [12]. These frequency control reserves can be activated automatically and/or manually. Following a disturbance, the automatic fast controllers aim to stabilize the frequency and then to bring the frequency back to its target value. The manual controls are used to manage the contingencies and to restore the automatic control reserves, frequency and interchanges to their target values.

These classifications are commonly taking into account the time scale decomposition of different control schemes. Likewise to the voltage control, the frequency control reserves can be provided from the preventive and/or corrective control actions.

1.2 Objectives and Contributions of the Thesis

This thesis focuses on the study of the security of interconnected power systems regarding the voltage and frequency controls. The effect of these two control services on the security of SAPS and MAPS are distinctly investigated. The objective of the study of the voltage control is the optimization of the voltage and reactive power controllers in the context of Tertiary Voltage Regulation (TVR) or Centralized Voltage Regulation (CVR). The study of the frequency control

aims to investigate the role of automatic and manual frequency control reserves on the risk of cascading outages and large blackouts.

The contributions of this thesis in the voltage control are as follow:

- The study and classification of current practices on voltage and reactive power control over different TSOs.
- The proposition of an original optimization approach for TVR or CVR based on the criteria of the maximization of effective reactive power reserve. This criterion takes into account the voltage stability margins of the system.
- The proposition of an original genetic algorithm optimization solution approach for the appropriate selection of the pilot nodes according to the abovementioned criteria.
- The investigation of the proposed methodologies for the inter-area voltage and reactive power management in the literatures.
- The classification of MAPS voltage and reactive power optimization methods based on different characteristics like coordinated/non-coordinated solution approaches in the context of collaborative/non-collaborative behavior of TSOs and on centralized/decentralized implementations.
- The proposition of an original unified mathematical formulation for various MAPS voltage and reactive power optimization. These optimizations benefit from the distributed slack bus model and the constraints on the voltage and reactive power in the interconnection links.
- The proposition of the distributed slack bus model for the modelling of loss participation of generating units with additional non-negative variables.
- The proposition of a new coordinated voltage and reactive power control for MAPS. It considers the criteria of the maximization of effective reactive power reserve. Appropriate modifications are proposed for the formulation in the case of the decentralized optimization implementation in order to consider the effect of complementarity constraints at border buses.

The contributions from the frequency control point of view are as follow:

- The study of the power law pattern in the blackouts data and its consequences on the short- and long-term dynamics of cascading outages and blackouts.
- The development of an original risk assessment method that considers the effect of frequency control reserves (automatic and manual) on cascading outages and blackouts.
- The assessment of the trade-off between the probability of small and large blackouts with respect to the value of frequency control reserves, particularly for the interconnected power systems. This part is proposed as an original contribution of this thesis.

1.3 Thesis Outline

A general overview of the context of this thesis and its main contributions are described in the introduction. The two following chapters present the performed studies on the voltage and frequency controls, respectively.

Chapter 2: Voltage and Reactive Power Control presents a concise review of the fundamental issues for the voltage and reactive power controls. An overview of several voltage and reactive power control practices in different TSOs is given in section 2.2. In section 2.3 different approaches for the secure provision of the voltage and reactive power control are investigated. The Effective Reactive Power Reserve (ERPR) is proposed as an effective criterion for the management of the voltage and reactive power resources. The issue of pilot node selection for the TVR is introduced and an optimization method is developed for this purpose in section 2.5. Then, several formulation approaches for the centralized and decentralized voltage and reactive power scheduling in MAPS are evaluated in section 2.4. In the following section 2.6, the proposed approach for the voltage and reactive power management based on ERPR in 2.3 is extended to MAPS using centralized/decentralized implementations. This method is proposed to improve the security of MAPS regarding the voltage and reactive power control.

Chapter 3: Frequency Control vs. Blackouts Risk presents a method to evaluate the effect of frequency control reserves on the risk of blackouts. At first, the blackouts data of the continental Europe are studied in 3.1. The power law distribution, as the output of this analysis, implies that the dynamics of blackouts can be associated with a complex system with short- and long-term dynamics. Besides, the definitions of frequency control reserves in the literatures and the impact of frequency control reserves on the cascading outages and blackouts are briefly explained in section 3.2. In section 3.3, a detailed risk assessment method is proposed which takes into account the cascading outages due to the transmission overloading and the hidden failure of protection systems. It also considers the automatic and manual response of frequency control reserves and under-frequency load shedding. Based on this, section 3.4, investigates the effect of frequency control reserves on the risk of cascading outages and blackouts mainly in the interconnected power systems.

The last chapter, **Conclusions 4**, summarizes the main findings of this research work and provides an outlook on potential future works.

2

Voltage and Reactive Power Control

Voltage and reactive power control service is a critical ancillary service used by all system operators for secure and reliable operation of power systems. In a deregulated power system environment, appropriate provision of the reactive power support and voltage control services are among the major challenging responsibilities of the system operator. In this respect, the main challenges are due to numerous physical constraints, lack of transparent procurement and remuneration policies, and possibilities of discriminatory actions with respect to different resources [13]. Moreover, unlike the active power ancillary services (frequency control reserves), the reactive power cannot be transmitted efficiently through long distances because it leads to additional active and reactive power losses. As a result, the voltage has to be controlled by using special devices dispersed throughout the system. Hence, the system operators usually provide the voltage control services from the resources within their own controlled area.

Although the voltage control is primarily a local problem, the widespread blackouts in the past two decades have demonstrated that the voltage instability and collapse could be considered as important as thermal overloads in major power outages worldwide [14]. Table 2.1 provides some examples for which the voltage collapse was a causal factor in the blackouts (left column) or participated in the blackouts as a consequence of different events (right column).

Table 2.1. The list of blackouts due to voltage collapse.

voltage collapse a causal factor in blackout	voltage collapse factored in blackout	
Belgium in 1982, West Tennessee in 1987, WSCC in 1996, West Coast in 1996, Greece in 2004.	France in 1978, Denmark in 1979, Canada in 1979, Sweden in 1983, South Florida in 1985, Czechoslovakia in 1985, Tokyo in 1987,	Western France in 1987, Québec in 1989, Southern Finland in 1992, North America in 2003, London in 2003, Sweden and Denmark in 2003.

As a result, insufficient voltage and reactive power support was an origin or a factor in the large power outages. Moreover, these events demonstrate that voltage control problem may involve several areas in the interconnected system and increase the scale of blackouts and even affect the intact areas [15].

Therefore, this chapter of the thesis is devoted to the investigation of several issues related to the voltage and reactive power control with respect to the security of single- and multi-area power systems. For this purpose, the following section 2.1 provides the fundamental definitions and classifications for the voltage and reactive power control. The current practices of several TSOs for the provision and remuneration of this control service is presented in section 2.2. Then, a new optimization is proposed in section 2.3 for the scheduling of the voltage and reactive power in SAPS with respect to the effective reactive power reserve. This optimization requires the appropriate selection of voltage sensitive nodes (pilot nodes) for which section 2.5 deals with this issue. Several aspects of the MAPS' voltage and reactive power management are studied in section 2.4. The proposed optimization for the effective reactive power reserve is extended to MAPS in section 2.6. It is expected that this optimization improves the security of voltage and reactive power management in power systems.

2.1 Fundamentals of Voltage and Reactive Power Control

This section reviews the basic definitions and classifications for the voltage and reactive power control. These categories are based on: time response of controllers, time scale of phenomena, analysis methods and time scale of studies. The presented terminologies and the preliminary studies are used in the development of the subsequent sections.

The voltage and reactive power control service is an important ancillary service for secure and reliable operation of power systems. The provision of this ancillary service should assure that the voltage of the entire system is kept at an acceptable level, both in normal operation and emergency conditions. The voltage and reactive power control is primarily a local issue since the reactive power cannot be transmitted effectively through long distances. As a result, the voltage has to be controlled by using special devices disseminated throughout the system to avoid excessive reactive power transmission. The proper selection and coordination of voltage and reactive power control devices is among the major responsibilities of the system operators. This challenging task should be properly studied according to different phenomena and for different design stages.

2.1.1 Classifications of Voltage and Reactive Power Control Studies

The voltage control can be studied in the scopes of power system planning, system protection design, operational planning, and real-time as shown in Table 2.2. In the power system planning stage, the system operator has to ensure the viability of voltage controls requirement of the future system. The system protection against voltage collapse consists of automatic control actions based on local or wide area measurements. The operational planning and the real-time control typically involve different actions aiming at maintaining appropriate voltage profile and reactive power reserves.

Table 2.2. Different design stages in voltage control studies.

Design Stage	Power System Planning	
	System Protection Design	
	Operational Planning	Procurement
		Scheduling
	Real-Time	

The system operator in the various voltage control studies deals with different phenomena in different time-scales. The voltage stability can be classified into two categories based on the size of the disturbance. Small-disturbance voltage stability concerns the system's ability to control voltages following small perturbations. This form of stability can be effectively studied by steady-state approaches based on load flow methods such as PV and VQ curves, Jacobian matrix, continuation power flow, and quasi steady state simulation. Large-disturbance voltage stability concerns the system's ability to control voltages following large disturbances. It can be studied by using non-linear time domain simulations in the short-term timeframe and steady state analysis in the long-term time frame [16].

In addition, according to the different time-scale of phenomena, the voltage stability can be classified into short and long-term stability [17]. The short-term voltage stability is characterized by fast acting dynamics of the power system and its components following a disturbance. The time frame is from less than one second to several seconds. The long-term voltage stability involves slow phenomena and slower acting equipments. Its time frame may extend from several minutes to hours.

The mechanisms that make the system unstable in short-term and long-term dynamics are (i) loss of post-disturbance equilibrium (ST1 and LT1)¹, (ii) lack of attraction toward stable equilibrium (ST2 and LT2), and (iii) post-disturbance oscillatory instability (ST3 and LT3). Usually the evolution of the long-term voltage instability, leads to a short-term instability. This

¹ ST is for the short-term and LT is for the long-term phenomena.

time scale decomposition perspective can be utilized to highlight time horizon of various phenomena and system components actions taking part in the voltage stability. Based on the equipments capability, voltage controllers could be applied in both preventive and corrective strategies [8].

The preventive and the corrective controls are two main defenses against instability incidents. These control actions must be taken appropriately to provide a sufficient security margin. The objective of the voltage security assessment in operational planning and real-time environments is to ensure the system security while taking into account both types of the remedial actions. In the case of a short-term voltage problem, there is not always enough time to implement the corrective actions. Therefore, sufficient reactive power margins should be provided as preventive action for the short-term voltage instability prior the disturbance by the automatic support of the control devices. The countermeasures for the long-term voltage instability contain both preventive and corrective actions, because in the long-term voltage instability usually there is time for operator actions. The various remedial actions for different time-scales of the voltage instability are shown in Table 2.3.

Table 2.3. Various preventive and corrective countermeasures for different time-scales of voltage instability

	preventive action	corrective action
short-term	PVR	Load shedding
long-term	SVR TVR Capacitor switching Load tap changer Generation redispatch	Capacitor switching Load tap changer blocking Generation redispatch (limited to ramp rate) Load shedding

In order to avoid voltage instability, three characteristics of countermeasures including amount, location, and execution time should be appropriately adjusted. The location of corrective actions should be selected so that the minimum amount could be achieved. The further the countermeasure is from the location with voltage instability, the more countermeasures are needed to secure the system. Moreover, the execution of corrective actions can restore the long-term equilibrium when they are performed before the time limit. If corrective actions were realized after the time limit, the system would be prone to LT2 instability. Otherwise, more corrective actions are required to restore the stable post-contingency equilibrium.

The provided emergency controls to protect the system against the voltage collapse are divided into two categories. The first group has no impact on consumers. If they were available, they would be the first controls to be utilized. Some of these actions such as generation rescheduling may involve additional cost to the utilities. The second group of emergency controls, like load shedding, have a direct impact on consumers and usually are used as the ultimate remedial actions. Inappropriate provision of these control services may lead to voltage instability and loss of post-disturbance equilibrium and consequently the voltage collapse and blackout.

2.1.2 Voltage Stability Analysis and Optimization

The study of the voltage control requires appropriate voltage stability analysis methods. These analysis methods are classified in four categories namely: contingency analysis; loadability limit determination; determination of security limits; and preventive and corrective control [18]. These analyses can be accomplished by time-domain simulations and/or steady state approaches. Among the numerous voltage stability analysis methods, the PV curve and VQ curve based approaches are widely employed in the practice and in the literatures. As an instance in the practice side, the established standard of Western Electricity Coordinating Council (WECC) [19] specifies the required active and reactive stability margins, for both transfer paths and load areas, through conducting PV and VQ analyses, respectively. The literatures frequently propose the management of voltage and reactive power resources for the improvement of the voltage stability using the PV and VQ curves [20], [21], [22], [23], [24], [25], [26], [27], [28]. For instance, several Optimal Power Flow (OPF) based approaches are proposed regarding pre- and post-contingencies state(s), namely: Security Constraint Optimal Power Flow (SCOPF) [21], Voltage Stability Constrained Optimal Power Flow (VSCOPF) [22], RPR-based Contingency Constrained Optimal Power Flow (RCCOPF) [23], maximum loadability [24], [25], [26], and Effective RPR (ERPR) [20], [27]. Moreover, the effectiveness of the optimization results, in terms of their steady state responses in the pre- and post-contingency states, is generally tested using PV and VQ curves [20], [22], [23], [24].

Voltage Stability Margins (VSMs) are generally defined as the difference between the value of a key system parameter at the current operating condition and at the voltage stability critical point [24]. According to [24], two main categories for the key system parameter are: (i) PV curve based, and (ii) VQ curve based. The PV curve (watt-volt) presents the variation of load voltage magnitude (V) with the increase of the active power (P) of an area load or power transfer across an interface. The VQ curve (volt-var) expresses the relationship between the reactive power support (Q_f) and the voltage magnitude (V) at a given bus [28]. The PV curve (resp. VQ curve) can be used to evaluate the system active (resp. reactive) power margin to the voltage collapse, specified by VSM_P (resp. VSM_Q), in the pre- and post-contingency states.

The two bus system, shown in Figure 2.1, is used to illustrate the various viewpoints of the VSMs. In the given system, the generator at bus 1 with voltage $E\angle 0$ ($E=1.1$ p.u.) feeds the load at bus 2 with active power P_d ($P_d=2$ p.u.) and reactive power Q_d ($Q_d=0.4$ p.u.) with a constant power factor. Three parallel transmission lines, each one with inductance X ($X=0.3$ p.u.), connect the generation bus to the consumption bus. The PV and the VQ curves are calculated for this system in pre-contingency, post-contingency #1 (outage of one transmission line), and post-contingency #2 (outage of two transmission lines) and are shown in Figure 2.2 and Figure 2.3, respectively. In these figures, the current operating points and the voltage collapse points are shown with the black and white circles, respectively.

2.1 Fundamentals of Voltage and Reactive Power Control

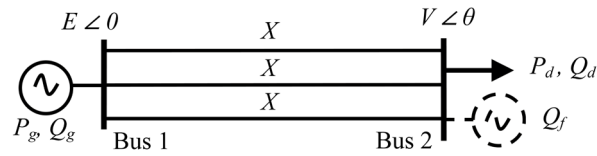


Figure 2.1. Single line diagram of the two bus system.

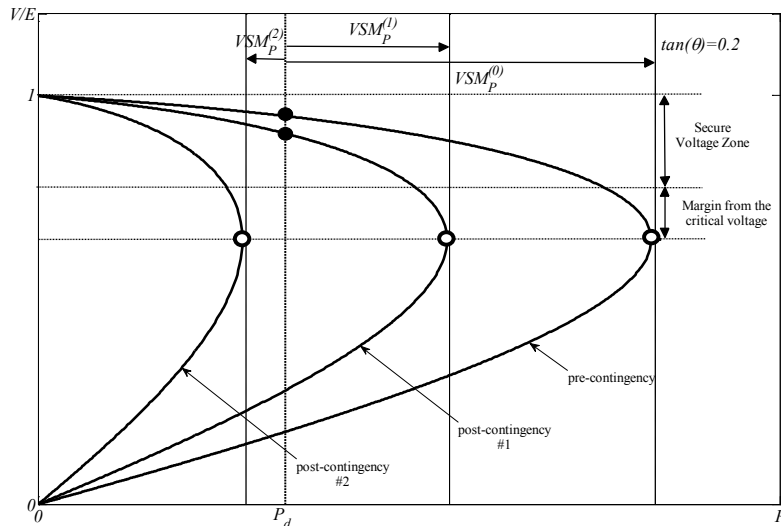


Figure 2.2. The PV curves of the two bus system.

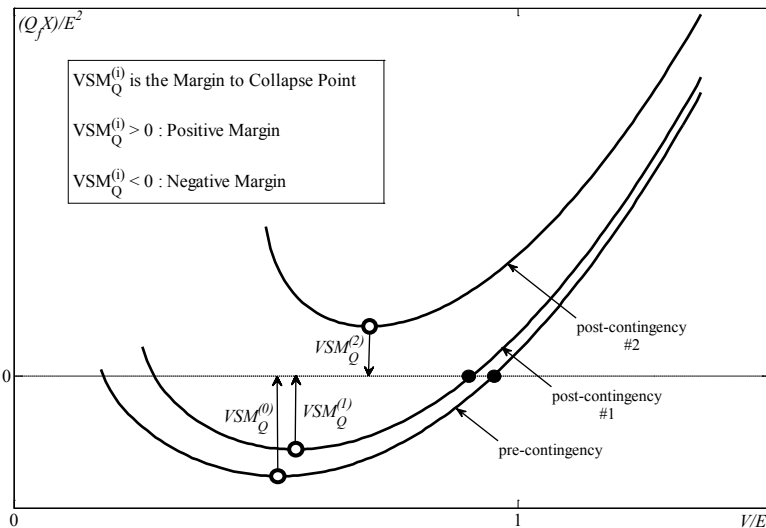


Figure 2.3. The VQ curves of the two bus system.

In Figure 2.2, the VSM_P is the distance of the operating point (black circle) to the nose-point on the PV curve. This margin for the post-contingency #1 ($VSM_P^{(1)}$) decreases in comparison to the pre-contingency ($VSM_P^{(0)}$) due to the loss of one transmission line ($VSM_P^{(1)} < VSM_P^{(0)}$). The

contingency #2 has a negative active power margin ($VSM_P^{(2)}$) with respect to the current operating point which means voltage instability. In this case, a corrective countermeasure like load shedding is required to restore the system to voltage stable area.

As shown in Figure 2.1, a fictitious reactive power injection (Q_f) is added to bus 2 to obtain the VQ curves. The VQ curves for the three aforementioned scenarios and the corresponding VSM_Q are depicted in Figure 2.3. The fictitious injections are equal to zero ($Q_f=0$) in the operating points (the black circles). The difference between the minimum of the VQ curve and the operating point is defined as the VSM_Q at the bus, which is equal to the negative value of the fictitious injected reactive power. The positive margins of the pre-contingency and post-contingency #1 are given by, $VSM_Q^{(0)}$ and $VSM_Q^{(1)}$, respectively. For the post-contingency #2, the reactive power margin ($VSM_Q^{(2)}$) became negative. This value ($VSM_Q^{(2)}$) is the reactive power margin to operability.

Furthermore, a qualitative comparison between the PV and VQ based voltage stability analysis methods is provided in [24], [6]. The advantages of the VQ curve method over the PV curve method are that: (i) it could be more readily derived for a non-radial system using conventional power flow programs, (ii) the power flow solution converges easily because of the fictitious reactive power injection, (iii) it is better suited for examining the requirements for reactive power compensation, (iv) it not only identifies the stability limit, but also defines the minimum reactive power requirement for stable operation. A drawback of VQ curve is that it is quite artificial and has no relation with the way the system is operated. Additionally, in order to completely assess the voltage stability of the system, the VQ curve has to be computed at every bus. On the other hand, only one PV curve computation can reveal the general stability margin of the system. Another advantage of the PV curve is that it provides a global measure of voltage security, such as maximum possible area load increase or maximum power transfer across an interface.

The critical information of the PV and VQ curves, such as VSM_P and VSM_Q , can be obtained in an efficient way using OPFs for the pre- and post-contingency states. For instances, the VSM_P can be readily defined as the maximum load that can be added to the system at a given operating point such that the system remains stable and within all operating limits [24]. This optimization problem is known as maximum loadability [24] or maximization of Loading Factor (LF) [25]. Likewise, the VSM_Q for a given bus can be calculated as the maximum fictitious reactive power load that can be added to that bus [20], [27].

In this thesis, the proposed optimizations for the voltage and reactive power management are based on the PV curve and VQ curve methods. Further aspects of these two optimization problems are investigated in section 2.3.

2.1.3 Provision of the Voltage and Reactive Power Control

The voltage and reactive power resources should be managed to preserve the security of the bulk power system against the short- and long-term instabilities and subsequent voltage

degradation and collapse. These resources are anticipated to keep the system voltages within established limits through automatic and manual actions of the controllers, under both pre- and post-contingency conditions [29]. For this purpose, appropriate control actions should be continuously acquired, deployed and maintained from the control resources in different design stages from planning to real-time. In the operational planning stage, these control actions comprise Reactive Power Reserve (RPR) and Emergency Countermeasures (EC) that can be considered, respectively, as preventive and corrective control actions. The main preventive actions are (i) management of voltage and reactive power resources, and (ii) active power rescheduling [23], which both of them effect on the RPR. The corrective actions include voltage and reactive power rescheduling, then active power rescheduling, and as the last resort load shedding [8].

2.1.3.1 *Reactive Power Reserve*

The RPR is a spare reactive power capability available in the system to assist the voltage control and to maintain the voltage stability. This capability should be held in reserve to respond to unforeseen events that lead to a sudden change of reactive power requirements. The RPR can be classified into static and dynamic RPR based on the resources. In case of contingency, both static and dynamic reactive resources are necessary for the system to survive the transitions and settle in to new operating conditions. An appropriate balance between them and their location need to be well determined [19]. In order to respond to the contingencies and to support the voltage during extreme system operating conditions, the system operator needs to carry sufficient RPRs according to the best response capability of the resources. Thus, it would be a wise practice to control the system in such a way to keep a maximum amount of RPRs on the generators.

The RPR can be viewed from the load's and the generator's perspective. The two bus system, shown in Figure 2.4-a, is used to illustrate the various viewpoints of the RPR. A generator and a load are connected to bus 1 and bus 2, respectively. The VQ curve method is used to obtain the reactive power margin to a voltage collapse point as shown in Figure 2.4-c. The voltage collapse point and the current operating point are indicated with white and black circles, respectively. The generator reactive power output of the current operating point and the voltage collapse point are shown on the generator capability curve in Figure 2.4-b.

The Load RPR (LRPR), shown in Figure 2.4-c, is defined as the minimum amount of the reactive load increase for which the system loses its operability. According to the literature, it is also referred to as the reactive power margin. The Generator RPR (GRPR) focuses on the effectiveness of the provided RPR by each generator. Technical Generator RPR (TGRPR) is defined as the difference between the maximum reactive power capability of the generator and its reactive power output at the current operating point. This quantity may not represent the useful quantity of the GRPR since at the collapse point the full amount of the TGRPR cannot be utilized. Effective Generator RPR (EGRPR), as achievable representative of the GRPR, is defined as the difference between the generator's reactive power output at the voltage collapse point and the generator's reactive power output at the current operating point. The TGRPR is an upper bound for the EGRPR. The LRPR, the TGRPR, and the EGRPR for the two bus system are shown in Figure 2.4-c and Figure 2.4-b.

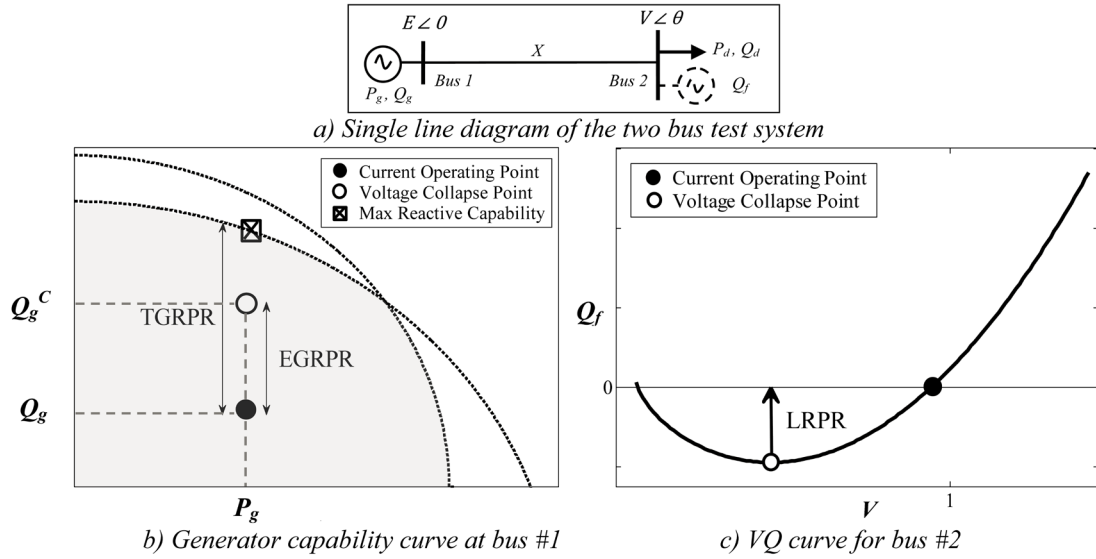


Figure 2.4. LRPR, TGRPR, and EGRPR for the two bus system.

This illustrative example shows that the main cause of voltage instability is the inability of power system generation and transmission network to deliver the required reactive power to load areas. As a result, the Effective RPRs (ERPRs) should be provided regarding both of the constraints of resources (e.g. generating units) and the ability of transmission systems to transfer this control service. Moreover, in order to provide ERPR appropriately, both reactive power generation and its reserve should be considered simultaneously in the procurement and the scheduling of the reactive power resources. The abovementioned issues should be taken in to account carefully for the provision of voltage and reactive power control.

2.1.3.2 Emergency Countermeasure

For some contingencies the provided RPRs cannot attain the desired voltage level and maintain voltage stability. In this case the corrective countermeasures such as reactive and active power redispatch of generators, load shedding schemes, etc., must be employed. The appropriate allocation and implementation of these emergency countermeasures are important in their effectiveness. The system operators must be able to recognize voltage instability related symptoms and take appropriate remedial actions. In this respect, reference [30] suggests an approach to corrective control of voltage instability using simulation and sensitivity. The Corrective Security Constrained Optimal Power Flow (CSCOPF) is also proposed in literatures [31], [32]. Some references propose a coupling security-constraint optimal power flow to determine an optimal combination of preventive and corrective controls ensuring long-term voltage stability [33]. For this purpose, both of the RPR and the emergency countermeasures have been considered.

Each TSO within its own voltage control area must identify and maintain required RPR and emergency countermeasure. However, the interaction of different control levels and actions between neighboring TSOs should be investigated for the security of the interconnected system.

For this aim, the following section studies the current practices of several TSOs for the voltage control within their own control areas.

2.2 Current Practices on Voltage Control

This section studies the current practices of several TSOs for the voltage control. The developed voltage regulation schemes are investigated in depth and their structures are classified as hierarchical and centralized voltage regulations. Moreover, the different provision and remuneration methods of several TSOs are reviewed.

The voltage control is primarily considered as a local issue for which each TSO has developed a particular control scheme within its own control area. However, the voltage instability and collapse may involve several control areas as reported for several blackouts in Table 2.1. Nevertheless, up to now, each TSO only developed a specific voltage and reactive power regulation for its own area. These regulation schemes can be classified into: (i) centralized voltage regulation (CVR) and (ii) hierarchical voltage regulation.

The definition, the implementation and the control objective of the centralized and the hierarchical voltage regulation vary from one TSO to another [34]. Generally, the centralized voltage regulation is divided into two classes: Primary Voltage Regulation (PVR) and Centralized Voltage Regulations (CVR) [8]. The PVR refers to the local response of the controllers (mainly generators). The CVR adjusts the set points of primary controllers from a control center. However, the hierarchical voltage regulation is usually implemented in three levels; primary, secondary and tertiary voltage regulation [5]. In addition to the PVR, the voltage control at a zonal level is related to a Secondary Voltage Regulation (SVR) whereas the Tertiary Voltage Regulation (TVR) is at regional or national system level (area) [35].

The generic schemes of the centralized and hierarchical regulations are illustrated in Figure 2.5 and Figure 2.6, respectively. Figure 2.5 represents a typical structure of the centralized control, where the CVR determines the set-points of the voltage/reactive power regulators (PVRs) based on an optimization criterion. The depicted control scheme in Figure 2.6, contains a TVR as a system control center which determines the optimal voltage set-points for the pilot buses based on a given optimization criterion applied to the whole system. These set-points are fed to the SVRs and they are used by local voltage/reactive power regulators, which are PVRs. A SVR controls the voltage at the given pilot bus(es) in such a manner that the generation of the reactive power is uniformly distributed among controllers inside the zone. It is worth mentioning that the application of SVR is effective for improving the RPR. Despite these efforts for Single Area Power System (SAPS), the coordinated voltage control in the context of interconnected power systems has received less attention.

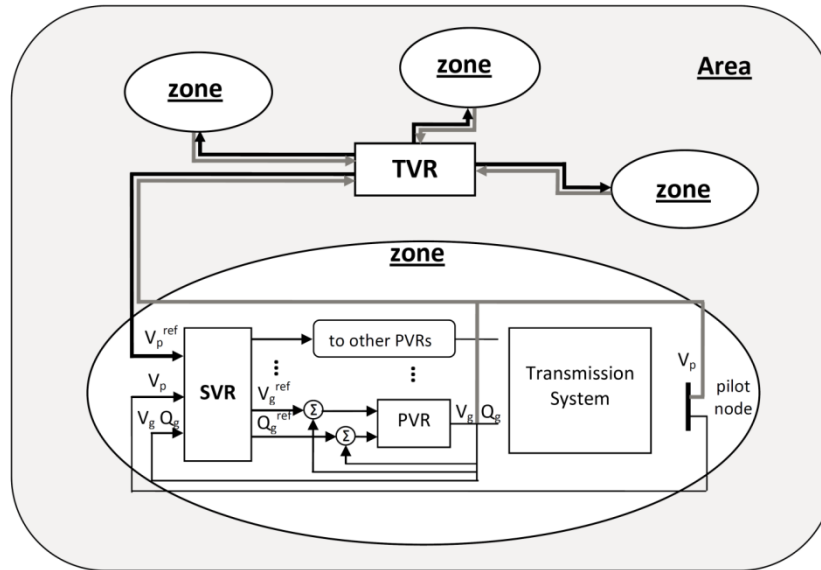


Figure 2.5. Structure of a typical hierarchical voltage regulation with SVR and TVR.

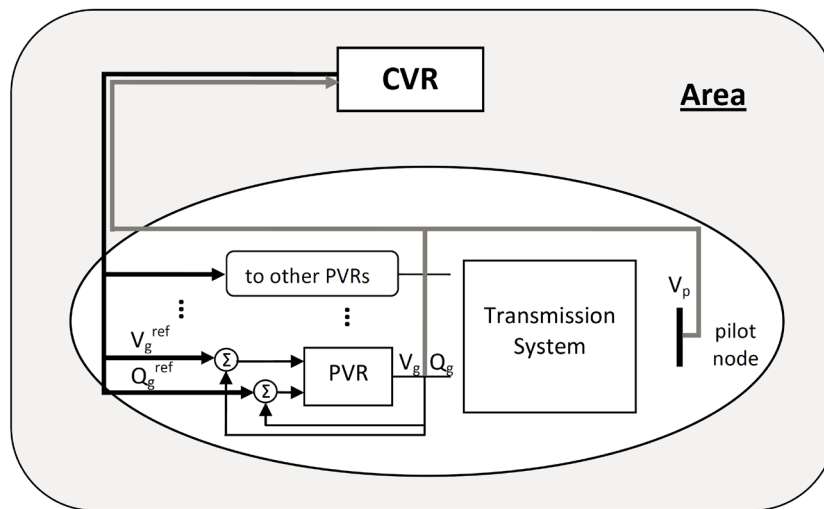


Figure 2.6. Structure of typical CVR.

Current practices of different TSOs in ENTSOE and NERC for the voltage and reactive power control and its provision and remuneration are studied in [15]. Table 2.4 summarizes the aforementioned practices. The corresponding provision and remuneration methods are provided in Table 2.5.

2.2 Current Practices on Voltage Control

Table 2.4. Summary of different practices in voltage and reactive power control.

System	TSOs	Centralized		Hierarchical Control			
		Voltage Control	Reactive Power Control	SVR		TVR	
				Voltage Control	Reactive Power Control	Voltage Control	Reactive Power Control
France	RTE			✓		✓	
Italy	ENEL			✓	✓	✓	
Belgium	Elia	Practice	✓	✓			
		Proposed				✓	✓
Switzerland	Swissgrid	✓					
Spain	REE	Practice	✓				
		Proposed			✓	✓	✓
Germany *	Vattenfal, EON, RWE, EnBW						
Nordic *	NORDEL						
Netherlands *	Tennet						
PJM	NERC	✓	✓				

* The cases indicated with * are not identified.

Table 2.5. Summary of different provision and remuneration methods in voltage and reactive power control.

System	Provision	Remuneration
France	Long term bilateral contract with generators	It is only specified for sensitive geographical zones. Energy generators at fix rate (€/MVar/hr). 50% increase if generator participates in SVR.
Italy	Hierarchical voltage control	Excess reactive energy withdrawal should pay (€/MVar/hr).
Belgium	Tender for providing voltage control resources based on price and location of generating units	The producers are paid for the actual consumed or generated reactive power (€/MVar/hr)
Switzerland	Day ahead reactive power planning, and bilateral agreement for enhanced reactive power support	The provided reactive energy is compensated by (CHF/MVar/hr)
Spain	For reactive power generation day ahead reactive planning, and voltage control ancillary service in annual and daily time scopes. Both through tendering process.	Monthly payment for both production and absorption considering: 1) utilized reactive power (€/MVar/hr), 2)availability of additional band (€/MVar)
Germany	1) Bilateral agreements between concerned parties 2) Supplementary reactive power support in daily operational planning	1) Opportunity cost has to be included 2) Financial compensation based on bilateral agreements
Nordic	1) generators compensatory reactive power supply 2) additional reactive power supply	1) without financial compensation 2) yearly negotiation between system operator and producer
Netherlands	bilateral contracts with local generators	They are only paid for the reactive capacity not for reactive energy
PJM	Compulsory basic voltage control	The generators remunerated based on a regulated price including fixed (\$/Month) plus opportunity cost

Table 2.4 and Table 2.5 demonstrate the intention of different system operators toward the implementation of more sophisticated schemes like centralized and hierarchical voltage

controls. Thus, different approaches and practices from one TSO to another highlight the complexity of the interactions between the different system operations. In addition, the issue of additional coordination in MAPS is important because TSOs' accessibility to the neighboring TSOs' information is limited. This issue could become even more significant whenever the operating limits are reached and control efforts are saturated in an area [36]. Also, as it is mentioned before, a local voltage control problem may spread in MAPS and affect the intact areas. Therefore, a higher level coordination in MAPS is necessary to ensure the security of the power system operation.

The survey of the current practices demonstrates the significance of the inter-area voltage coordination, although the provision of voltage control services is local. In this respect, the ENTSOE operational handbook [35] recommends that interconnected TSOs should coordinate their actions and agree on an acceptable voltage range at each interconnection link, which can be roughly formulated as a zero reactive power flow at every interconnection link [37]. However, no reactive power flow at the interconnection links is difficult to realize. Observations show that reactive power flows are rarely negligible at the interconnection links [38]. In this respect, there are little relevant works to define required additional coordination between TSOs; consequently the voltage and reactive power control in MAPS needs to receive more attention. The further required coordination can be obtained by using centralized and decentralized control schemes.

In spite of different developed voltage control schemes by various TSOs and also in the literatures, there are still ongoing research attempts to well-define the voltage control even in single area. Therefore, in the next section we deal with the single area voltage control regarding the system security.

2.3 Security of Voltage Control in SAPS

This section studies the management of the voltage and reactive power resources regarding the voltage stability margins. In this respect, the maximization of system loadability and the maximization of effective reactive power reserve are investigated in depth. The studied optimizations can be utilized by the centralized voltage regulators or the tertiary voltage regulators in hierarchical voltage control for adjusting the set points of the voltage and reactive power controllers. The details of formulations and the simulation results on several systems are presented and discussed.

2.3.1 Preliminaries

The voltage and reactive power resources have to be managed for the secure and reliable operation of the system. For this purpose, appropriate stability margins should be provided for the voltage control. The system operator defines the set-points of the voltage and reactive power controllers by using different optimization criteria such as: minimization of reactive power injection (or maximization of TGRPR), minimization of voltage profile deviation, minimization of transmission losses, etc. These different objectives would result in different amounts of RPR and consequently different security margins. Nevertheless, the RPRs should be appropriately managed from the available resources to enhance the VSM. It should consider the management of both reactive power generation and its reserve simultaneously in the procurement and the scheduling of the reactive power resources.

The improvement of VSM has been considered in the literature in different ways. The proposed VAR scheduling methods in [39], [40], [41] add a penalty factor to the OPF to maximize the VSM. The penalty factor is derived from the eigenvectors and/or the generators' participation factors related to the Jacobian matrix. The provision of RPR is proposed based on: (i) SCOPF with different constraints [23], [21] and (ii) VSCOPF to determine preventive [22], [42] and corrective controls [22].

Regarding the literatures on LRPR, [43] defines a reactive reserve as the sum of the exhausted reactive reserves at the minimum point of the VQ curve. The RCCOPF presented in [23] utilizes a decomposition method to solve the preventive voltage control in normal state while considering the active power margin of post-contingency states. The proposed RPR management in [20] utilizes a two level Benders decomposition, including a base case and stressed cases, to ensure the feasibility of the stressed cases.

Most of the studies on GRPR like in [44] and [45] are performed on TGRPR since it can be calculated easily regardless of stability analysis. On the other hand, EGRPR depends on the generators capability curve and the network characteristics [46]. That means the maximization of TGRPR doesn't imply necessarily the maximization of EGRPR. The GRPR is studied from the EGRPR point of view more in depth in [46] and [47]. The EGRPR for a bus or an area is determined in [48] as the weighted sum of the individual RPR of generators at the minimum of the VQ curve. The proposed approach in [49], determines the minimum RPR to face a contingency, while stressing the system in its pre-contingency state, until reaching an unacceptable post-contingency response. The maximization of EGRPR is studied in [27] as the main preventive action against voltage instability. This optimization determines the reactive power generation and its reserve for each generator such that maximum voltage stability can be attained for the system.

Reference [50] investigates the correlative relationship between the GRPR and the system VSMs for on-line monitoring. A nonlinear relationship between the GRPR and the VSMs and the voltage limits violations is investigated in [51].

This brief survey demonstrates the significant effect of RPR on the voltage stability. Thus, as mentioned in section 2.1.3, the role of RPR is quite significant as the preventive action for the

system security. This preventive action, by increasing the security margin, can decrease or even remove the necessity of the corrective action in case of contingency. In the following subsection, two optimization methods which consider the VSM_P and VSM_Q are studied more in depth.

2.3.2 Investigation of PV and VQ Curve Based Optimizations

Several optimization problems can be proposed for the voltage and reactive power scheduling which takes into account the voltage stability criteria mentioned in section 2.1.2. These kinds of optimization problems usually consider two operating points, namely: a current operating point and a collapse point. The subscripts “ o ” and “ c ” correspond to the variables and constraints at the current operating point and at the collapse point, respectively. A relationship is assumed between the system variables at these two points [52]. This section of thesis investigates the following two optimizations for the voltage and reactive power scheduling: (i) maximization of Loading Factor ($max.LF$) [25], and (ii) maximization of ERPR ($max.ERPR$) [27]. These two optimizations look similar since both of them consider the analysis of a current operating point and a collapse point. However, the specifications of the objective function and the collapse point for the maximization of LF and $ERPR$ are quite different. Actually, the collapse point for the maximization of LF is obtained by increasing the loading level of the whole system linearly in one direction until reaching a bifurcation point whereas the collapse point in the case of $ERPR$ maximization is attained based on the reactive power reserve of generators and VSMS at the pilot nodes. Note that for the $max.ERPR$, the VQ curve method is used to obtain the reactive power margin to a voltage collapse point. For this purpose fictitious reactive power supports Q_f 's are connected to certain load buses referred to as pilot nodes. Here, the term “pilot node” is explicitly used for this purpose. The pilot nodes are assumed to be the most voltage sensitive nodes. Thanks to the a priori selected pilot nodes, a single VQ based optimization ($max.ERPR$) can provide the solution of the system. Therefore, it is not required to calculate the VQ based VSMS for each load bus individually.

It is worth noting that in these optimizations, it is assumed that the management of the active and reactive power is decoupled. It is due to the fact that the system operator usually has to manage his or her reactive power resources for a specified active power dispatch obtained from the active power market. Moreover, literatures [53] and [54] show that distributed slack bus model gives a better model for the response of the generators to the active power imbalances (here active power losses). Thus, no assumption is made a priori about the slack bus being unique or distributed. Any generating unit can play a role in active power losses without introducing a set of participation factors. For this purpose, the proposed distributed slack bus model is considered using an additional non-negative variable that models the participation of every generating unit in the active power losses. Therefore, the total injected power of each generator is decomposed into a constant term (P_G), specified beforehand in the active power market, and a variable power (P_L) representing its unknown contribution to the active power losses [53].

Furthermore, it is worth mentioning that in traditional maximum stability problems, the current operating point is not incorporated into the optimization model and only the collapse point is considered [52]. As a result, the obtained control variables of these methods may result into the violation of constraints in the current operating point. Hence, these optimization approaches cannot be used for the voltage and reactive power scheduling.

Another important issue in these optimizations is the modeling of the generators reactive power limits which has received lots of attention [20], [25], [26], [27], [52]. As discussed in [26], choosing a priori fixed value for the reactive power limits is an approximation that may lead to errors in the optimization results. For a given active power output, the maximum reactive power support of a generator (Q_{Gg}^{max}) is constrained by the limitation of the field current (\bar{Q}_{GRg}), the limitation of the armature current (\bar{Q}_{GAg}) and the under-excitation limit [55]. The under-excitation limit is considered by the inequality constraint $Q_{Gg} \geq Q_{Gg}^{min}$, where Q_{Gg}^{min} is negative and represents the generator minimum reactive power output. The maximum produced reactive power regarding the field and armature limitations are given by (2-1.a) and (2-1.b), respectively.

$$Q_{Gg}^{max} = \min \begin{cases} \bar{Q}_{GRg} = -\frac{V_g^2}{X_{sg}} + \sqrt{\frac{V_g^2 \cdot \bar{I}_{fg}^2}{X_{sg}^2} - (P_{Gg} + P_{Lg})^2} & (2-1.a) \\ \bar{Q}_{GAg} = \sqrt{V_g^2 \cdot \bar{I}_{ag}^2 - (P_{Gg} + P_{Lg})^2} & (2-1.b) \end{cases}$$

where g is the index of the generators, V_g is the generator terminal voltage, P_{Gg} is the generator active power output, \bar{I}_{fg} is the maximum field current, \bar{I}_{ag} is the maximum armature current, and X_{sg} is the synchronous reactance. Moreover, three modes of generator operation, namely within voltage control range, over-excitation and under-excitation strongly influence the operational limits of the system's reactive power suppliers and consequently the voltage stability limits. Over/Under excitation is considered when the maximum/minimum reactive power limit is reached [21]. The generator switch between the constant terminal voltage and the constant reactive power output is handled by the following complementarity constraints [52]:

$$0 \leq (Q_{Gg}^{(c)} - Q_{Gg}^{min}) \perp V_g^{ue} \geq 0 \quad (2-2.a)$$

$$0 \leq (Q_{Gg}^{max} - Q_{Gg}^{(c)}) \perp V_g^{oe} \geq 0 \quad (2-2.b)$$

$$V_g^{(c)} = V_g^{(0)} + V_g^{ue} - V_g^{oe} \quad (2-2.c)$$

where the operator \perp denotes the complementarity of two quantities. The voltage magnitudes at the collapse point ($V_g^{(c)}$) are defined as the sum of the voltage at the operating point ($V_g^{(0)}$) plus the under-excitation correction voltage (V_g^{ue}) and minus the over-excitation correction voltage (V_g^{oe}) [52]. In this formulation $Q_{Gg}^{(c)}$ is the generator reactive power output at the collapse point. Q_{Gg}^{max} is the maximum reactive power output obtained from (2-1). Q_{Gg}^{min} is the minimum reactive power output that represents the under-excitation limit.

Generally, the optimization problems with complementarity constraints increase the computational complexity. Nevertheless, the explicit representation of generator capability limits plays a dominant role in emergency states [26], [27]. These complementarity constraints

(2-2.a) and (2-2.b) could be, respectively, taken into consideration by the following nonlinear constraints:

$$(Q_{Gg}^{(c)} - Q_{Gg}^{min}).V_g^{ue} \leq 0 \quad (2-3.a)$$

$$(Q_{Gg}^{max} - Q_{Gg}^{(c)}).V_g^{oe} \leq 0 \quad (2-3.b)$$

In order to prevent a strict complementarity constraint and the related problems [52], the righthand sides' zeros of (2-3) are replaced by a small positive number ($\epsilon=10^{-7}$). It should be noted that at the collapse point, the generators switching to the under-excited mode is not taken into consideration. In fact, in response to the increase of the loading level (for *max.LF*) or the increase of the fictitious reactive power loads at the pilot nodes (for *max.ERPR*), the generators need rather to switch from the voltage control mode to the over-excited mode in order to increase their reactive power support at the collapse point. Moreover, in the case without consideration of the complementarity constraints the over-excitation correction voltage (V_g^{oe}) is assumed equal to zero.

The detailed modeling of the generator's switch mode with complementarity constraints effectively improves the optimization results since it allows the voltage levels to be changed when generators reach their reactive power limits. Reference [52] demonstrates that this additional degree of freedom permits higher critical loading level, specifically when the network is lightly loaded. In this work, it is demonstrated that for certain loading levels the complementarity modeling may increase the value of the objective function, whereas, for other loading levels for which the objective value remains unchanged, the complementarity constraints may allow to decrease the generators reactive power output in the current operating point. The corresponding illustrative examples are presented in simulation results in section 2.3.4.

Furthermore, the optimization problem of *max.ERPR* is formulated by the author of this thesis using both one-stage and two-stage approaches [47]. The two-stage method decomposes the problem into two smaller problems. The first stage determines an operating point and the second stage calculates the collapse point based on the results of the first stage. The Subgradient method is used to correlate these two stages and to fix the operating point. These two smaller problems are generally solved much simpler than a single larger one. However, a drawback of this approach is that the solution of the two-stage optimization is obtained iteratively. It is demonstrated that for small systems, a two-stage approach is more efficient than a one-stage, but it is not effective in larger study cases, since it iteratively solves a large problem at the voltage collapse point. Hence, in this thesis the one-stage approach is used only.

In addition, the *PV* curve and *VQ* curve based methods along with the post-contingency stability margin of a certain number of postulated contingencies are used in the literature for the voltage and reactive power scheduling regarding the system security. For instance, reference [20] proposes a two level benders' decomposition to handle several contingency scenarios and their post-contingency stability margins based on *VQ* analysis approach. Similarly, the *PV* curve based stability margin for a set of contingencies is proposed in [25] for the voltage and reactive

power scheduling. Here, the investigated optimizations (*max.LF* and *max.ERPR*) only consider a contingency scenario (the collapse point) which is obtained by the increase of the loading level or the reactive power injection at pilot nodes.

The next subsection presents the related formulations for the optimizations based on *PV* and *VQ* methods.

2.3.3 Formulations

This section presents the formulation for the optimization problems and the contingency analysis. These optimizations can be considered as the preventive action whose results are used for the adjustment of the voltage and reactive power controllers. Then, the proposed contingency analysis evaluates the effectiveness of the provided preventive actions as well as the required corrective countermeasures.

The proposed optimizations (*max.LF* and *max.ERPR*) are generally formulated as follow:

$$\max_{u, \phi} f(x_0, x_c, u, \phi) \quad (2-4.a)$$

s.t.

$$g_0(x_0, u) \leq 0 \quad (2-4.b)$$

$$h_0(x_0, u) = 0 \quad (2-4.c)$$

$$g_c(x_c, u, \phi) \leq 0 \quad (2-4.d)$$

$$h_c(x_c, u, \phi) = 0 \quad (2-4.e)$$

In the presented general formulation the objective function $f(.)$ is for *LF* or *ERPR*. The vector of the control variables (u) includes the voltage of *PV* generators and the reactive power output of *PQ* generators. The control variables could be considered as the complicating variables since they are present for the current operating point and for the voltage collapse point. x indicates the vector of the state variables and ϕ is the variable of active power increase (for *max.LF*) or the vector of fictitious reactive power injections (for *max.ERPR*). $g(.)$ and $h(.)$ correspond to inequality and equality constraints, respectively. The equality constraints are the power flow equations and the equality of control variables at the current operating point and the collapse point. The inequality constraints include the operating limits of generating units, transmission lines and voltage magnitude of nodes. The complementarity constraints are modeled with a certain number of nonlinear constraints according to (2-3). The obtained control variables from the optimization of (2-4) are given by u^* .

The contingency analysis is formulated as an optimization problem that aims to find the stability margin of post-contingency state using *max.LF* or *max.ERPR*. The constraints of this optimization are the same as in the case of the collapse point. The general form of optimization is as follows:

$$\max_{\phi} f(x_s, u^*, \phi) \quad (2-5.a)$$

s.t.

$$g_s(x_s, u^*, \phi) \leq 0 \quad (2-5.b)$$

$$h_s(x_s, u^*, \phi) = 0 \quad (2-5.c)$$

where subscript “s” represents the s-th scenario. If this optimization does not converge or its result demonstrates instability, other optimizations are employed. In order to obtain the appropriate corrective action alternate optimizations are employed: initially, voltage and reactive power rescheduling (Δu), then the active power rescheduling (Δp_g) and lastly the load shedding (Δp_c). The objective of these alternate optimizations is the minimization of the deviation from the scheduled set-points which characterize the minimum required corrective actions. These optimizations only consider the voltage collapse point. The general form of this optimization is given as follows:

$$\min_{\Delta u, \Delta p_g, \Delta p_c} f(x_s, u^* + \Delta u, \Delta p_g, \Delta p_c) \quad (2-6.a)$$

s.t.

$$g_s(x_s, u^* + \Delta u, \Delta p_g, \Delta p_c) \leq 0 \quad (2-6.b)$$

$$h_s(x_s, u^* + \Delta u, \Delta p_g, \Delta p_c) = 0 \quad (2-6.c)$$

The provided corrective actions by (2-6) are initially in terms of the voltage and reactive power rescheduling. If this corrective action is not enough then the active power rescheduling is employed. In this way, generators are able to change their active power outputs for obtaining appropriate corrective action. If the rescheduling of the voltage and reactive and active power are not sufficient, the load shedding is employed to restore the system operability. In this formulation the load shedding is performed with a constant power factor.

In the presented formulations (2-4) – (2-6) the distributed slack bus model is used to characterize the response of generators to the active power losses. This model assumes a non-negative variable for each generator which can participate in the compensation of active power imbalances. The explicit formulation for *max.LF*, *max.ERPR* and contingency analysis are presented in the following.

2.3.3.1 Maximization of Loading Factor

The maximization of loading factor (*max.LF*) is given by (2-7). It is subjected to the given equality and inequality constraints:

$$\max LF \quad (2-7.a)$$

- at the operating point (2-7.b) – (2-7.h):

$$P_{Gi} + P_{Li}^{(0)} - P_{Di} - \sum_j P_{ij}^{(0)}(V^{(0)}, \theta^{(0)}) = 0 \quad i \in \Omega_B \quad (2-7.b)$$

$$Q_{Gi}^{(0)} - Q_{Di} - \sum_j Q_{ij}^{(0)}(V^{(0)}, \theta^{(0)}) = 0 \quad i \in \Omega_B \quad (2-7.c)$$

$$(P_{ij}^{(0)})^2 + (Q_{ij}^{(0)})^2 \leq (S_l^{max})^2 \quad \{i, j\} \in l, l \in \Omega_T \quad (2-7.d)$$

$$0 \leq P_{Lg}^{(0)} \leq \bar{P}_{Gg} - P_{Gg} \quad g \in \Omega_G \quad (2-7.e)$$

$$\underline{Q}_{Gg} \leq Q_{Gg}^{(0)} \leq \bar{Q}_{GRg}^{(0)} \quad g \in \Omega_G \quad (2-7.f)$$

$$\underline{Q}_{Gg} \leq Q_{Gg}^{(0)} \leq \bar{Q}_{GAg}^{(0)} \quad g \in \Omega_G \quad (2-7.g)$$

$$V_i^{min} \leq V_i^{(0)} \leq V_i^{max} \quad i \in \Omega_B \quad (2-7.h)$$

- and at the voltage collapse point (2-7.i) – (2-7.u):

$$P_{Gi} \cdot (1 + LF) + P_{Li}^{(c)} - P_{Di} \cdot (1 + LF) - \sum_j P_{ij}^{(c)}(V^{(c)}, \theta^{(c)}) = 0 \quad i \in \Omega_B \quad (2-7.i)$$

$$Q_{Gi}^{(c)} - Q_{Di} \cdot (1 + LF) - \sum_j Q_{ij}^{(c)}(V^{(c)}, \theta^{(c)}) = 0 \quad i \in \Omega_B \quad (2-7.j)$$

$$(P_{ij}^{(c)})^2 + (Q_{ij}^{(c)})^2 \leq (S_l^{max})^2 \quad \{i, j\} \in l, l \in \Omega_T \quad (2-7.k)$$

$$0 \leq P_{Lg}^{(c)} \leq \bar{P}_{Gg} - P_{Gg} \quad g \in \Omega_G \quad (2-7.l)$$

$$V_i^{min} \leq V_i^{(c)} \leq V_i^{max} \quad i \in \Omega_B \quad (2-7.m)$$

$$V_g^{(c)} = V_g^{(0)} - V_{Ag}^{oe(c)} - V_{Rg}^{oe(c)} \quad g \in \Omega_{G-PV} \quad (2-7.n)$$

$$(\bar{Q}_{GAg}^{(c)} - Q_{Gg}^{(c)}) \cdot V_{Ag}^{oe(c)} \leq \varepsilon \quad g \in \Omega_{G-PV} \quad (2-7.o)$$

$$(\bar{Q}_{GRg}^{(c)} - Q_{Gg}^{(c)}) \cdot V_{Rg}^{oe(c)} \leq \varepsilon \quad g \in \Omega_{G-PV} \quad (2-7.p)$$

$$V_{Ag}^{oe(c)} \geq 0 \quad g \in \Omega_{G-PV} \quad (2-7.q)$$

$$V_{Rg}^{oe(c)} \geq 0 \quad g \in \Omega_{G-PV} \quad (2-7.r)$$

$$\underline{Q}_{Gg} \leq Q_{Gg}^{(c)} \leq \bar{Q}_{GAg}^{(c)} \quad g \in \Omega_G \quad (2-7.s)$$

$$\underline{Q}_{Gg} \leq Q_{Gg}^{(c)} \leq \bar{Q}_{GRg}^{(c)} \quad g \in \Omega_G \quad (2-7.t)$$

$$Q_{Gg}^{(c)} = Q_{Gg}^{(0)} \quad g \in \Omega_{G-PQ} \quad (2-7.u)$$

In this formulation Ω_B , Ω_T and Ω_G are the set of buses, the set of lines and the set of generators, respectively. Ω_{G-PV} and Ω_{G-PQ} represent the set of PV and PQ generators such that $\Omega_G = \{\Omega_{G-PV} \cup \Omega_{G-PQ}\}$. i and j are the index of buses, l is the index of lines and g is the index of generators. V_i is the voltage magnitude of bus i , and θ is the voltage angle difference between the buses connecting two nodes together. The active power and the reactive power are shown by P and Q , respectively. P_{Gi} , P_{Li} and P_{Di} are the active power generation, losses and demand in bus i , respectively. P_{ij} is the active power flow from bus i to bus j . Similarly, Q_{Gi} and Q_{Di} are the reactive power generation and demand in bus i and Q_{ij} is the reactive power flow from bus i to bus j . The reactive power capacity of each generator is limited by a lower bound \underline{Q}_{Gg} and two upper bounds of the field and armature currents that are \bar{Q}_{GRg} and \bar{Q}_{GAg} , given by (2-1). V_{Rg}^{oe} and V_{Ag}^{oe} are the corresponding complementarity variables which models the generators switch mode

between the constant voltage and the over excitation mode. The upper limit of the active power generation is specified by \bar{P}_{Gg} . The limits of voltages at bus i are V_i^{min} and V_i^{max} . The maximum transfer capability of the transmission lines is given by S_l^{max} .

At the current operating point (resp. voltage collapse point) the active and reactive power balance equality constraints are given by (2-7.b) – (2-7.c) (resp. (2-7.i) – (2-7.j)). Note that the active and reactive power balance equality constraints at the collapse point contain the loading factor (LF). The transmission lines flow limit is considered in (2-7.d) (resp. (2-7.k)). The limits of the generators active and reactive power and the voltage magnitude at each bus are considered in (2-7.e), (2-7.f), (2-7.g) and (2-7.h), respectively. At the voltage collapse point, the limitations of the generators active and reactive power outputs and the voltage of the buses are given by (2-7.l), (2-7.s), (2-7.t) and (2-7.m), respectively.

$V_g^{(0)}$ and $Q_{Gg}^{(0)}$ in (2-7.n) and (2-7.u) are the voltage and reactive power of the PV and PQ generators at the operating point, respectively. These two equality constraints in addition to the inequality constraints (2-7.o) – (2-7.p) correlate the current operating point and the collapse point while considering the complementarity constraints mentioned by (2-2.c) and (2-3). Besides the fact that the PQ generators reactive power output are the same at the current operating point and at the voltage collapse point (according to (2-7.u)), they can participate in the optimization process.

2.3.3.2 Maximization of ERPR

The maximization of $ERPR$ is given by (2-8). This optimization consists in the minimization of the difference between the sum of the generators reactive power output at the operating ($\sum Q_{Gg}^{(0)}$) and the collapse point ($\sum Q_{Gg}^{(c)}$). It is subjected to the given equality and inequality constraints:

$$\begin{aligned} \max ERPR &= \max \sum_{g \in \Omega_G} \{Q_{Gg}^{(c)} - Q_{Gg}^{(0)}\} & (2-8.a) \\ &\cong \min \sum_{g \in \Omega_G} \{Q_{Gg}^{(0)} - Q_{Gg}^{(c)}\} \end{aligned}$$

- at the operating point (2-8.b) – (2-8.h):

$$P_{Gi} + P_{Li}^{(0)} - P_{Di} - \sum_j P_{ij}^{(0)}(V^{(0)}, \theta^{(0)}) = 0 \quad i \in \Omega_B \quad (2-8.b)$$

$$Q_{Gi}^{(0)} - Q_{Di} - \sum_j Q_{ij}^{(0)}(V^{(0)}, \theta^{(0)}) = 0 \quad i \in \Omega_B \quad (2-8.c)$$

$$(P_{ij}^{(0)})^2 + (Q_{ij}^{(0)})^2 \leq (S_l^{max})^2 \quad \{i, j\} \in l, l \in \Omega_T \quad (2-8.d)$$

$$0 \leq P_{Lg}^{(0)} \leq \bar{P}_{Gg} - P_{Gg} \quad g \in \Omega_G \quad (2-8.e)$$

$$\underline{Q}_{Gg} \leq Q_{Gg}^{(0)} \leq \bar{Q}_{GRg}^{(0)} \quad g \in \Omega_G \quad (2-8.f)$$

$$\underline{Q}_{Gg} \leq Q_{Gg}^{(0)} \leq \bar{Q}_{GAg}^{(0)} \quad g \in \Omega_G \quad (2-8.g)$$

$$V_i^{min} \leq V_i^{(0)} \leq V_i^{max} \quad i \in \Omega_B \quad (2-8.h)$$

- and at the voltage collapse point (2-8.i) – (2-8.u):

$$P_{Gi} + P_{Li}^{(c)} - P_{Di} - \sum_j P_{ij}^{(c)}(V^{(c)}, \theta^{(c)}) = 0 \quad i \in \Omega_B \quad (2-8.i)$$

$$Q_{Gi}^{(c)} - Q_{Pi}^{(c)} - Q_{Di} - \sum_j Q_{ij}^{(c)}(V^{(c)}, \theta^{(c)}) = 0 \quad i \in \Omega_B \quad (2-8.j)$$

$$(P_{ij}^{(c)})^2 + (Q_{ij}^{(c)})^2 \leq (S_l^{max})^2 \quad \{i, j\} \in l, l \in \Omega_T \quad (2-8.k)$$

$$0 \leq P_{Lg}^{(c)} \leq \bar{P}_{Gg} - P_{Gg} \quad g \in \Omega_G \quad (2-8.l)$$

$$V_i^{min} \leq V_i^{(c)} \leq V_i^{max} \quad i \in \Omega_B \quad (2-8.m)$$

$$V_g^{(c)} = V_g^{(0)} - V_{Ag}^{oe(c)} - V_{Rg}^{oe(c)} \quad g \in \Omega_{G-PV} \quad (2-8.n)$$

$$(\bar{Q}_{GAg}^{(c)} - Q_{Gg}^{(c)}) \cdot V_{Ag}^{oe(c)} \leq \varepsilon \quad g \in \Omega_{G-PV} \quad (2-8.o)$$

$$(\bar{Q}_{GRg}^{(c)} - Q_{Gg}^{(c)}) \cdot V_{Rg}^{oe(c)} \leq \varepsilon \quad g \in \Omega_{G-PV} \quad (2-8.p)$$

$$V_{Ag}^{oe(c)} \geq 0 \quad g \in \Omega_{G-PV} \quad (2-8.q)$$

$$V_{Rg}^{oe(c)} \geq 0 \quad g \in \Omega_{G-PV} \quad (2-8.r)$$

$$\underline{Q}_{Gg} \leq Q_{Gg}^{(c)} \leq \bar{Q}_{GAg}^{(c)} \quad g \in \Omega_G \quad (2-8.s)$$

$$\underline{Q}_{Gg} \leq Q_{Gg}^{(c)} \leq \bar{Q}_{GRg}^{(c)} \quad g \in \Omega_G \quad (2-8.t)$$

$$Q_{Gg}^{(c)} = Q_{Gg}^{(0)} \quad g \in \Omega_{G-PQ} \quad (2-8.u)$$

In addition to the presented nomenclatures in section 2.3.3.1, Q_{Pi} is the vector of fictitious reactive power injection at i -th bus. This vector has non-zero elements only for the pilot nodes and it is added to reactive power balance equality constraint at the collapse point as shown in (2-8.j).

2.3.3.3 Contingency analysis

The post-contingency stability margin of a scenario can be obtained by *max.LF* or *max.ERPR* for which the corresponding optimization only considers the collapse point. In the case of negative stability margin or infeasibility or non-convergence of these optimizations, a corrective action is required.

The minimization of the required corrective actions for a given scenario is given by (2-9). This optimization only considers the voltage collapse point and it is subjected to the given equality and inequality constraints (2-9.b) – (2-9.o). Here, the quadratic costs (the second norm) are considered in order to obtain the deviation from the current operating point. The first norm can also be taken into consideration.

$$\min \sum_{g \in \Omega_G, d \in \Omega_D} (\Delta V_g)^2 + (\Delta Q_{Gg})^2 + K_1 \cdot (\Delta P_{Gg})^2 + K_2 \cdot (P_{Lsd}) \quad (2-9.a)$$

subject to

$$P_{Gi} + \Delta P_{Gi}^{(s)} - P_{Di} + P_{LSi}^{(s)} - \sum_j P_{ij}^{(s)}(V^{(s)}, \theta^{(s)}) = 0 \quad i \in \Omega_B \quad (2-9.b)$$

$$Q_{Gi}^{(s)} - Q_{Di} + Q_{LSi}^{(s)} - \sum_j Q_{ij}^{(c)}(V^{(c)}, \theta^{(c)}) = 0 \quad i \in \Omega_B \quad (2-9.c)$$

$$(P_{ij}^{(s)})^2 + (Q_{ij}^{(s)})^2 \leq (S_l^{max})^2 \quad \{i, j\} \in l, l \in \Omega_T \quad (2-9.d)$$

$$0 \leq \Delta P_{Gg}^{(s)} \leq \bar{P}_{Gg} - P_{Gg} \quad g \in \Omega_G \quad (2-9.e)$$

$$V_i^{min} \leq V_i^{(s)} \leq V_i^{max} \quad i \in \Omega_B \quad (2-9.f)$$

$$V_g^{(s)} = V_g^{(*)} - V_{Ag}^{oe(s)} - V_{Rg}^{oe(s)} + \Delta V_g^{(s)} \quad g \in \Omega_{G-PV} \quad (2-9.g)$$

$$(\bar{Q}_{GAg}^{(s)} - Q_{Gg}^{(s)}) \cdot V_{Ag}^{oe(s)} \leq \varepsilon \quad g \in \Omega_{G-PV} \quad (2-9.h)$$

$$(\bar{Q}_{GRg}^{(s)} - Q_{Gg}^{(s)}) \cdot V_{Rg}^{oe(s)} \leq \varepsilon \quad g \in \Omega_{G-PV} \quad (2-9.i)$$

$$V_{Ag}^{oe(s)} \geq 0 \quad g \in \Omega_{G-PV} \quad (2-9.j)$$

$$V_{Rg}^{oe(s)} \geq 0 \quad g \in \Omega_{G-PV} \quad (2-9.k)$$

$$\underline{Q}_{Gg} \leq Q_{Gg}^{(s)} \leq \bar{Q}_{GAg}^{(s)} \quad g \in \Omega_G \quad (2-9.l)$$

$$\underline{Q}_{Gg} \leq Q_{Gg}^{(s)} \leq \bar{Q}_{GRg}^{(s)} \quad g \in \Omega_G \quad (2-9.m)$$

$$Q_{Gg}^{(s)} = Q_{Gg}^{(*)} + \Delta Q_{Gg}^{(s)} \quad g \in \Omega_{G-PQ} \quad (2-9.n)$$

$$0 \leq P_{LSd}^{(s)} \leq 0 \quad d \in \Omega_D \quad (2-9.o)$$

where subscript ‘*’ represents the current operating point obtained from the optimization problems (2-7) or (2-8). ΔV_g , ΔQ_{Gg} and ΔP_{Gg} are the variables for the voltage, reactive and active power rescheduling. P_{LS} is devoted for the load shedding at every bus. d is the index of demands and Ω_D is the set of buses with demands.

In order to consider the active power rescheduling, the constraint (2-9.e) is replaced with the following equation (2-9.p). In this way, generators are able to change their active power outputs for obtaining appropriate corrective action.

$$-P_{Gg} \leq \Delta P_{Gg}^{(s)} \leq \bar{P}_{Gg} - P_{Gg} \quad g \in \Omega_G \quad (2-9.p)$$

If the above mentioned corrective actions are not sufficient, the load shedding is employed to restore the system operability. In this respect, the inequality (2-9.o) is replaced with the following inequality (2-9.q).

$$0 \leq P_{LSd}^{(s)} \leq P_d \quad d \in \Omega_D \quad (2-9.q)$$

In this formulation the load shedding is performed with a constant Power Factor (PF) and the value of Q_{LSd} is calculated from the following equation (2-9.r).

$$Q_{LSd}^{(s)} = P_{LSd}^{(s)} \cdot \frac{\sqrt{1 - PF^2}}{PF} \quad d \in \Omega_D \quad (2-9.r)$$

2.3.4 Simulation Results

The aforementioned optimization approaches are tested on 6-bus system, New England 39-bus system and IEEE 57-bus system, shown in Figure 2.7, Figure 2.8 and Figure 2.9, respectively. The data of generators, loads and transmission components are given in [27] and [56]. The

further parameters of generators which they are not available in standard load flow data (e.g. synchronous reactance, maximum armature and field current) are calculated according to the proposed method in [26]. The buses shown in bold and red represent the pilot nodes used for *max.ERPR*. The selection of pilot nodes is based on the developed principle pointed out in section 2.5. It is well-known that the voltage and reactive power management effectively depends on the loading level (L) of the system. In order to obtain more general conclusions, simulations are performed for different loading levels from 0.2 to 1.0 times of the nominal loading. Furthermore, the simulations are carried out for the cases with PV generators only and the cases including both PV and PQ generators. The voltage deviation of all buses is acceptable within $\pm 10\%$ of the nominal voltage. Several aspects of the optimization and the evaluation of stability margin are studied as listed below.

- 1) The effect of detailed modeling of generators.
- 2) The effect of distributed slack bus modeling.
- 3) The scheduling of voltage and reactive power resources based on *PV* curve method (*max.LF*) and *VQ* curve method (*max.ERPR*).
- 4) The evaluation of the post-contingency stability margin.

The proposed OPF models are nonlinear optimization problems which they are solved using “fmincon” with interior-point algorithm in MATLAB R2011b. In order to improve the performance of the optimizations, the gradients of the objective function and constraints are provided using the symbolic toolbox according to [57]. Moreover, the multi-start algorithm with parallel computation [58] is used to search thoroughly for a global optimum solution. To this end, a set of custom starting points are provided by adding a random noise to the provided initial point.

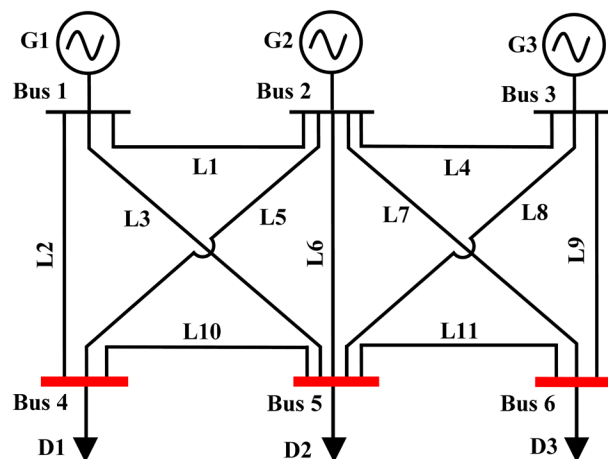


Figure 2.7. One line diagram of 6-bus system.

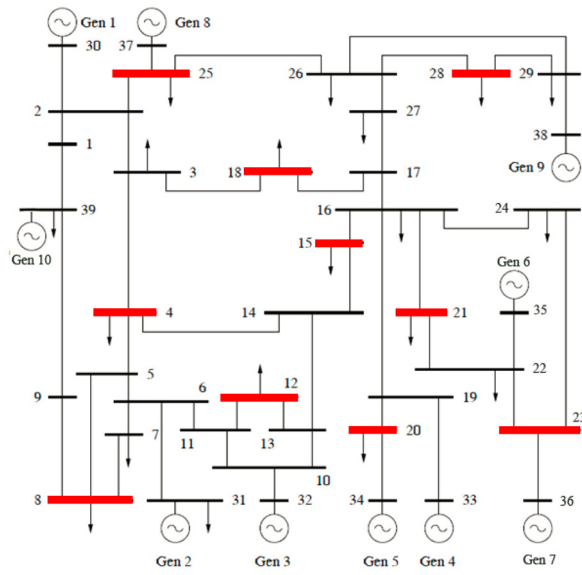


Figure 2.8. One line diagram of New England 39-bus system.

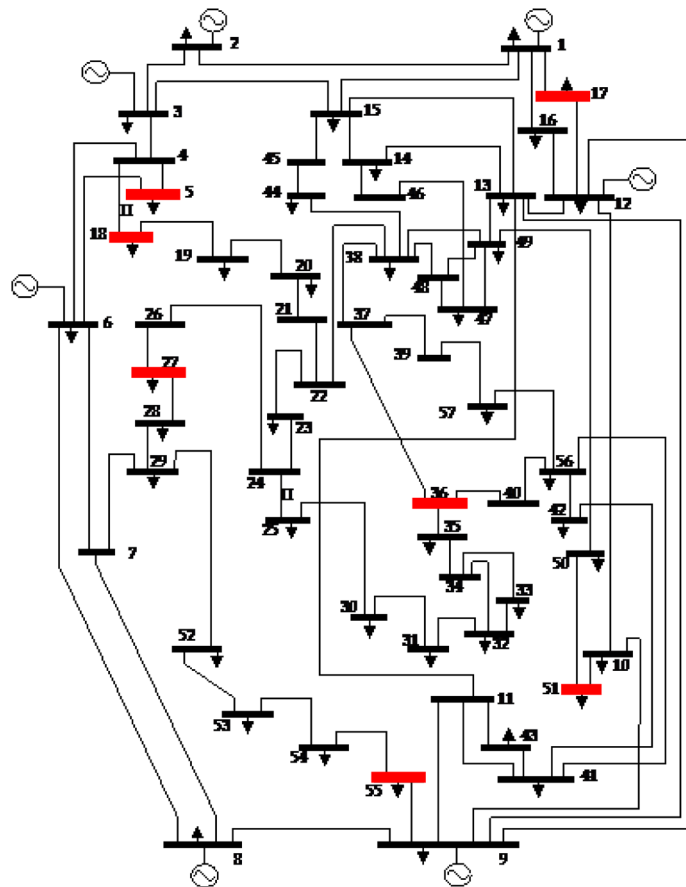


Figure 2.9. One line diagram of IEEE 57-bus system.

2.3.4.1 The effect of detailed modeling of generators

The introduced optimizations for $max.LF$ and $max.ERPR$ are tested on 6-bus system for different loading levels with and without considering the complementarity constraints. The results for the $max.LF$ and the $max.ERPR$ are presented in Figure 2.10 and Figure 2.11, respectively. One simulation considers all generators as PV generators (3pv) and another one considers G3 as PQ generator (2pv,1pq). The values of objective functions (LF or $ERPR$) are generally higher in the case of 3PV generators than the case with 2PV and 1PQ generators, because the number of voltage control generators is lower in the latter.

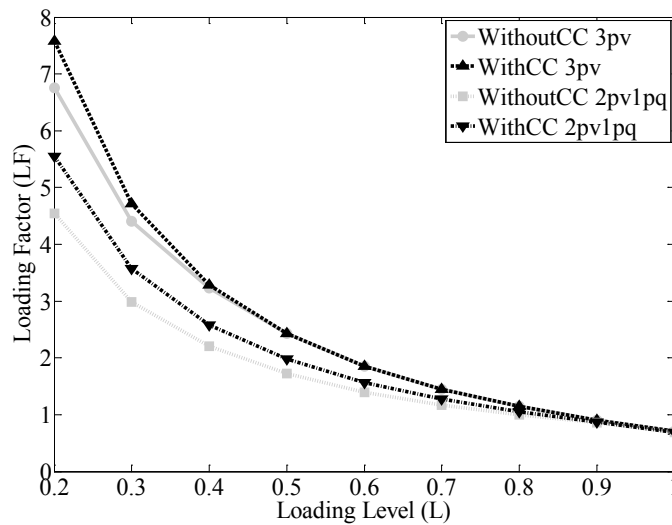


Figure 2.10. The results of maximization of the loading factor (LF) for different loading levels for 6-bus system.

* CC: Complementarity Constraints

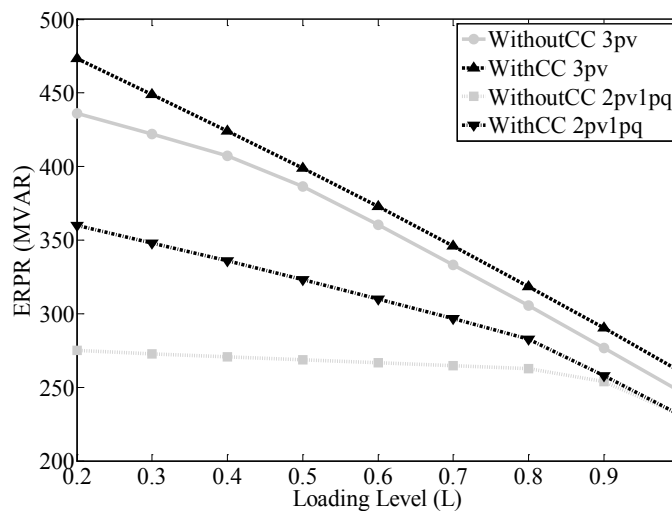


Figure 2.11. The results of maximization of the ERPR for different loading levels for 6-bus system.

As shown in Figure 2.10, thanks to the complementarity constraints the value of the objective function (LF) is always higher at lower loading levels. It is due to the fact that this modeling allows the generators to change their voltages in order to increase their reactive power output at the collapse point. For the higher loading levels, although the value of the objective function remains unchanged, this modeling allows to decrease the required reactive power generation at the current operating point, because the control variables at the operating point and collapse point can be different. For instance, for the loading level equal to 1 and with three PV generators, the value of objective function (LF) is 0.7147 for both cases with and without consideration of the complementarity constraints. In this case, the consideration of the complementarity constraints decreases the total reactive power output of generators at the current operating point from 182.28 MVAR to 176.63 MVAR. It clearly decreases the operating cost of the system.

The presented results in Figure 2.11 demonstrate that the effect of the complementarity constraints becomes more distinctive for $max.ERPR$ than $max.LF$. For instance, in the case of three PV generators, the ERPR with consideration of complementarity constraints is higher than in the case without their consideration for all loading levels. However, the effect of these constraints is more significant for lower loading levels. This is similar with the observations for $max.LF$ in Figure 2.10. Moreover, this observation is verified for 6-bus system with 2 PV and 1 PQ generators as shown in Figure 2.11. It is worth mentioning that in this case and for loading level equal to 1, the value of objective function without and with complementarity constraints are 231.42 MVAR and 231.55 MVAR, respectively. Although these two values are so close, the consideration of the complementarity constraints decreases the total generated reactive power at the operating point from 251.23 MVAR to 227.71 MVAR. It effectively decreases the operating cost of the system. For this case, the comparison between the results of $max.LF$ and $max.ERPR$ demonstrate that the total generated reactive power at the current operating point is lower in the case of $max.ERPR$ (227.71 MVAR) than in the case of $max.LF$ (231.56 MVAR). This conclusion is more discussed in section 2.3.4.3.

Similar studies are performed for the New England 39-bus and IEEE 57-bus systems. The New England 39-bus system is studied for two cases; first one with 10 PV generators and the second with 8 PV and 2 PQ generators ($\Omega_{G-PQ}=\{G_7, G_8\}$). The results of $max.LF$ are given in Figure 2.12 and Figure 2.13 and the results of $max.ERPR$ are presented in Figure 2.14 and Figure 2.15. Firstly, Figure 2.12 and Figure 2.13 demonstrate that the value of objective function decreases with the increase of the loading level for both systems. This phenomenon was shown in Figure 2.10 as well. Secondly, the value of objective function is slightly lower in the case with less number of PV generators (8pv2pq). Thirdly, Figure 2.13 demonstrates that the complementarity constraints effectively improve the value of the objective function in 57-bus system while they are not effective for 39-bus system (Figure 2.12). As a result, the consideration of the complementarity constraints for the $max.LF$ does not necessarily improve the optimization results. However, the results of $max.ERPR$ in Figure 2.14 and Figure 2.15 demonstrate that the complementarity constraints improve the optimization results for all loading levels for both systems. Indeed the complementarity constraints are more effective for $max.ERPR$ than for $max.LF$ since the generators switch between the different operating modes directly increases the value of the objective function. Moreover, the ERPR is higher for the 39-

bus system than for the 57-bus system due to the higher number of generators. Generally, it is observed that the complementarity constraints are more effective for lower loading levels.

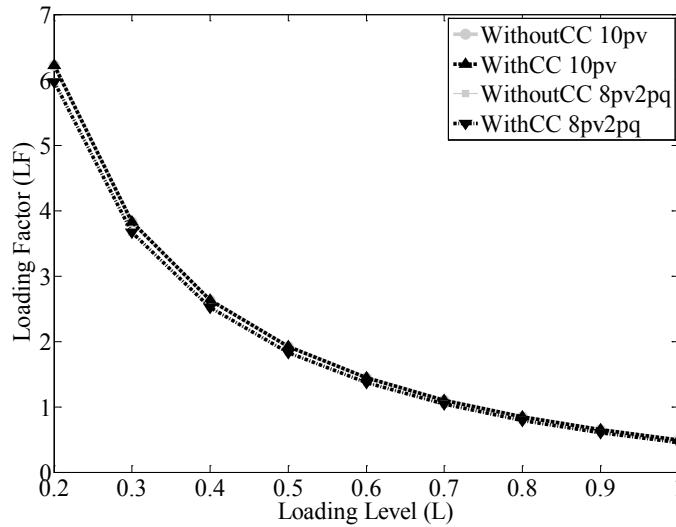


Figure 2.12. The results of maximization of the loading factor (LF) for different loading levels for 39-bus system.

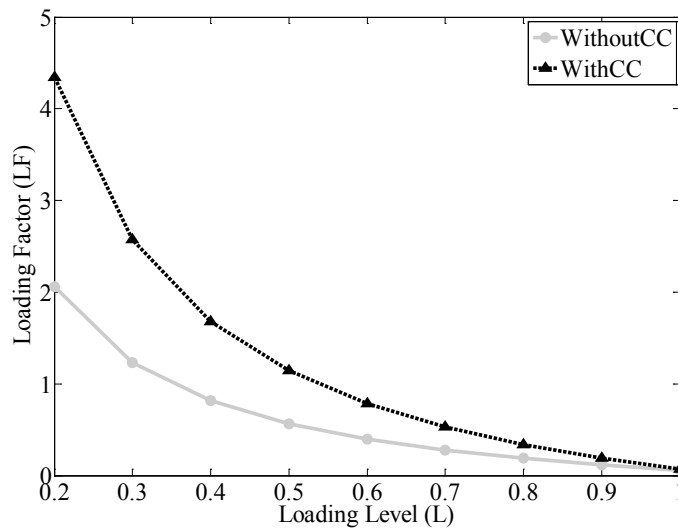


Figure 2.13. The results of maximization of the loading factor (LF) for different loading levels for 57-bus system.

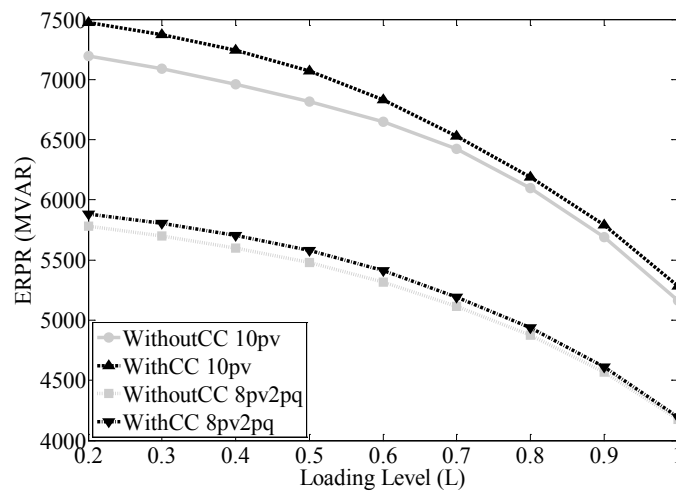


Figure 2.14. The results of maximization of the ERPR for different loading levels for 39-bus system.

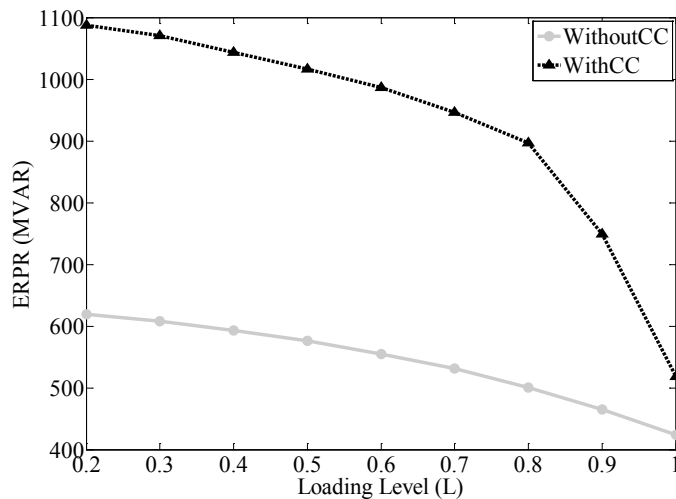


Figure 2.15. The results of maximization of the ERPR for different loading levels for 57-bus system.

2.3.4.2 The effect of distributed slack bus modeling

In this work the response of generators to the active power imbalances is taken into account with a distributed slack bus model as mentioned in section 2.3.2. In this respect, a vector of variables (P_L) represents the active power losses and every generator can take different portion of the losses. The simulation results for $max.LF$ and $max.ERPR$ are given in Table 2.6 and Table 2.7, respectively, with and without consideration of complementarity constraints. The comparison of the results of distributed slack bus with the results of single slack bus demonstrates that the distributed slack bus model slightly improves the objective function value regardless of the consideration of the complementarity constraints and also regardless of the loading level.

Table 2.6. The effect of distributed slack bus model on $max.LF$ for some loading levels (unit:-).

		6 bus		39 bus		57 bus	
		with CC	without CC	with CC	without CC	with CC	without CC
Single Slack Bus	$L=0.2$	7.4937	6.6000	6.1336	6.1336	4.3360	2.0530
	$L=0.6$	1.8312	1.8312	1.4093	1.4093	0.7860	0.3952
	$L=1.0$	0.6987	0.6987	0.4560	0.4560	0.0716	0.0566
Distributed Slack Bus	$L=0.2$	7.5736	6.7584	6.2196	6.2196	4.3397	2.0598
	$L=0.6$	1.8579	1.8579	1.4413	1.4413	0.7872	0.3997
	$L=1.0$	0.7147	0.7147	0.4874	0.4874	0.0723	0.0600

CC: Complementarity Constraint.

Table 2.7. The effect of distributed slack bus model on $max.ERPR$ for some loading levels (unit:MVAR).

		6 bus		39 bus		57 bus	
		with CC	without CC	with CC	without CC	with CC	without CC
Single Slack Bus	$L=0.2$	472.65	426.05	7470.62	7192.56	1083.23	603.04
	$L=0.6$	371.95	359.08	6798.76	6625.39	985.21	552.93
	$L=1.0$	259.71	245.48	5211.20	5077.76	514.01	419.73
Distributed Slack Bus	$L=0.2$	473.17	435.95	7471.66	7193.26	1086.92	619.43
	$L=0.6$	372.67	360.27	6833.08	6646.96	986.33	555.01
	$L=1.0$	261.20	247.28	5280.56	5153.57	518.68	423.87

2.3.4.3 The scheduling of voltage and reactive power resources based on PV and VQ curve methods

The scheduling of the voltage and reactive power resources considering the voltage stability can be performed based on the PV curve and/or VQ curve analyses. In this respect, two optimizations are proposed for: (i) $max.LF$ and (ii) $max.ERPR$. They are implemented according to equation (2-4). These two optimizations lead to different values for the control variables and consequently different stability margins.

The values of the control variables (here, the voltage of generators) for 6-bus, 39-bus and 57-bus systems are given in Table 2.8, Table 2.9 and Table 2.10, respectively. In the presented results all generators are assumed as PV generators and the loading level is equal to 1. These values are obtained for $max.LF$ and $max.ERPR$ with and without consideration of complementarity constraints. As it is mentioned earlier in section 2.3.2, the consideration of the complementarity constraints is effective in the obtained control variables for all loading levels. The sensitivities of these two objective functions to the different loading levels are already demonstrated in Figure 2.10 to Figure 2.15.

Table 2.8. The value of the control variables for 6-bus system with 3 PV generators for loading level equal to 1.

		control variables		
		V_{g1}	V_{g2}	V_{g3}
<i>max.LF</i>	withCC	1.0893	1.0608	1.0590
	withoutCC	1.0893	1.0282	1.0338
<i>max.ERPR</i>	withCC	1.1000	1.1000	1.1000
	withoutCC	1.0750	1.0104	1.0198

Table 2.9. The value of the control variables for 39-bus system for loading level equal to 1.

		control variables									
		V_{g1}	V_{g2}	V_{g3}	V_{g4}	V_{g5}	V_{g6}	V_{g7}	V_{g8}	V_{g9}	V_{g10}
<i>max.LF</i>	withCC	1.0998	1.1000	1.1000	1.1000	1.1000	1.1000	1.1000	1.0960	1.1000	1.0884
	withoutCC	1.0998	1.1000	1.1000	1.1000	1.1000	1.1000	1.1000	1.0960	1.1000	1.0884
<i>max.ERPR</i>	withCC	1.0932	1.1000	1.1000	1.1000	1.1000	1.1000	1.1000	1.1000	1.1000	1.0889
	withoutCC	1.0193	1.0699	1.1000	1.1000	1.1000	1.0479	1.1000	1.1000	1.1000	1.0785

Table 2.10. The value of the control variables for 57-bus system for loading level equal to 1.

		control variables						
		V_{g1}	V_{g2}	V_{g3}	V_{g4}	V_{g5}	V_{g6}	V_{g7}
<i>max.LF</i>	withCC	1.1000	1.0879	1.1000	1.1000	1.1000	1.0826	1.1000
	withoutCC	1.1000	1.0878	1.1000	1.0965	1.0924	1.0761	1.1000
<i>max.ERPR</i>	withCC	1.1000	1.1000	1.0967	1.0986	1.1000	1.0830	1.1000
	withoutCC	1.1000	1.0982	1.0889	1.0841	1.1000	1.0796	1.1000

It is worth mentioning that the total generated reactive power output of generators is generally lower in the case of *max.ERPR* than in the case of *max.LF*. It is due to the fact that *max.ERPR* inherently aims to decrease the reactive power output of generators at the operating point in order to increase these outputs at the collapse point. This is shown in Table 2.11 for the studied systems for loading level equal to 1. If we assume that the reactive power remuneration is according to the generators' reactive power output, the operating cost of the system for the voltage control becomes lower in the case of *max.ERPR* than in the case of *max.LF*.

Furthermore, the active power rescheduling can be taken into consideration as another preventive action, whenever the obtained stability margin is not sufficient. Here, this preventive control action is studied for both of *max.LF* and *max.ERPR*. It is implemented with additional control variables for every generator. A further equality constraint is added to ensure that the sum of these control variables is equal to zero. It guarantees the balance of the active power generation and demand at the operating and collapse points. These variables should be considered for both of the operating and collapse points. Table 2.12 demonstrates that the consideration of this control action increases the value of the objective function. This improvement is obtained with the cost of active power rescheduling. However, in the presented

results, the cost of active power rescheduling is not added to the objective function. In other words, the given results demonstrate the maximum attainable stability margin using the preventive actions. The required active power rescheduling, for the given objective function values in Table 2.12, are presented in Table 2.13 to Table 2.15.

Table 2.11. Total reactive power output of generators for studied systems in loading level equal to 1.

		6 bus	39 bus	57 bus
<i>max.LF</i>	withCC	176.63	1024.51	311.93
	withoutCC	182.28	1024.51	320.49
<i>max.ERPR</i>	withCC	171.17	1006.01	273.89
	withoutCC	185.07	1459.66	297.89

Table 2.12. The effect of active power rescheduling on the value of the objective functions for the studied systems for loading level equal to 1.

		6 bus	39 bus	57 bus
<i>max.LF</i>	with APR*	0.7246	0.5652	0.0817
	without APR	0.7147	0.4874	0.0723
<i>max.ERPR</i>	with APR	263.57	5617.94	572.94
	without APR	261.20	5280.56	518.68

* APR: Active Power Rescheduling

Table 2.13. The active power rescheduling to improve the VSMs for 6-bus system.

	ΔP (MW)		
	G_1	G_2	G_3
<i>max.LF</i>	-36.70	20.92	15.78
<i>max.ERPR</i>	-41.63	23.76	17.87

Table 2.14. The active power rescheduling to improve the VSMs for 39-bus system.

	ΔP (MW)									
	G_1	G_2	G_3	G_4	G_5	G_6	G_7	G_8	G_9	G_{10}
<i>max.LF</i>	38.00	-60.51	-71.67	-2.51	24.22	-79.88	105.77	102.14	-71.59	16.03
<i>max.ERPR</i>	65.81	-42.73	-66.96	-40.83	-57.15	-146.18	-75.77	-94.56	-61.32	519.68

Table 2.15. The active power rescheduling to improve the VSMs for 57-bus system.

	ΔP (MW)						
	G_1	G_2	G_3	G_4	G_5	G_6	G_7
<i>max.LF</i>	77.57	-99.93	-139.98	2.32	64.55	-64.47	159.93
<i>max.ERPR</i>	23.73	-90.18	-74.50	-54.59	141.55	-48.16	102.15

The effectiveness of the obtained control variables should be specified using the contingency analysis and the evaluation of the voltage stability margin of the post-contingency states.

2.3.4.4 The evaluation of the post-contingency stability margin

The post-contingency stability margin of the system is assessed using the proposed optimization in equation (2-5). This optimization problem can be solved for assessing VSM_P or VSM_Q . The obtained VSMs which take into account the operational constraints (e.g. voltage upper/lower limits) are not necessarily consistent with each other. In other words, the VSM_P globally quantifies the VSM of the system while the VSM_Q locally considers the VSM at every bus. For a given contingency scenario and under specified operational constraints, the system can be feasible according to the global indicator (VSM_P) while the system at some of the buses may be infeasible according to the local indicator (VSM_Q). Note that the infeasibility results from either voltage instability or voltage operational constraints violation. For instance, the stability margins of the 6-bus system for loading level equal to 1 with 2 PV and 1 PQ generators after the outage of line L5 are given in Table 2.16. The value of control variables are taken from both optimizations ($max.LF$ and $max.ERPR$) as indicated in Table 2.16 by ‘‘Optimization’’. In order to precisely understand the reason of infeasibility, the VSM_Q regardless of the constraints on the voltage of buses, given by VSM_Q^V , is calculated for each case.

Table 2.16. Evaluation of post-contingency VSMs and required corrective actions for 6-bus system with 2 PV and 1 PQ generators for loading level equal to 1.

Contingency	Optimization	Post-contingency VSMs		Required Corrective Actions	
		VSM_P	VSM_Q	ΔV_g (pu)	ΔQ_g (MVAR)
L5	$max.LF$	0.1296	$VSM_{Q4} = \text{Inf}^*$	$\Delta V_1 = -0.0090$	-
			$VSM_{Q4}^V = 63.94$		
			$VSM_{Q5} = 59.34$	$\Delta V_2 = 0.0074$	-
			$VSM_{Q5}^V = 151.60$		
			$VSM_{Q6} = 96.07$	-	$\Delta Q_3 = -0.0048$
	$VSM_{Q6}^V = 156.20$				
	$max.ERPR$	0.0564	$VSM_{Q4} = \text{Inf}^*$	$\Delta V_1 = -0.0053$	-
			$VSM_{Q4}^V = 61.63$		
			$VSM_{Q5} = 34.92$	$\Delta V_2 = 0.0065$	-
			$VSM_{Q5}^V = 153.20$		
$VSM_{Q6} = 76.62$			-	$\Delta Q_3 = -0.0040$	
$VSM_{Q6}^V = 158.10$					

* Inf: Infeasible

The $VSM_P > 0$ demonstrates that the system is voltage stable after the contingency according to the PV curve. Moreover, the positive values of VSM_Q in bus 5 and bus 6 demonstrate that these two buses are voltage stable according to the VQ curve. However, the infeasibility of optimization of VSM_Q demonstrates that an operationally acceptable solution does not exist for the voltage at bus 4. In this case $VSM_{Q4}^V > 0$ demonstrates that the infeasibility is due to the operational constraints on the voltage of buses. As a result, the system is feasible regarding VSM_P while it is infeasible according to VSM_Q . Actually, it is possible that VSM_P cannot indicate the infeasibility of the post-contingency state, whereas the VSM_Q can since it particularly calculates the stability margin of the post-contingency state for each bus. As a result, it effectively demonstrates possible infeasibility as well as the corresponding bus(es). Therefore, a positive VSM_P could be considered as insufficient condition to guarantee the voltage stability and feasibility throughout the system. On the other hand, whenever the VSM_Q 's are positive for all the buses we may intuitively conclude that VSM_P is certainly positive. At least this is the case for all of the performed simulations in this thesis. Therefore, $VSM_Q > 0$ for all buses can be a sufficient condition that guarantees the existence of voltage feasible solution.

In addition, the system may require a sort of corrective action after the occurrence of the contingency in order to ensure the feasibility. In this example, the required corrective actions are in terms of voltage and reactive power rescheduling as indicated in Table 2.16. They are obtained using optimization (2-6).

As a result, the VSM_Q provides more accurate information about the stability and feasibility of the post-contingency state. Its disadvantage for obtaining the post-contingency stability margin under specified constraints is that the optimization (2-5) should be solved for each load bus individually. This drawback can be further mitigated by evaluating only the stability margin of certain voltage sensitive buses instead of all buses. These buses are assumed to be representative of the voltage stability of the system. However, the VSM_P can be obtained with only one optimization problem.

2.4 Voltage and Reactive Power Scheduling for MAPS

This section focuses on the multi-area voltage and reactive power management. Different aspects of the mathematical formulation of the optimization problem for interconnected power system, including objective function, constraints and appropriate modeling of neighboring areas, are revisited in depth. Various implementations of solution approaches, including centralized and decentralized implementations, as well as coordinated and non-coordinated solution approaches in the context of collaborative and non-collaborative environments are proposed and illustrated. In this respect, new contributions are proposed by using the distributed slack bus model and the limitation on the voltage and reactive power in the interconnection links. The comparative analyses between the available and proposed methods are discussed in terms of sub-optimality and time to convergence.

2.4.1 Preliminaries

The review of the current practices in section 2.2 has demonstrated the importance of the inter-area voltage coordination, although the voltage control has been considered primarily as a local service. The MAPS without inter-area voltage coordination may be operated in a non-optimum state which means less security margin. For instance, reference [59] demonstrates that in MAPS, the optimization solution of a TSO for reducing the active power losses in its own region might lead to increase the losses globally in the interconnected area. Moreover, automatic and non-coordinated voltage control may lead to unacceptable reactive power flow or voltage level in the controlled area or even in its neighbors. Hence, a wide coordinated control within control areas will bring additional value by proposing a global optimum solution. For this purpose, different TSOs must develop coordinated voltage control schemes inside their own area, and between control areas, to prevent voltage control concerns. However, up to now, each TSO only developed a specific voltage and reactive power regulation for its own area. Therefore, the issue of multi-area voltage and reactive power regulation (MAVR) could be considered between neighboring areas in interconnected power systems. Here, the investigations are performed on the optimization of the voltage and reactive power controllers in the operational planning stage. The obtained conclusions could be useful for the other design stages as well.

This section firstly focuses on the proposed methodologies in literatures for the inter-area voltage and reactive power management. Then, the optimization methods are classified based on several criteria, like coordinated/non-coordinated solution approaches in the context of collaborative/non-collaborative behavior of TSOs and different coordination approaches including centralized/decentralized. A unified mathematical formulation is proposed for various optimization approaches. The distributed slack bus model and the reactive power limits in the interconnection links are proposed as original contributions in this work to improve the optimization methods. Section 2.4.3 presents in depth the advantages and drawbacks of the different optimization approaches for the voltage and reactive power management in the MAPS. The case studies and discussions on practical use/implementation of results are provided in section 2.4.4.

2.4.2 Multi-Area Voltage and Reactive Power Optimization

The coordinated voltage and reactive power control in MAPS has been recently investigated in the literatures [37], [60], [61], [62], [63], [45], [64]. A new layer of hierarchical control to coordinate long-term control actions over several control areas in normal operating conditions is proposed in [38]. The corresponding time horizon for the proposed MAVR is shown in Figure 2.16, in comparison with the different levels of hierarchical voltage regulation (PVR, SVR, and TVR). The absence of the MAVR and non-coordinated operation of the system would result into the responses of PVR and SVR that reduces reactive power reserve and consequently security margin.

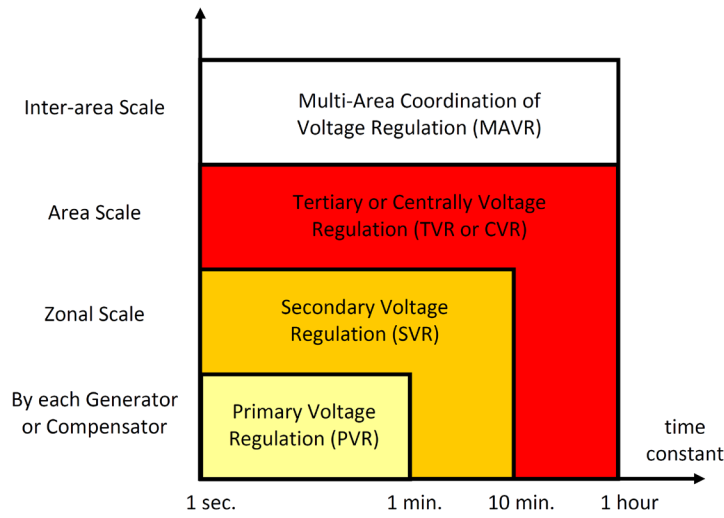


Figure 2.16. Structure and time constant of the multi-area voltage regulation in comparison with different level of voltage regulation [38].

The various MAVR approaches are classified based on the coordination and collaboration between TSOs, as shown in Figure 2.17. Two main trends are developed for the MAVR coordination, namely centralized and decentralized manners. These two optimization approaches and the corresponding formulations are explained more in depth in the following sub-sections. Note that these approaches could be implemented according to a collaborative or non-collaborative behavior of TSOs. More details on the advantages and disadvantages of these approaches are presented in section 2.4.3.

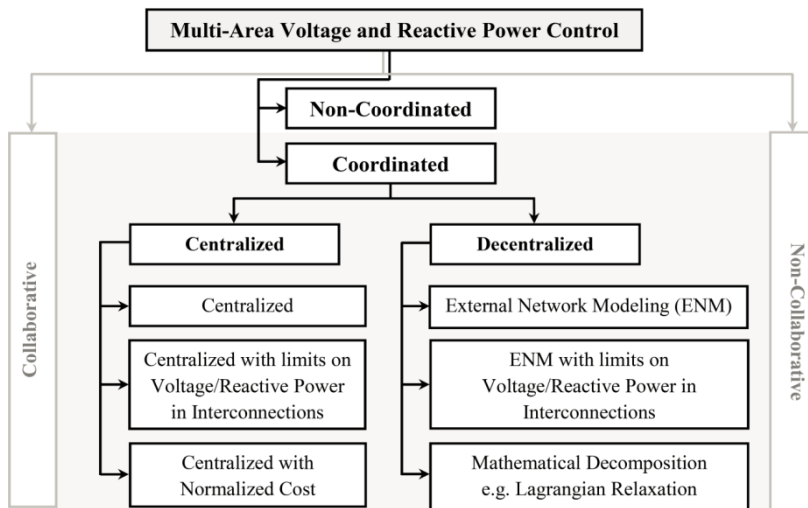


Figure 2.17. Classification of the MAVR based on different coordination approaches and collaborative/non-collaborative behavior of TSOs.

In this respect the problem of interest, which is a general Optimal Power Flow (OPF) of a TSO (a single area), is formulated as follows:

$$\min_u C(x, u) \quad (2-10.a)$$

subject to

$$g(x, u) \leq 0 \quad (2-10.b)$$

$$h(x, u) = 0 \quad (2-10.c)$$

where $C(x, u)$ is the objective function. u and x indicate the vector of control variables and the vector of the state variables, respectively. The inequality constraints such as transmission line flow limits and generators capability limitations as well as node voltage limits are given by $g(x, u)$. The equality constraints, given by $h(x, u)$, correspond to the power flow equations.

The system operator usually has to manage its reactive power resources for a specified active power dispatch (P_G) obtained from the active power market. Therefore, in this optimization the control variables are the voltage of PV nodes and the reactive power of PQ nodes where control devices are connected to. These elements could be generators, transformers tap changer, synchronous condenser, capacitor banks, static VAR compensators and FACTS devices.

Each TSO has provided a particular formulation for its objective function $C(x, u)$ according to its network structure and specific requirements. Usually, a multi-objective function represents the objective function of one area. For instance, a general $C(x, u)$ can be written in the following form.

$$OF = \omega_1 \cdot \sum_{g \in \Omega_G} Q_{Gg}^2 + \omega_2 \cdot \sum_{g \in \Omega_G} P_{Lg} + \omega_3 \cdot \sum_{i \in \Omega_B} (V_i - V_i^{spc})^2 \quad (2-11)$$

where $\sum(Q_{Gg})^2$ is the quadratic sum of reactive power injection (QSQ)¹, $\sum P_{Lg}$ is the total active power losses, and $\sum(V_i - V_i^{spc})^2$ is the voltage deviation from a specified value or the voltage profile. Here, all voltage reference values (V_i^{spc}) are set to 1 p.u. ω_i are the weight coefficients of the corresponding objectives. Other control objectives like effective reactive power reserve [27] and voltage stability criteria [52] could also be considered.

The objective function is subjected to the inequality and equality constraints given by (2-4.b) – (2-4.c). The active and reactive power balance equality constraints are given by (2-7.b) and (2-7.c), respectively. The transmission lines capacity limits are considered with (2-7.d). The generators participation in the active power losses is limited by (2-7.e). The limits of the voltage magnitudes for each bus are given by (2-7.h). The maximum reactive power support of a

¹ Quadratic objective is quite effective since there are well-known quadratic optimization methods. Also, there is similarity between the quadratic objective and the reactive power cost function. Besides, all generators that participate in the voltage and reactive power control could be remunerated according to their participation, whether reactive power generation (injection) or consumption (absorption).

generator is considered using the limitation of the field current and the limitation of the armature current according to (2-1).

It must be mentioned when a single central control satisfies a certain objective function for the interconnected system, the result would be the system wide optimal solution. However, in the multi-TSO system, where there are several entities, specifying a certain optimization for the whole system is challenging. Different aspects of the centralized optimization of MAPS are investigated in the following sub-section.

2.4.2.1 Centralized Optimization

A centralized control scheme addresses the multiple areas as one contiguous area with multiple parties. Thus, an optimization problem over all areas is solved by a single central controller [60]. In this respect, it is assumed that each TSO_k has its own objective function $C_k(x, u)$ and constraints $g_k(x, u)$ and $h_k(x, u)$. The objective of each TSO can be selected with different combinations of the multi-objective function in (2-11). Note that the TOSs can provide their objectives and constraints information to the control center either in a collaborative or non-collaborative manner. The multi-objective optimization for $NTSO$ number of TSOs could be represented by (2-12) subject to the constraints in (2-10.b) and (2-10.c) [61].

$$\min_u [C_1(x, u), \dots, C_k(x, u), \dots, C_{NTSO}(x, u)] \quad (2-12)$$

Generally, the objective function of the centralized optimization is presented as the sum of all TSOs cost functions $\sum_{k \in NTSO} C_k(x, u)$. This optimization defines the system wide optimal solution. The main concern of the centralized optimization is the effort of the TSOs to fulfill the individual and possibly conflicting objectives. Thus, the objective of a single TSO may adversely affect other TSOs [62]. For this issue, a compromise method is proposed in [61] to obtain the Pareto-front solution. In this method that is called centralized with Normalized Cost (NC), each TSO solves an initial optimization to minimize its own cost function while respecting all constraints in the system. For the k -th TSO, the obtained initial solution is given by u_k^* . Then, another optimization minimizes the distance of final solution from the obtained initial solutions in a normalized multi-dimensional space, as shown in (2-13).

$$\min_u \sum_{k \in NTSO} (\bar{C}_k(u) - \bar{C}_k(u_k^*))^2 \quad (2-13)$$

where $\bar{C}_k(u)$ is the normalized cost function of area k , given by (2-14).

$$\bar{C}_k(u) = \frac{C_k(u)}{C_k^0 \times \chi_k} \quad (2-14)$$

In this formulation C_k^0 and χ_k are given by (2-15) and (2-16), respectively. C_k^0 is the average of the overcost supported by TSO_k for the other NTSO areas. χ_k penalizes the detrimental impact of TSO_k on the other TSOs.

$$C_k^0 = \sum_{j \in NTSO} \frac{C_k(u_j^*) - C_k(u_k^*)}{NTSO} \quad (2-15)$$

$$\chi_k = \sum_{j \in NTSO} \frac{C_j(u_k^*) - C_j(u_j^*)}{C_j^0} \quad (2-16)$$

The objectives are normalized to ensure that the solution of the problem has some properties of fairness. The fairness of the solution is studied in the economic sense by some criteria, namely efficiency, accountability and altruism. The proposed scheme is quite effective in collaborative strategy of TSOs. Moreover, it is shown that this scheme is not robust (see 2.4.4.3) to biased information of TSOs. Whenever they provide wrong information about their objectives and constraints, they may affect the allocation of resources in certain circumstances [61].

Although the centralized and the centralized with NC optimization procedures could define the system wide optimal and fair solutions, respectively, they suffer from several drawbacks. The first disadvantage is that the centralized solutions are susceptible to single point failure (centralized control center). Another difficulty to implement a centralized control in MAPS is due to the TSOs intention to not reveal their operational information to the other TSOs. Moreover, implementation of a wide area control scheme would be technically more expensive and requires more communication. Furthermore, some issues, like the fairness of the solution, provoke challenges when the TSOs have different objectives and constraints, specifically in the case of a non-collaborative environment. In addition to the aforementioned difficulties and limitations, a major reason to implement a decentralized control in MAPS comes from the facile adaptation to the current structurally decentralized control situation of the system in Europe.

2.4.2.2 Decentralized Optimization

In the decentralized optimization scheme, the overall optimization in the interconnected system is divided into sub-problems according to the area's topological and control limits. Each TSO maintains its prerogatives and optimizes its own control area according to a specific procedure [64]. In such cases, coordination is needed because the chosen setting of one area possibly impacts the entire system as well as the choice of the setting of the other areas [65].

The non-coordinated reactive power scheduling in MAPS, when each TSO only solves its own optimization, increases the cost of the interconnected system as well as the cost of each area, specifically when neighboring TSOs apply conflicting objectives [66]. Even if the neighboring TSOs satisfy a same objective separately by their own, not only a communication would be necessary between the areas, but also the obtained results would be sub-optimal in comparison with the centralized one [44]. The coordination could be achieved by exchanging some information between neighboring areas.

In order to investigate the appropriate coordination in the MAPS, the decentralized optimization can be formulated as follow. Generally, every TSO_k confronts the following optimization.

$$\min_{u_k} C_k(x_k, u_k, \bar{z}_k) \quad (2-17.a)$$

subject to

$$g_k(x_k, u_k) \leq 0 \quad (2.17.b)$$

$$h_k(x_k, u_k) = 0 \quad (2.17.c)$$

$$g_{k-\zeta}(x_k, u_k, \tilde{z}_k) \leq 0 \quad (2.17.d)$$

$$h_{k-\zeta}(x_k, u_k, \tilde{z}_k) = 0 \quad (2.17.e)$$

where (2-17.b) – (2-17.c) are its own inequality and equality constraints. (2-17.d) and (2-17.e) depend on the decision variables of the problems related to the other areas and they are so-called coupling equality and inequality constraints, respectively. For each area, the number of coupling constraints depends on the set of interconnections ($\Omega_{k-\zeta}$). \tilde{z}_k represents the complicating variables which belongs to both TSO_k and $TSO_{k'}$ ($k' \neq k$). The number of these border variables depends on the number of the buses that the interconnections are connected to. These optimizations cannot be solved separately for each area k , because \tilde{z}_k is involved in the objective function (2-17.a) and/or in the coupling constraints (2-17.d) – (2-17.e) of more than one TSO. In other words, these variables and the subsequent constraints bring the need for coordination and communication.

Note that decentralized optimizations are iterative in nature. Additional subscript t specifies the objectives and variables in t^{th} iteration. For instance $C_{k,t}$ refers to the objective function of TSO_k at iteration t . Here, this subscript is not shown in the formulation, except when it is needed, to avoid the complex formulation.

In general, there is no coordination between control areas. The lack of coordination can be eliminated by implementing different decomposition approaches [67]. Literatures [60], [63], [45], [65], [67] propose various decomposition approaches for the voltage and reactive power management in the MAPS. These approaches are divided into External Network Modeling (ENM) and mathematical decomposition methods.

2.4.2.2.1 External network modeling

Phulpin et al. [45] suppose that each TSO assumes an external network equivalent for its neighboring areas and solves its own optimization defined by (2-18.a) regarding its own constraints given by (2-17.b) – (2-17.c) and regardless to the neighboring systems' objectives. The external network equivalents are considered as equality constraints given by (2-18.b), where \tilde{z}_k^* denotes the parameters of the external network equivalent. The superscript * indicates the variables which are calculated in previous iteration and are kept constant in this iteration. Note that it is supposed that every TSO fairly uses the same type of equivalent to compute the neighboring area's model at the interconnections.

$$\min_{u_k} C_k(x_k, u_k) \quad (2-18.a)$$

$$h_{k-\zeta}(x_k, u_k, \tilde{z}_k^*) = 0 \quad (2-18.b)$$

Then, it is assumed that all TSOs apply the solution to their own systems as a part of the interconnected system and each TSO measures variables to set up the external network equivalents. Although the proposed scheme doesn't need any information exchange between

TSOs, each TSO should communicate with a central control center which performs a power flow to determine the overall system state. It is possible that this power flow doesn't converge.

Similarly, a coordinated decomposition can be proposed for a specific time interval. For this, a center like TSC – TSO Security Cooperation –in Europe [3] could receive the calculated control actions of each TSO and perform a load flow to evaluate the state of the interconnected system. Then, the load flow results are sent back to each area. The load flow results in the interconnections could be considered as common knowledge of all TSOs. The TSOs improve their external network equivalents corresponding to the tie-line flows. Note that this load flow should be performed by distributed slack bus model according to the active power loss participation factors, obtained from the OPF of each area. The algorithm is repeated until convergence is reached $|C_{k,t} - C_{k,t-1}| \leq \varepsilon$. In this approach, each TSO applies a parameter fitting method on the load flow results in the interconnection to obtain the external network equivalents as follows [45]:

$$\min_{z_k} \sum_{t=1}^T \beta^{T-t} \times \|z_k - z_{k,t}^*\|^2 \quad (2-19)$$

In (2-19) $\beta \in [0,1]$ is a memory factor and $z_{k,t}^*$ is the parameter of the external network equivalent in t^{th} iteration. Here, β is considered to be equal to 0.75. The simulation results for $\beta=0$ swing as shown in [60]. Various external network models are studied in [63] and [45] including PQ-equivalent, PV-equivalent, Thevenin-equivalent and more advanced models like REI equivalent and non-reduced power system equivalent. It is shown that PQ-equivalent could achieve better performance in terms of convergence and sub-optimality. It should be mentioned that in the first iteration, the interconnections are modeled by a fixed active power, obtained from a DC load flow. It can be deliberated as an agreed active power flow in the interconnections between neighboring TSOs.

2.4.2.2.2 Mathematical decomposition method

Mathematical decomposition of optimizations is widely proposed in literature [60], [65], [67], [68], [69], based on Lagrangian, augmented Lagrangian, approximate Newton directions and primal dual interior point methods. The decomposed sub-problems are then solved in an iterative way, independently but in coordinated way. Two coordination approaches based on Lagrangian methods at the existing or fictitious border buses [60] are: (i) the coordination via an adjustment at the interfaces (borders) to the neighboring areas, and (ii) the coordination by exchange of variables which belong to neighboring areas. In these approaches the neighboring areas exchange the value of the border variables and the Lagrangian multipliers related to the complicating variables and the coupling constraints.

a) Decomposition based on adjustment at the border

In the first approach, each area independently solves a modified optimization that includes its own variables and the border variables (\tilde{z}_k) shared with the other areas. The coordination is attained via a coupling constraint, forcing the border variables to be equal [67]. By considering these coupling constraints into the objectives, the following optimization is reached subject to (2-17.b) – (2-17.c).

$$\min_{u_k} C_k(x_k, u_k, \tilde{z}_k) + \sum_{k' \neq k} \lambda_{k'}^* (\tilde{z}_k - \tilde{z}_{k'}^*) \quad (2-20)$$

In this formulation $\lambda_{k'}^*$ is the vectors of the Lagrangian multipliers corresponding to the border variable ($\tilde{z}_{k'}^*$) determined by the sub-problems of the neighboring areas ($k' \neq k$).

In fact in this approach, all TSOs with shared borders calculate the corresponding complicating border variables (\tilde{z}_k). Then, TSOs use the observations from borders to model the influence of other areas on their own areas.

b) Decomposition based on passing adjacent variables

In the second approach, the coordination is attained through exchanging some dedicated variables between neighboring areas. The sub-problem of TSO_k is obtained by accounting for the coupling constraints of the foreign areas ($h_{k'-\zeta}$ and $g_{k'-\zeta}$) and adding them to the objective function while maintaining its own coupling constraints [65], [67], [68]. Therefore, TSO_k solves the following optimization.

$$\min_{u_k} C_k(x_k, u_k, \tilde{z}_k, \tilde{z}_{k'}^*) + \sum_{\Omega_{k'-\zeta}} \lambda_{k'-\zeta}^* h_{k'-\zeta}(x_k, u_k, \tilde{z}_k, \tilde{z}_{k'}^*) + \sum_{\Omega_{k'-\zeta}} \mu_{k'-\zeta}^* g_{k'-\zeta}(x_k, u_k, \tilde{z}_k, \tilde{z}_{k'}^*) \quad (2-21.a)$$

subject to (2-17.b) – (2-17.c) as well as the following constraints.

$$g_{k-\zeta}(x_k, u_k, \tilde{z}_k) \leq 0 \quad : \quad \mu_{k-\zeta} \quad (2-21.b)$$

$$h_{k-\zeta}(x_k, u_k, \tilde{z}_k) = 0 \quad : \quad \lambda_{k-\zeta} \quad (2-21.c)$$

In this formulation, the second and the third part of (2-21.a) demonstrate the coupling constraints of the other sub-problems ($k' \neq k$) as relaxed constraints in the objective function. (2-21.b) – (2-21.c) give the coupling constraints of the sub-problem k as hard constraints. $\lambda_{k-\zeta}$ and $\mu_{k-\zeta}$ are the Lagrangian multipliers obtained from the solution of the sub-problems k . They could be interpreted as the cost of providing power from the neighboring areas.

The coupling constraints could be the power balance equations at the existing border buses. In [68] and [70] these coupling constraints are the interconnections active and reactive power flow equations ($h_{k-\zeta}$) but not their power flow limits ($g_{k-\zeta}$). The active and reactive power flows from bus i to bus j at the interconnection ζ are calculated using (2-22.a) and (2-22.b), respectively.

$$P_{ij-\zeta} = V_i^2 G_{ij} - V_i V_j G_{ij} \cos \theta_{ij} - V_i V_j B_{ij} \sin \theta_{ij} \quad (2-22.a)$$

$$Q_{ij-\zeta} = -V_i^2 (B_{ij} - (B_{sh}/2)) + V_i V_j B_{ij} \cos \theta_{ij} - V_i V_j G_{ij} \sin \theta_{ij} \quad (2-22.b)$$

where B_{sh} is the tie-line shunt susceptance. It must be noted that if several tie-lines are connected to a bus, $P_{ij-\zeta}$ and $Q_{ij-\zeta}$ are the sum of all tie-lines power flows connected to that bus.

The interconnections power flow tolerances calculated on both sides are used as convergence criteria. Here, no specific treatment is needed to define the reference bus, since a distributed slack bus is utilized for the active power losses. Besides, the initial values of parameters in the first iteration are equal to zero except the voltages which are equal to one.

2.4.2.2.3 *Implementation and evaluation of the decentralized optimization*

Every decomposition approach can be implemented in a sequential way or in a synchronized way [60]. In the synchronized way, also referred to as the parallel way, every TSO solves its own optimization simultaneously and then exchanges the variables. In the sequential way, TSOs solve their optimizations in turn by updating the variables of the neighboring areas obtained from their previous solutions. The sequential approach has the disadvantage of being slower than the parallel one. On the other hand, the synchronized approach may not keep the system inside its feasible operating region at every moment since each TSO ignores the other TSOs control actions. This infeasibility could be due to the non-convergence of the TSO's OPF or load flow (in the case of ENM). In these cases, additional coordination should be designated to bring the solution back inside the feasible region [71]. For instance, reference [68] introduces the fictitious reactive power sources in order to obtain feasibility of nodal reactive power balance. These fictitious sources are added in the buses with reactive loads and the sum of square of them is added in the objective function with a high cost (reactive load shedding). This method could be used for both decentralized approaches with ENM and Lagrangian Relaxation (LR).

The result of the decentralized optimization can be evaluated based on the distance to the solution of the centralized optimization [38], [64]. This is usually referred to as sub-optimality or additional cost of the decentralized operation. Besides, the results of the decentralized optimization scheme can be evaluated using the required number of iterations for converging to a solution. This can be literally considered as the required communication between areas.

One of the main specifications of the decentralized approach in comparison to the centralized approach is that it deals with smaller problems in an iterative manner. Here, the complexity of the simulation time, results from the interaction between the number of iterations and the size of the problem. The simulation results in [68] particularly demonstrate that the decentralized approach is more time consuming when the power system size increases, while in the small test systems it is the contrary.

2.4.3 Various Approaches for Collaborative Optimization of Voltage and Reactive Power in MAPS

The difficulties for the voltage and reactive power control in MAPS are discussed in section 2.4.1. Then, general formulations for the voltage and reactive power control in SAPS and MAPS are presented in section 2.4.2. This section classifies various approaches that could be proposed for the collaborative coordination of the voltage and reactive power control in MAPS. Advantages and disadvantages of these approaches are investigated more in depth.

It is worth remembering the assumptions taken into consideration here:

- The optimization variables are voltage/reactive power of generators, voltage magnitudes and voltage phase angles of buses, and active power losses provided by generators.

- Distributed slack bus models the generators responses to the active power losses. This modeling improves the optimization results in comparison with single slack bus, specifically in high loading levels.
- The generators active power output is composed of a fixed and a variable term. The former is known through active power market and the latter changes by a distribution of losses among the generators.
- The TSOs work in a collaborative frame work and they do not provide biased information. The effect of non-collaborative strategies including biased formulation of the constraints and objectives on various approaches will be studied in section 2.4.4.
- AC power flow is calculated using distributed slack bus with a given participation factor obtained from the result of OPF in each area.
- The variables at the other side of the interconnection are assumed as the border variables.
- In this way, the interconnections belong to both areas. Thus, it is not needed to define a dummy bus in the middle of each tie-line to identify the border variables.
- For decentralized optimization approaches, TSOs solve their own optimizations in a synchronized way. That means at each iteration, all areas perform their own optimization concurrently and then the exchange information between areas are updated.

The different approaches implemented in this thesis are explained below:

- a) Non-Coordinated:** Each TSO solves its own sub-problem and implements the solution without further coordination. A power flow determines the state of the system for the obtained control actions. The main features of the non-coordinated operation are higher amounts of sub-optimality and possible infeasibility in the sub-problems or the load flow due to conflictual decisions.

All of the next approaches are coordinated.

- b) Centralized:** All TSOs send their objectives and constraints to a center. This center combines information and solves an optimization for the entire system. The obtained solution is considered as the Utopian optimum or the system wide optimal solution. This solution is not necessarily fair for all TSOs.
- c) Centralized - Normalized Cost (NC):** This approach solves (NTSO + 1) optimization problems to obtain control actions using the formulation presented by (2-12) – (2-16). Note that there is a distance between the solution of the Centralized and the Centralized NC that is the additional cost to obtain a fair solution. This additional cost in the long term can lead TSOs to improve the voltage control in their own areas.
- d) Decentralized - External Network Modeling (ENM):** Every TSO solves its own problem with a PQ model for each interconnection. The obtained control actions are sent to a center and a power flow calculates the whole system state. The results at the interconnections are sent back to areas to update the model of neighboring systems using (2-19), iteratively. In general the solution suffers from sub-optimality.
- e) Decentralized – Lagrangian Relaxation (LR):** Every TSO solves its own problem by exchanging the border variables including the voltages magnitudes and phase angles as

well as Lagrangian multipliers for the active and reactive power flow equality constraints on tie-lines. In comparison with Decentralized ENM, Decentralized LR has negligible sub-optimality and it doesn't need the AC power flow to determine the system state, but more information exchange and iterations are required.

One can propose to limit the reactive power flows on interconnections to further localize the reactive power provision within each area in order to increase the transfer capability of the interconnections. However, in this case the inter-area reactive power support of neighboring areas will become more limited. In this respect, the objective function changes as follows:

$$OF + \omega_4 \cdot \sum_{\Omega_{k-\zeta}} (Q_{ij-\zeta}^2 + Q_{ji-\zeta}^2) + \omega_5 \cdot \sum_{\Omega_{k-\zeta}} (V_{i-\zeta} - V_{j-\zeta})^2 \quad (2-23)$$

where the first term shown by OF is the main objective function given in (2-11). The second term is the sum of the square of the reactive power flows at both ends of the interconnections. The last term is the square of the voltage differences between the interconnection ends. ω_i are weighting coefficients that should be selected in such a way to compensate the effect of different objective functions, and to minimize the total cost of the system. One may propose to add the reactive flow in the middle of interconnection to the objective function in order to minimize the transferred reactive power. However, in this case the results would be dependent on the interconnection model (π -model and T -model).

Reformulating the objective function in the form given by (2-23) could bring advantages for the Centralized and Decentralized ENM approaches. Thus, the following two approaches are investigated in addition.

- f) Centralized with additional limits on voltage/reactive power in the interconnections (Centralized LI):** In the centralized approach, additional limits on voltage/reactive power in the interconnections reduce the effect of different (and even conflicting) objectives of neighboring TSOs on the others. In other words it can improve fairness of the centralized optimization. In a non-collaborative environment it decreases the impact of conflicting decisions of the neighboring TSOs. However, the total cost becomes higher than in the case of the centralized approach. This additional cost is paid to oblige TSOs to provide their requested reactive power within their own area. This cost could be shared among TSOs.

For the centralized optimization, the limits on the reactive power in the interconnections and the limits on the voltage in the interconnections have similar effects on the optimization results. However, the first is more effective than the latter ($\omega_4 \neq 0, \omega_5 = 0$). Here, the term effective means less reactive power flow in the interconnections while the objective functions maintain the same objective value by adjusting the weights in (2-23). The reason is that, the transmitted reactive power between areas is directly minimized in the objective function.

- g) Decentralized ENM with additional limits on voltage/reactive power in the interconnections (Decentralized ENM LI):** Additional limits on voltage/reactive power in the interconnections in the decentralized ENM decrease the sub-optimality and

the required communication. Furthermore, if the controller fails in one area the effects are more limited.

For Decentralized ENM, the limits on the voltage in the interconnections result in lower total cost than in the case of the limits on reactive power ($\omega_4 = 0, \omega_5 \neq 0$).

It is worth mentioning that for the approaches which require power flow to determine the system state (Non-Coordinated and Decentralized ENM); the obtained voltage magnitudes may not satisfy their limits. It occurs more frequently in the first iterations as shown in [45].

These optimization approaches for MAVR are studied for the case study in the next section. The specifications, advantages and disadvantages of these approaches are discussed based on illustrative example as well as the results and conclusions in the literatures.

2.4.4 Case Studies and Discussions on Practical Use/Implementation of Results

The aforementioned approaches are evaluated on New England 39-bus system. The one line diagram of the system is represented in Figure 2.18 and its description and data can be found in [27]. The voltage deviation of all buses is acceptable within $\pm 6\%$ of the nominal voltage. This system is partitioned into three areas, namely area A, B and C. The areas are selected such that at least one border bus (bus 4 and 14) is connected to more than one interconnection line and one border bus (bus 39) is connected to a generator. This particular system allows verifying the presented general formulation when there are different number of complicating variables and coupling constraints.

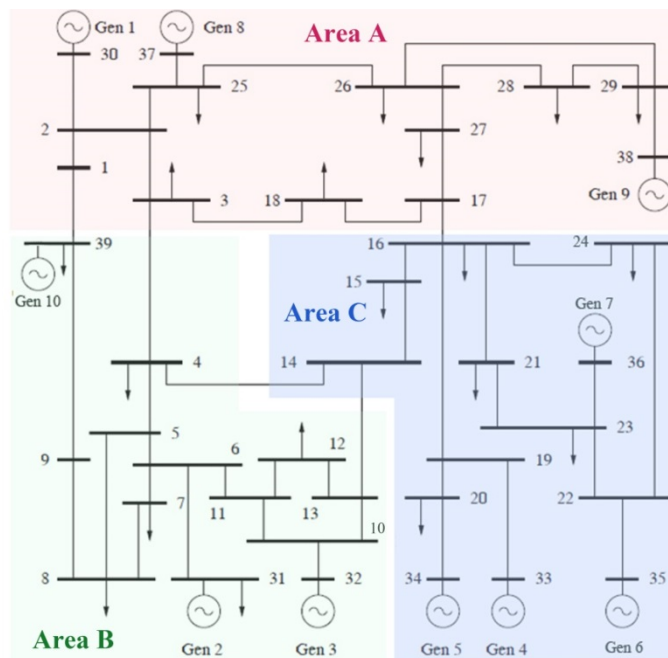


Figure 2.18. One line diagram of New England 39-bus system with 3 areas.

It is well-known that the reactive power generation effectively depends on the loading level in the system. In order to obtain more general conclusions, simulations are performed for two loading patterns with different quantities of loads namely high (7011.66 MW + 1620.22 MVAR) and low (6110 MW + 1409.70 MVAR). The simulations results provided in this section are carried out for the high and low loading patterns.

The approaches mentioned in section 2.4.3 for MAVR are investigated with three different study cases when neighboring areas hold:

- Same Objective Functions
- Different Objective Functions
- Non-Collaborative Strategies

In the non-collaborative strategy, one area can provide biased information on the constraints/objectives to increase its own benefit. All the optimizations contain nonlinear equality and inequality constraints. The non-linear optimization problems are solved using “fmincon” with interior-point algorithm in MATLAB R2011b.

2.4.4.1 Same objective functions

In this subsection TSOs apply the same objective function given by (2-11) where ($\omega_1 = 1$) and ($\omega_2, \omega_3 = 0$). The generators voltage set point and their reactive power output for the high and low loading patterns are reported in Table 2.17 and Table 2.18, respectively. The total cost (objective function value) for the high and low loading patterns are presented in Figure 2.19 and Figure 2.20, respectively. The horizontal axis demonstrates the numbers of iterations since the decentralized approaches are iterative.

Table 2.17. The value of control variables for New England 39-bus system for high loading pattern when areas apply the same objective function.

		Area A			Area B			Area C			
		G1	G8	G9	G2	G3	G10	G4	G5	G6	G7
Non-coordinated	V (pu)	1.0155	1.0197	0.9854	1.0600	1.0600	1.0492	1.0600	1.0600	1.0528	1.0600
	Q (MVAR)	49.26	39.17	47.76	305.07	316.39	270.50	208.36	175.66	246.08	190.99
Centralized	V (pu)	1.0600	1.0600	1.0600	1.0365	1.0359	1.0467	1.0600	1.0600	1.0500	1.0600
	Q (MVAR)	131.35	63.05	92.73	243.67	245.55	223.04	187.53	164.13	214.24	182.62
Centralized NC	V (pu)	1.0600	1.0600	1.0600	1.0182	1.0190	1.0259	1.0557	1.0600	1.0425	1.0600
	Q (MVAR)	162.11	80.70	102.64	233.74	237.65	197.75	188.12	179.20	205.47	203.07
Decentralized ENM	V (pu)	1.0198	1.0284	1.0120	1.0600	1.0600	1.0600	1.0600	1.0600	1.0528	1.0600
	Q (MVAR)	33.42	39.05	65.06	291.38	303.03	285.36	199.18	171.50	236.18	185.40
Decentralized LR	V (pu)	1.0600	1.0600	1.0600	1.0365	1.0359	1.0468	1.0600	1.0600	1.0500	1.0600
	Q (MVAR)	131.32	63.05	92.74	243.63	245.52	223.01	187.53	164.13	214.23	182.62
Centralized LI	V (pu)	1.0579	1.0600	1.0600	1.0600	1.0524	1.0547	1.0600	1.0600	1.0565	1.0600
	Q (MVAR)	103.61	53.69	86.08	279.59	255.82	217.12	173.79	157.91	224.22	166.09
Decentralized ENM LI	V (pu)	1.0188	1.0280	1.0168	1.0600	1.0507	1.0600	1.0600	1.0600	1.0544	1.0600
	Q (MVAR)	31.31	38.54	71.23	302.75	275.91	290.64	200.14	171.93	243.58	183.90

Table 2.18. The value of control variables for New England 39-bus system for low loading pattern when areas apply the same objective function.

		Area A			Area B			Area C			
		G1	G8	G9	G2	G3	G10	G4	G5	G6	G7
Non-coordinated	V (pu)	0.9912	0.9935	0.9561	1.0600	1.0600	1.0493	1.0600	1.0600	1.0534	1.0600
	Q (MVAR)	-25.66	-17.74	-17.52	250.54	262.49	226.04	170.17	144.32	194.97	151.76
Centralized	V (pu)	1.0600	1.0600	1.0600	1.0270	1.0271	1.0440	1.0600	1.0600	1.0498	1.0600
	Q (MVAR)	97.89	34.87	38.56	162.97	164.56	149.95	140.57	129.79	150.19	138.77
Centralized NC	V (pu)	1.0600	1.0600	1.0600	0.9996	1.0004	1.0185	1.0434	1.0463	1.0309	1.0439
	Q (MVAR)	146.92	64.26	58.24	151.75	154.30	130.82	138.81	139.43	146.37	146.06
Decentralized ENM	V (pu)	0.9777	0.9738	0.9400	1.0600	1.0600	1.0600	1.0600	1.0600	1.0518	1.0600
	Q (MVAR)	-44.37	-46.37	-13.04	253.08	267.99	275.28	179.37	148.50	198.88	159.22
Decentralized LR	V (pu)	1.0600	1.0600	1.0600	1.0270	1.0271	1.0440	1.0600	1.0600	1.0498	1.0600
	Q (MVAR)	97.89	34.87	38.56	162.97	164.56	149.95	140.57	129.79	150.19	138.77
Centralized LI	V (pu)	1.0514	1.0600	1.0600	1.0539	1.0481	1.0523	1.0600	1.0600	1.0553	1.0600
	Q (MVAR)	45.72	32.75	33.84	204.17	186.10	145.91	127.50	123.89	156.74	124.18
Decentralized ENM LI	V (pu)	0.9814	0.9789	0.9400	1.0600	1.0428	1.0600	1.0600	1.0600	1.0544	1.0600
	Q (MVAR)	-34.78	-36.00	-14.89	272.06	216.44	279.33	180.70	149.10	210.41	156.78

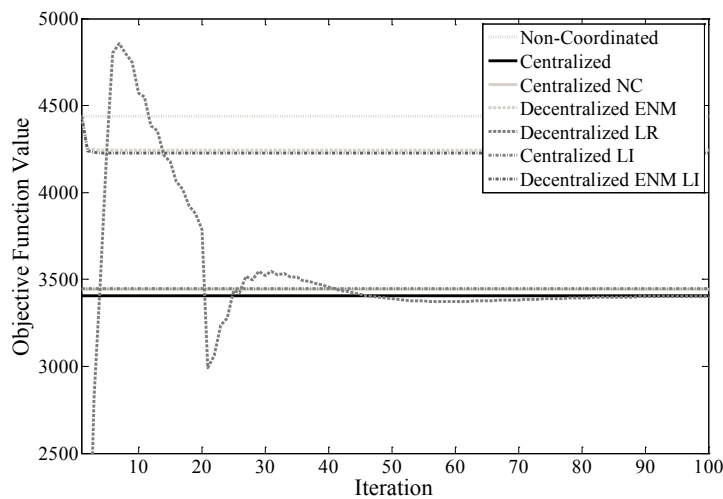


Figure 2.19. MAVR for New England 39-bus system for high loading pattern when areas apply the same objective function.

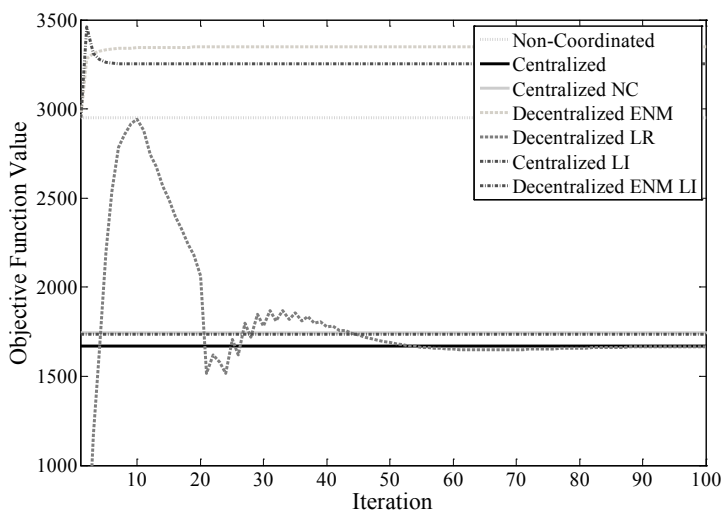


Figure 2.20. MAVR for New England 39-bus system for low loading pattern when areas apply the same objective function.

For both loading patterns, Centralized has the lowest cost and the distance of the other approaches to this solution is considered as sub-optimality. Decentralized LR converges to Centralized with negligible sub-optimality. Although Non-Coordinated solutions don't have infeasibility, there is high sub-optimality. Centralized NC provides an economically fair solution by accepting a small sub-optimality. Decentralized ENM converges to an operating point that does not have necessarily lower cost than in the case of Non-coordinated. For instance, the cost of Decentralized ENM is higher than Non-coordinated in low loading pattern while it is the contrary in high loading pattern. As a result, lower sub-optimality is not guaranteed by Decentralized ENM. However, Decentralized ENM LI effectively reduce the sub-optimality of Decentralized ENM and the number of iterations as well. The total cost of Centralized LI increases in comparison with Centralized case. However, this solution is close to the solution of Centralized NC. The higher is the ω_4 , the higher is the total cost because each area should provide its own reactive power resource.

2.4.4.2 Different objective functions

In this subsection each area applies different objective function. It is assumed that TSO_A applies minimization of QSQ ($\omega_1 = 1, \omega_2, \omega_3 = 0$). TSO_B minimization of active power losses ($\omega_2 = 1, \omega_1, \omega_3 = 0$), and TSO_C minimization of the voltage deviation ($\omega_3 = 1, \omega_1, \omega_2 = 0$). In other words the cost is defined in different ways for every TSO. Here, it is assumed that the total cost is the sum of the cost of all areas. The generators voltage set point and their reactive power output for the high and low loading patterns are given in Table 2.19 and Table 2.20, respectively. The simulation results for the high and low loading patterns are presented in Figure 2.21 and Figure 2.22, respectively.

Table 2.19. The value of control variables for New England 39-bus system for high loading pattern when areas apply different objective functions.

		Area A			Area B			Area C			
		G1	G8	G9	G2	G3	G10	G4	G5	G6	G7
Non-coordinated	V (pu)	1.0155	1.0197	0.9854	1.0600	1.0600	1.0121	1.0600	1.0600	1.0600	1.0600
	Q (MVAR)	76.02	53.18	51.80	329.53	335.39	181.63	208.30	173.54	280.41	183.84
Centralized	V (pu)	0.9889	0.9888	0.9400	1.0600	1.0600	1.0600	1.0600	1.0600	1.0600	1.0600
	Q (MVAR)	7.34	9.64	30.98	313.37	328.53	331.73	220.13	178.89	288.42	189.83
Centralized NC	V (pu)	0.9786	0.9867	0.9956	1.0237	1.0363	1.0493	1.0296	1.0179	1.0325	1.0316
	Q (MVAR)	7.52	22.11	109.03	273.15	339.49	367.37	229.66	147.61	291.64	192.55
Decentralized ENM	V (pu)	1.0493	1.0600	1.0600	1.0497	1.0519	1.0009	1.0600	1.0600	1.0600	1.0600
	Q (MVAR)	122.04	89.51	98.65	293.08	300.89	113.20	185.17	163.06	255.00	169.81
Decentralized LR	V (pu)	0.9889	0.9888	0.9400	1.0600	1.0600	1.0600	1.0600	1.0600	1.0600	1.0600
	Q (MVAR)	7.34	9.64	30.98	313.39	328.54	331.77	220.13	178.89	288.42	189.83
Centralized LI	V (pu)	0.9956	1.0033	0.9828	1.0600	1.0119	1.0359	1.0600	1.0600	1.0600	0.9903
	Q (MVAR)	36.55	43.10	73.83	391.17	210.15	286.94	247.66	191.33	407.04	33.63
Decentralized ENM LI	V (pu)	1.0451	1.0600	1.0600	1.0600	1.0064	1.0600	1.0600	1.0600	1.0600	1.0600
	Q (MVAR)	72.92	77.18	96.47	339.62	135.08	272.67	188.10	164.39	258.23	171.59

Table 2.20. The value of control variables for New England 39-bus system for low loading pattern when areas apply different objective functions.

		Area A			Area B			Area C			
		G1	G8	G9	G2	G3	G10	G4	G5	G6	G7
Non-coordinated	V (pu)	0.9912	0.9935	0.9561	1.0512	1.0543	1.0044	1.0600	1.0600	1.0600	1.0600
	Q (MVAR)	10.25	1.38	-11.02	262.71	279.90	128.28	175.20	145.43	229.92	147.65
Centralized	V (pu)	0.9938	0.9981	0.9739	1.0381	1.0394	1.0189	1.0599	1.0599	1.0599	1.0599
	Q (MVAR)	0.07	0.07	0.10	230.70	240.65	166.50	173.92	144.61	225.47	146.00
Centralized NC	V (pu)	0.9989	1.0069	0.9695	1.0086	1.0084	1.0291	1.0125	1.0155	1.0144	1.0173
	Q (MVAR)	51.02	47.33	20.28	210.94	222.94	245.84	142.31	142.78	202.38	146.45
Decentralized ENM	V (pu)	0.9738	0.9747	0.9400	1.0503	1.0534	1.0094	1.0600	1.0600	1.0600	1.0600
	Q (MVAR)	-17.87	-18.47	-5.15	268.20	287.86	164.50	185.40	150.05	241.11	153.80
Decentralized LR	V (pu)	0.9939	0.9981	0.9741	1.0380	1.0394	1.0189	1.0600	1.0600	1.0600	1.0600
	Q (MVAR)	0.07	0.07	0.10	230.40	240.33	166.03	173.77	144.80	225.37	146.10
Centralized LI	V (pu)	0.9693	0.9752	0.9552	1.0600	0.9751	1.0030	1.0600	1.0600	0.9849	0.9400
	Q (MVAR)	16.81	20.09	34.82	426.94	108.26	201.91	284.47	194.81	206.38	8.26
Decentralized ENM LI	V (pu)	1.0059	1.0108	0.9899	1.0600	0.9727	1.0600	1.0600	1.0600	1.0600	1.0600
	Q (MVAR)	2.33	3.00	6.04	339.88	12.94	275.24	174.70	145.21	229.39	147.35

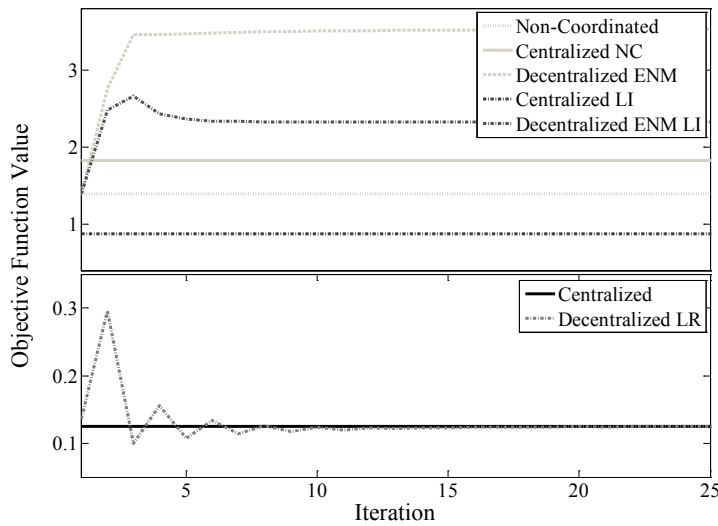


Figure 2.21. MAVR for New England 39-bus system for high loading pattern when areas apply different objective functions.

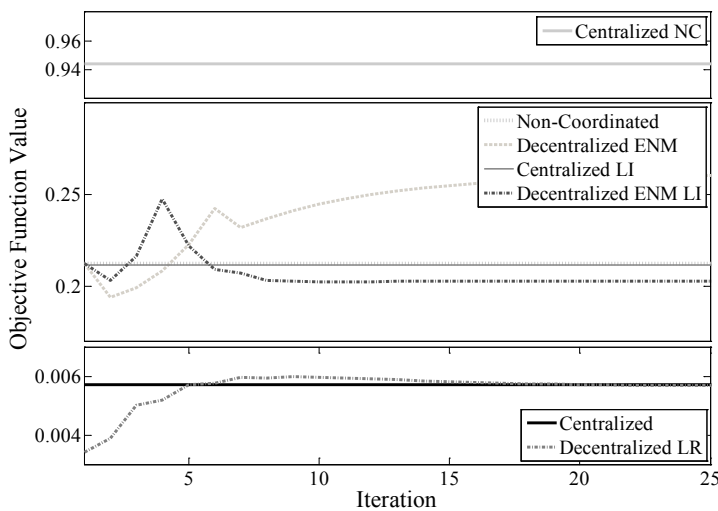


Figure 2.22. MAVR for New England 39-bus system for low loading pattern when areas apply different objective functions.

In comparison with the case when TSOs apply the same objective function:

- * The difference between Non-coordinated and Centralized solutions is relatively higher due to the disparate nature of the TSOs objectives.
- * The sub-optimality of Centralized NC increases in comparison with other approaches since in the proposed fair solution, the normalized objective functions impose higher costs to certain areas.

Similar to the case with the same objective functions:

- * Decentralized ENM has significant sub-optimality.
- * Decentralized LR converges to Centralized with negligible sub-optimality. The convergence is clearly shown in the bottom of Figure 2.21 and Figure 2.22.
- * Centralized LI gives a solution that is not far-off the solution of Centralized NC.

Decentralized ENM LI reduces the sub-optimality and the required number of iterations for Decentralized ENM.

2.4.4.3 *Non-collaborative strategy*

In these simulations all TSOs apply the same objective function given by (2-11) where ($\omega_1 = 1$) and ($\omega_2, \omega_3 = 0$). It is assumed that TSO_B aims to provide incorrect information of its own network to other TSOs. These strategic behaviors could be applied on various information e.g. the generator limits, voltage limits and objective functions. The solution of every approach for different non-collaborative strategies is compared with the result of the Centralized case with the same objective function (Centralized Ref.) given in 2.4.4.1. An optimization approach is called robust against a strategic behavior if the results of non-collaborative and collaborative strategies become similar. Here, the simulation results are not presented and only the conclusions are discussed. It is interesting to mention that for all strategies and approaches, the sub-optimality in high loading pattern is rather lower than in the case of low loading pattern, since in the former, the system is closer to its limits and the feasible region of the solution is more limited.

2.4.4.3.1 *Generator limits*

In this strategy, TSO_B applies fifty percent of the limit for the maximum generators reactive power. Therefore, reactive power output of area B is limited and the costs of its neighbors increase. Centralized and Decentralized LR approaches approximately have the same sub-optimality regarding to Centralized Ref. case. This sub-optimality is close to zero at low loading pattern while it increases at high loading pattern. The reason is that at low loading pattern the generators maximum reactive power constraints are not reached but at the high loading pattern these constraints are active. Centralized NC is not robust against this strategy and the total cost goes higher. For Decentralized ENMs and Centralized LI the total cost increases (decreases) at low (high) loading pattern. Note that the decentralized approaches here, including Decentralized ENMs and Decentralized LR, require fictitious reactive power sources in infeasible iterations, as special treatment mentioned in 2.4.2.2.3, to avoid the infeasibility.

2.4.4.3.2 Voltage limits

For this strategy, TSO_B applies the voltage deviation within ten percent instead of six percent (disclose). The Centralized approach is robust against this strategy behavior while Decentralized LR has sub-optimality. The result of Centralized NC in high (low) loading pattern has higher (lower) cost. The sub-optimality increases for the other approaches. Furthermore, TSO_B may apply the voltage deviation within six percent but inform the other areas that ten percent voltage deviation is acceptable for this area (non-disclose). Centralized and Centralized LI approaches are immune against this strategy. The total cost of Centralized NC in high (low) loading increase (decrease). For the other approaches the sub-optimality decreases. Generally, these strategies don't improve the objective of area B necessarily, and even they may effect adversely on its objective [61].

2.4.4.3.3 Objective functions

It is assumed that TSO_B declares its cost function as $2 \times OF$ and OF^2 , respectively. The first strategy is linear transformation of the objective function. The results of Non-Coordinated, Centralized NC and Decentralized ENM are robust against this strategy. In both loading patterns, the sub-optimality of Centralized LI decrease. In contrast, the sub-optimality increases for Centralized, Decentralized LR and Decentralized ENM LI. In the second strategy TSO_B minimizes the square of its cost. Simulation results demonstrate that Non-Coordinated, Centralized NC and Decentralized ENM are robust against this strategy. The sub-optimality increases for the other approaches. The robustness of the different approaches to the non-collaborative strategies is summarized in Table 2.21.

Table 2.21. The robustness of different approaches to the strategic behavior of TSO_B.

Generator limits	Voltage limits		Objective functions	
	Disclose	Non-disclose	$2 \times OF$	OF^2
Non-Coordinated			✓	✓
Centralized	✓	✓		
Centralized NC			✓	✓
Decentralized ENM			✓	✓
Decentralized LR				
Decentralized ENM LI				
Centralized LI		✓		

2.4.4.4 Discussions and conclusions

This section investigated the inter-area optimal voltage and reactive power control. The state of the art in practice and research are studied and the necessity of MAVR is highlighted. Several centralized and decentralized approaches are examined to investigate their effectiveness for the voltage and reactive power control in MAPS. The proposed formulation benefits from the distributed slack bus model for the response of generators to the active power losses. This modeling allows an easier implementation of the optimization approaches and also improves the optimization results.

In collaborative environment the solution of Centralized approach is considered as the reference case to obtain sub-optimality of other approaches. Decentralized LR practically always converges to zero sub-optimality but it requires more iteration and more information exchange between neighboring areas. Decentralized ENM converges with less number of iterations but with high sub-optimality. Additional limits on the voltage difference at both ends of interconnections effectively reduce the sub-optimality of Decentralized ENM while the number of iterations decreases a little. Non-coordinated operation always has high sub-optimality and non-feasibility is also possible. Centralized NC proposes an economically fair solution with low sub-optimality for the same objective functions and higher sub-optimality when the objective functions are different. The solution of Centralized with limits on the reactive power flow at interconnections is close to the solution of Centralized NC.

The discussed approaches are not robust against all kinds of strategic behaviors. Therefore, a collaborative framework should be realized for an appropriate MAVR. The non-collaborative behaviors can be avoided for instance by improving the power system monitoring. However, additional limits on the difference of the voltage of both ends of the interconnections and reactive power flow limits in the interconnections are effective against strategic behaviors when limiting the strategic decisions of one TSO within its own area.

2.5 Pilot Node Selection for *max.ERPR*

This section focuses on the problem of optimal selection of pilot nodes for the suggested optimization of $max.ERPR$. This optimization is an integer nonlinear programming problem. An approach is developed based on genetic algorithm to effectively find the appropriate pilot nodes in SAPS. The robustness of the obtained solutions for the pilot nodes is tested for several contingencies. Several decentralized methods are studied to extend the proposed approach for MAPS.

2.5.1 Preliminaries

The pilot nodes are the most voltage sensitive nodes that reflect the state of the voltage in a control zone. Any control action to maintain the voltage profile of these nodes will be propagated inside the zone. Thus keeping the voltage of pilot buses at an admissible level means that every bus in that zone has an acceptable voltage level. The appropriate selection of these nodes plays an important role in the proper implementation of the voltage control schemes. The optimal selection of the pilot nodes for SVR is studied in several literatures [72]. These methods can be classified in two main categories, namely: (i) heuristic rules based methods and (ii) evolutionary optimization based methods.

The heuristic rules based methods are dependent on the field experience to efficiently formulate and solve a problem. For instance in France, the buses with the highest short circuit current are selected as the pilot nodes [73]. However, the evolutionary based methods consider the pilot node selection as an optimization problem [74]. Regarding the optimization based methods, [75] proposes an extensive search of all the possible pilot nodes in the system using simulated annealing algorithm. The definition of convergence criteria for the annealing algorithm is difficult as it is empirical and case dependent. A method based on search procedure approach is used in [76] for the pilot nodes selection. This search procedure considers all the nonlinearities of the power system such as full load flow equations. However, there is no guarantee that the obtained selection of pilot nodes is the global optimal solution. [77] addresses the problem of pilot node selection for SVR by applying the bifurcation theory on the differential-algebraic equations of the power system. The solution of this method is dependent on the selection of optimization criteria and operator's knowledge of the system. Another evolutionary optimization method is immune based selection algorithm, which solves an optimization problem using pattern recognition and memorization [74]. It has an inherent drawback of slower convergence to optimal solution. In addition, there are other methods based on complex network theory [78], [79]. These methods use the so called community structure for system partitioning which ensures that the regions are decoupled from each other to reduce control complexity. Then centrality degree index is used to determine pilot nodes. These different optimization methods result in different pilot node selections. It is worth noting that all of the above mentioned methods only consider the pilot node selection for SVR. In [80] the pilot node selection for SVR is initially discussed and then extended for TVR. The reference [80] concerns a master diploma project performed under supervision of the author of this thesis.

In this thesis the issue of pilot node selection for TVR is particularly introduced for the optimization of *max.ERPR*. As mentioned in section 2.3.2, this optimization maximizes the ERPR of generators in order to improve the VSMs at the pilot nodes. Therefore, these network representative nodes should be appropriately selected to demonstrate the most voltage sensitive nodes. The proposed method in [80] for the optimal pilot node selection of TVR is based on the genetic algorithm. The effectiveness of selected pilot nodes are investigated using contingency analyses for the outages of transmission equipments and generating units.

2.5.2 Problem Formulation

The objective function of the optimization for the pilot node selection, given by $I(X)$, can be represented using (2-24) [81]. A small value of $I(X)$ means that the choice of pilot nodes is effective and the control effect provides better results.

$$\min_x I(X) \tag{2-24}$$

In this objective function $I(X)$ is the stabilization effect, and it is calculated according to the following formula:

$$I(X) = E\{\Delta V_L^T \times Q_l \times \Delta V_L\} \tag{2-25}$$

where $E\{\cdot\}$ is the expected value, Q_l is the matrix of reactive power at all load buses and ΔV_l is the vector of voltage deviation for all load buses. The objective is to minimize (2-24) that is a binary nonlinear programming problem. The buses whose voltage deviation is zero at minimum value of (2-24) are considered as pilot nodes. This minimum value is also called stabilization effect of pilot nodes.

This formula (2-25) takes into account the sensitivity matrices determined from Jacobian matrix related to imaginary part of admittance matrix as well as the effect of the controlled (load) and the controlling (generator) buses. The detailed formulation of (2-24) can be found in [80] and [81]. Note that the voltage deviation vector (ΔV_l) is dependent on the matrix corresponding to pilot node choices (X). The matrix of X is defined as follows:

$$X = [x_{ij}]_{n_p \times n_l} \quad x_{ij} = \begin{cases} 1 & \text{if bus } j \text{ is the } i^{\text{th}} \text{ pilot bus} \\ 0 & \text{otherwise} \end{cases} \quad (2-26)$$

where n_p and n_l show the number of pilot nodes and load buses and constitute the dimensions of X . It is worth mentioning that the pilot nodes are a subset of load buses. Moreover, the number of pilot nodes should be less than or equal to the number of controlling nodes. It brings an inequality constraint to the introduced optimization [79]. This optimization is an integer nonlinear programming problem which is solved using different approaches for SVR and TVR.

2.5.2.1 Pilot Node Selection for SVR

The proposed method in [79] for the pilot node selection for SVR initially divides the power system into different zones. It ensures the decoupling of zones from each other and thus simplifying the implementation of control function. Then, pilot nodes in each zone are selected independently using control centrality index [79] which determines their importance for the control objective given by (2-24). In this approach, the computational time is reduced since the number of possible combinations of controlled buses, constituting pilot node set, is reduced. The effectiveness of these combinations is evaluated using (2-24), namely $I_i(X)$, for each zone. The number of pilot nodes in each combination cannot be greater than the number of controlling buses in that particular zone. The combinations of candidate pilot nodes of each zone which give the optimal stabilization effect are chosen as the set of pilot nodes of the system. Then an overall system stabilization effect is calculated using (2-24).

2.5.2.2 Pilot Node Selection for TVR

The pilot node selection for TVR is similarly defined based on (2-24). In this optimization the whole system is considered. It highly increases the computation burden due to the increase of the combinatorial possibilities. Therefore, the presented approach for SVR is not applicable for TVR. In order to solve this nonlinear combinatorial problem, genetic algorithm is used. The genetic algorithm is appropriate for highly nonlinear integer programming problems and global search. Moreover, it is independent of its initial settings and is easy to be implemented. The related parameters should be carefully tuned to avoid converging to suboptimal solutions. The genetic algorithm starts from a population of randomly generated individuals (solutions). It modifies the population of individuals, while judiciously selecting individuals from the current population for parenting children for the next generation. Over subsequent generations, the population evolves towards an optimal solution [82]. For the presented optimization, the

number of individuals in the population is equal to the number of controlled buses and the initial pilot node set is randomly selected from this population. The values assigned to the individuals are either “1” or “0” where “1” representing their status as a pilot node and “0” otherwise. In each population pilot nodes are selected and then they are tested for their effectiveness using (2-24).

2.5.3 Simulation and Results

The New England 39-bus system and IEEE 57-bus system area used to evaluate the effectiveness of the proposed methods for the pilot node selection. The single line diagrams of the studied systems are given in Figure 2.8 and Figure 2.9. The selected pilot nodes for these study cases are shown in these figures with bold and red buses. In order to further investigate this optimization problem, additional simulations are performed for the New England 39-bus system for two loading levels namely; low and high loading levels. These loading levels are similar to the given loading values in section 2.4.4.

Regarding the pilot node selection for SVR, the system is partitioned into five zones based on the complex network theory and according to the presented results in [79], whereas for the pilot node selection for TVR the whole system is considered.

Table 2.22 shows the pilot nodes selected for SVR and TVR with their stabilization indices. As the loading level increases the stabilization effect increases as well, but the selected pilot nodes are not affected. This specifies that the higher is the loading of a system, the higher is the possibility of instability. But as far as the pilot node selection is concerned, the optimization solution is independent of the loading level of the system.

Table 2.22. Selected pilot nodes for SVR and TVR for New England 39-bus system.

pilot nodes		$I(X)$	
		Low Loading	High Loading
SVR	4, 7, 8, 12, 20, 21, 23, 24 , 25, 28	0.0033	0.0055
TVR	4, 8, 12, 16¹ , 18 , 20, 21, 23, 25, 28	0.0031	0.0043

Table 2.22 also presents a comparison of the selected pilot nodes for SVR and TVR as well as their stabilization indices. These differences demonstrate that in the case of TVR that considers the whole grid, the pilot node selection is different from the case of SVR. It is observed that the

¹ The selection of this bus is different from the presented pilot nodes in Figure 2.8 since in the original data of this study case the reactive load at bus 24 is negative, whereas in the simulation of the section 2.5 this load is assumed positive.

stabilization factor of TVR has a lower value in comparison with SVR. Therefore, the selected pilot nodes for TVR have a higher system stabilization capability.

The robustness of the selected pilot nodes for TVR is verified for several contingencies. These contingencies include the single outage of generating units and transmission elements. Since this thesis is focused on TVR, the effect of contingencies is studied only for TVR. In this respect, the optimization problem for the pilot node selection is solved to obtain the effective pilot nodes for every contingency. Figure 2.23 shows the percentage that a certain bus is selected as pilot node. As it is illustrated, the selected buses as the pilot nodes using the optimization for TVR have the highest percentage of selection. These results confirm that the selected pilot nodes are robust against different kind of contingencies.

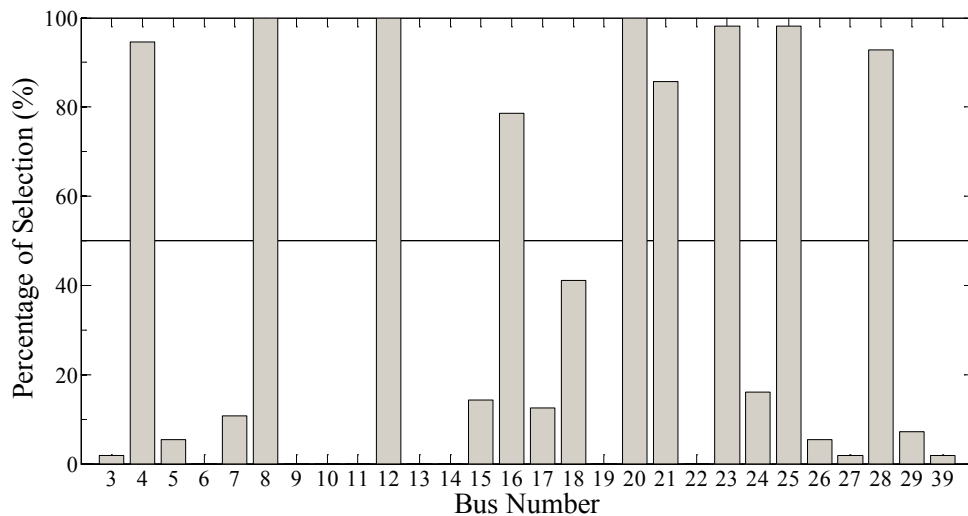


Figure 2.23. The percentage of selection of buses as pilot node for different contingencies for New England 39-bus system.

The issue of the optimal pilot node selection is also investigated in the context of MAPS in [80] using the centralized and decentralized approaches. The results of the centralized approach are similar to those presented in Table 2.22 for TVR in the case of SAPS. It is due to the fact that the centralized optimization for MAPS deals with the entire interconnected network with a single optimization problem. Several decentralized approaches are also studied in [80], however, their results are dependent on the borders of areas in MAPS. A major difficulty for using a decentralized approach comes from the fact that the genetic algorithm does not provide the value of Lagrangian multipliers. As a result, the implementation of a decentralized method based on mathematical decomposition cannot be achieved as in section 2.4.2.2.2. Moreover, the methods based on the external network modeling are not effective since the studied models (e.g. equivalent PQ, PV, impedance, etc.) of neighboring areas do not change with the variation of the selected pilot nodes. Therefore, further investigation is required to formulate and solve the decentralized optimization for the pilot node selection for MAPS.

2.6 Security Constrained Voltage and Reactive Power Scheduling in MAPS

The multi-area voltage and reactive power management regarding the voltage stability is studied in this section. In this respect, the maximization of effective reactive power reserve is proposed using the centralized and decentralized implementations. The simulation results demonstrate that the well-known decentralized implementation does not converge whenever there are PV generators at border buses. It is illustrated that this problem occurs when the complementarity constraints are considered. Appropriate modifications are proposed for the formulation of the decentralized optimization in order to consider the effect of the complementarity constraints at border buses. The presented results demonstrate the effectiveness of the proposed formulation to handle such optimization problems.

2.6.1 Preliminaries

The various possible implementations of the centralized and decentralized voltage and reactive power optimizations are studied in section 2.4 and [9] where the comparative analysis between the different methods is discussed in terms of sub-optimality and time to convergence. However, the MAVR regarding the voltage stability has not been studied in the literatures so far. The aim of this section is to develop a coordinated MAVR which takes into account the voltage stability margin. In this respect, the maximization of effective reactive power reserve (*max.ERPR*), which considers the voltage stability, is studied using the centralized and decentralized approaches. The proposed formulations benefit from the detailed modeling of generators reactive power limits as well as the distributed slack bus model for the compensation of active power imbalances. Moreover, the generator switch between the constant terminal voltage and the constant reactive power output is modeled by the complementarity constraints. It is illustrated that the consideration of the complementarity constraints asks for further modification in the formulation of the decentralized optimization.

The presented assumptions in section 2.3.2 are taken into consideration in the proposed optimizations for MAVR. Using these assumptions, section 2.6.2 proposes a centralized and a decentralized formulation for the coordinated voltage and reactive power optimization in MAPS. Then, section 2.6.3 evaluates the effectiveness of the proposed optimization with reference to New England 39-bus system.

2.6.2 Problem Formulation

This section presents the MAVR regarding the maximum stability margin. Generally, an optimization problem in the context of MAPS can be solved using the centralized or decentralized approaches. The formulation of the optimization problems are presented in the two following sub-sections.

2.6.2.1 Centralized optimization

For the centralized optimization, it is assumed that each TSO_k has the similar objective function which is $max.ERPR$. Also TOSs provide their objectives and constraints information to the control center in a collaborative manner. Then, an optimization problem is solved by the control center for all areas. The general and detailed formulations for the $max.ERPR$ are similar to the given equations by (2-4) and (2-8), respectively.

2.6.2.2 Decentralized optimization

The appropriate coordination in the MAPS should be studied using decentralized optimization approaches. The decentralized optimization of every TSO_k can be generally formulated as follows:

$$\max_{u_k, \phi_k} f_k(x_{0k}, x_{ck}, u_k, \tilde{z}_{0k}, \tilde{z}_{ck}, \phi_k) \quad (2-27.a)$$

subject to

$$g_{0k}(x_{0k}, u_k) \leq 0 \quad (2-27.b)$$

$$h_{0k}(x_{0k}, u_k) = 0 \quad (2-27.c)$$

$$g_{ck}(x_{ck}, u_k, \phi_k) \leq 0 \quad (2-27.d)$$

$$h_{ck}(x_{ck}, u_k, \phi_k) = 0 \quad (2-27.e)$$

$$g_{0k-\zeta}(x_{0k}, u_k, \tilde{z}_{0k}) \leq 0 \quad (2-27.f)$$

$$h_{0k-\zeta}(x_{0k}, u_k, \tilde{z}_{0k}) = 0 \quad (2-27.g)$$

$$g_{ck-\zeta}(x_{ck}, u_k, \tilde{z}_{ck}, \phi_k) \leq 0 \quad (2-27.h)$$

$$h_{ck-\zeta}(x_{ck}, u_k, \tilde{z}_{ck}, \phi_k) = 0 \quad (2-27.i)$$

where (2-27.b) – (2-27.e) are its own inequality and equality constraints. The coupling equality and inequality constraints are given by (2-27.f) – (2-27.i). Similar to (2-17) coordination and communication are required and these optimizations cannot be solved independently for each area k , because \tilde{z}_k is involved in the objective function (2-27.a) and/or in the coupling constraints (2-27.f) – (2-27.i) of more than one TSO problem.

The decomposed sub-problems are then solved in an iterative way, independently but in coordinated way. In the proposed method the coordination is obtained based on passing adjacent variables at the existing border buses [60]. In this approach the neighboring areas exchange the value of the border variables and the Lagrangian multipliers related to the complicating

variables and the coupling constraints. The exchanged variables include the values of complicating variables at both of the current operating point (\tilde{z}_{0k}) and the collapse point (\tilde{z}_{ck}).

More precisely, the sub-problem of TSO_k is obtained by accounting for the coupling constraints of the foreign areas at the current operating point ($h_{0k'-\zeta}$ and $g_{0k'-\zeta}$) and at the collapse operating point ($h_{ck'-\zeta}$ and $g_{ck'-\zeta}$) and adding them as penalties to the objective function while maintaining its own coupling constraints. Therefore, TSO_k solves the following optimization problem.

$$\begin{aligned} \max_{u_k, \phi_k} \quad & f_k(x_{0k}, x_{ck}, u_k, \tilde{z}_{0k}, \tilde{z}_{ck}, \phi_k) & (2-28.a) \\ & + \sum_{\Omega_{k'-\zeta}} \mu_{0k'-\zeta}^* g_{0k'-\zeta}(x_{0k}, u_k, \tilde{z}_{0k}, \tilde{z}_{0k}^*) \\ & + \sum_{\Omega_{k'-\zeta}} \lambda_{0k'-\zeta}^* h_{0k'-\zeta}(x_{0k}, u_k, \tilde{z}_{0k}, \tilde{z}_{0k}^*) \\ & + \sum_{\Omega_{k'-\zeta}} \mu_{ck'-\zeta}^* g_{ck'-\zeta}(x_{ck}, u_k, \tilde{z}_{ck}, \tilde{z}_{ck}^*, \phi_k) \\ & + \sum_{\Omega_{k'-\zeta}} \lambda_{ck'-\zeta}^* h_{ck'-\zeta}(x_{ck}, u_k, \tilde{z}_{ck}, \tilde{z}_{ck}^*, \phi_k) \end{aligned}$$

subject to

$$g_{0k}(x_{0k}, u_k) \leq 0 \quad (2-28.b)$$

$$h_{0k}(x_{0k}, u_k) = 0 \quad (2-28.c)$$

$$g_{ck}(x_{ck}, u_k, \phi_k) \leq 0 \quad (2-28.d)$$

$$h_{ck}(x_{ck}, u_k, \phi_k) = 0 \quad (2-28.e)$$

$$g_{0k-\zeta}(x_{0k}, u_k, \tilde{z}_{0k}) \leq 0 \quad : \mu_{0k-\zeta} \quad (2-28.f)$$

$$h_{0k-\zeta}(x_{0k}, u_k, \tilde{z}_{0k}) = 0 \quad : \lambda_{0k-\zeta} \quad (2-28.g)$$

$$g_{ck-\zeta}(x_{ck}, u_k, \tilde{z}_{ck}, \phi_k) \leq 0 \quad : \mu_{ck-\zeta} \quad (2-28.h)$$

$$h_{ck-\zeta}(x_{ck}, u_k, \tilde{z}_{ck}, \phi_k) = 0 \quad : \lambda_{ck-\zeta} \quad (2-28.i)$$

In this formulation, the second to the fifth part of (2-28.a) demonstrate the coupling constraints of the other sub-problems ($k' \neq k$) as relaxed constraints in the objective function. (2-28.b) – (2-28.i) give the coupling constraints of the sub-problem k as hard constraints. The Lagrangian multipliers obtained from the solution of the sub-problems k at the current operating points are given by $\lambda_{0k-\zeta}$ and $\mu_{0k-\zeta}$ and at the collapse operating point are given by $\lambda_{ck-\zeta}$ and $\mu_{ck-\zeta}$. They could be interpreted as the cost of providing power from the neighboring areas at both operating and collapse points. Note that the superscript * indicates the variables which are calculated in previous iteration and they are kept constant in this iteration.

The coupling constraints are the interconnections active and reactive power flow equations ($h_{k-\zeta}$) but not their power flow limits ($g_{k-\zeta}$). The active and reactive power flows from bus i to bus j at the interconnection ζ are calculated for both of the current and collapse operating points. In addition, whenever there is a PV generator at the border buses, the equality constraint (2-8.n)

should be treated also as further coupling constraint. Otherwise, the solutions of those areas for which PV generators are connected to the border buses become oscillatory and their optimizations do not converge. It is worth mentioning that this equality constraint (2-8.n) results from the consideration of the complementarity constraints. This constraint is a nodal equality constraint within one of the interconnected areas whereas the power flow equality constraints are defined between two nodes of the neighboring areas sharing an interconnection line. This particular treatment for the complementarity constraints is not required when the generator at the border bus is a PQ generator. The issue of the decentralized optimization with complementarity constraints is discussed more in depth using illustrative example in section 2.6.3.

The interconnections power flow tolerances at the current operating and collapse points calculated on both sides are used as convergence criteria. Thanks to the distributed slack bus model for the active power losses, specific treatment is not needed to define the reference bus. Note that the initial values of parameters in the first iteration are equal to zero except the voltages which are equal to one.

It is worth mentioning that the solution of every area may not keep the system inside its feasible operating region at every iteration since each TSO ignores the other TSOs control actions. In these cases, additional fictitious reactive power sources (Q_s) is designated in the buses with reactive loads. The sum of square of them is added in the objective function with a high cost (large W) in order to obtain feasibility of nodal reactive power balance [14]. This can be considered as the reactive power load shedding. Note that this vector should be added to both of the current and collapse operating points ($Q_s^{(0)}$ and $Q_s^{(c)}$). The results of the decentralized optimization scheme are evaluated based on the sub-optimality of solution and the required number of iterations.

The detailed formulation of the proposed optimization for the $max.ERPR$ for every TSO_k is given as follow.

$$\max \sum_{\Omega_{G-k}} (Q_{Ggk}^{(c)} - Q_{Ggk}^{(0)}) - W \cdot \sum_{\Omega_{B-k}} ((Q_{Si}^{(0)})^2 + (Q_{Si}^{(c)})^2) + \sum_{\Omega_{k'-\zeta}} \left\{ \begin{array}{l} (\lambda_{P_0k'-\zeta}^* \times P_{jik'-\zeta}^{(0)}) + (\lambda_{Q_0k'-\zeta}^* \times Q_{jik'-\zeta}^{(0)}) - \\ (\lambda_{P_c k'-\zeta}^* \times P_{jik'-\zeta}^{(c)}) - (\lambda_{Q_c k'-\zeta}^* \times Q_{jik'-\zeta}^{(c)}) + \\ (\lambda_{PVk'-\zeta}^* \times (V_{gk'-\zeta}^{(0)} - V_{gk'-\zeta}^{(c)} - V_{gk'-\zeta}^{oe(c)})) \end{array} \right\} \quad (2-29.a)$$

subject to

$$P_{Gi} + P_{Li}^{(0)} - P_{Di} - \sum_j P_{ij}^{(0)}(V^{(0)}, \theta^{(0)}) = 0 \quad i \in \Omega_{B-k} \quad (2-29.b)$$

$$Q_{Gi}^{(0)} - Q_{Di} - Q_{Si}^{(0)} - \sum_j Q_{ij}^{(0)}(V^{(0)}, \theta^{(0)}) = 0 \quad i \in \Omega_{B-k} \quad (2-29.c)$$

$$(P_{ij}^{(0)})^2 + (Q_{ij}^{(0)})^2 \leq (S_i^{max})^2 \quad \{i, j\} \in l, l \in \Omega_{T-k} \quad (2-29.d)$$

$$0 \leq P_{Lg}^{(0)} \leq \bar{P}_{Gg} - P_{Gg} \quad g \in \Omega_{G-k} \quad (2-29.e)$$

$$\underline{Q}_{Gg} \leq Q_{Gg}^{(0)} \leq \bar{Q}_{Gg}^{(0)} \quad g \in \Omega_{G-k} \quad (2-29.f)$$

$$V_i^{min} \leq V_i^{(0)} \leq V_i^{max} \quad i \in \Omega_{B-k} \quad (2-29.g)$$

$$P_{ijk-\zeta}^{(0)} = (V_i^{(0)})^2 G_{ij} - V_i^{(0)} V_j^{(0)} G_{ij} \cos \theta_{ij}^{(0)} - V_i^{(0)} V_j^{(0)} B_{ij} \sin \theta_{ij}^{(0)} \quad : \lambda_{P_0k-\zeta} \quad i \in \Omega_{k-\zeta}, j \in \Omega_{G-PV k'-\zeta} \quad (2-29.h)$$

$$Q_{ijk-\zeta}^{(0)} = -(V_i^{(0)})^2 \cdot (B_{ij} - (B_{sh}/2)) + V_i^{(0)} V_j^{(0)} B_{ij} \cos \theta_{ij}^{(0)} - V_i^{(0)} V_j^{(0)} G_{ij} \sin \theta_{ij}^{(0)} \quad : \lambda_{Q_0k-\zeta} \quad i \in \Omega_{k-\zeta}, j \in \Omega_{G-PV k'-\zeta} \quad (2-29.i)$$

$$P_{ij k-\zeta}^{(0)} = (V_i^{(0)})^2 G_{ij} - V_i^{(0)} V_j^* G_{ij} \cos \theta_{ij}^{(0)} - V_i^{(0)} V_j^* B_{ij} \sin \theta_{ij}^{(0)} \quad : \lambda_{P_0k-\zeta} \quad i \in \Omega_{k-\zeta}, \quad (2-29.j)$$

$$\begin{aligned}
 Q_{ijk-\zeta}^{(0)} &= -(V_i^{(0)})^2 \cdot (B_{ij} - (B_{sh}/2)) + V_i^{(0)} V_j^* B_{ij} \cos \theta_{ij}^{(0)} - V_i^{(0)} V_j^* G_{ij} \sin \theta_{ij}^{(0)} & : \lambda_{Q_0 k-\zeta} & \begin{aligned} j &\in \{\Omega_{k'-\zeta} - \Omega_{G-PVK'-\zeta}\} \\ i &\in \Omega_{k-\zeta}, \end{aligned} & (2-29.k) \\
 P_{Gi} + P_{Li}^{(c)} - P_{Di} - \sum_j P_{ij}^{(c)}(V^{(c)}, \theta^{(c)}) &= 0 & & \begin{aligned} j &\in \{\Omega_{k'-\zeta} - \Omega_{G-PVK'-\zeta}\} \\ i &\in \Omega_{B-k} \end{aligned} & (2-29.l) \\
 Q_{Gi}^{(c)} - Q_{Pi}^{(c)} - Q_{Di} - Q_{Si}^{(c)} - \sum_j Q_{ij}^{(c)}(V^{(c)}, \theta^{(c)}) &= 0 & & i \in \Omega_{B-k} & (2-29.m) \\
 (P_{ij}^{(c)})^2 + (Q_{ij}^{(c)})^2 &\leq (S_l^{max})^2 & & \{i, j\} \in l, l \in \Omega_{T-k} & (2-29.n) \\
 0 \leq P_{Lg}^{(c)} &\leq \bar{P}_{Gg} - P_{Gg} & & g \in \Omega_{G-k} & (2-29.o) \\
 V_i^{min} &\leq V_i^{(c)} \leq V_i^{max} & & i \in \Omega_{B-k} & (2-29.p) \\
 V_g^{(c)} &= V_g^{(0)} - V_g^{oe(c)} & : \lambda_{PVk-\zeta} & g \in \Omega_{G-PVK} & (2-29.q) \\
 (\bar{Q}_{Gg}^{(c)} - Q_{Gg}^{(c)}) \cdot V_g^{oe(c)} &\leq \varepsilon & & g \in \Omega_{G-PVK} & (2-29.r) \\
 V_g^{oe(c)} &\geq 0 & & g \in \Omega_{G-PVK} & (2-29.s) \\
 \underline{Q}_{Gg} &\leq Q_{Gg}^{(c)} \leq \bar{Q}_{Gg}^{(c)} & & g \in \Omega_{G-k} & (2-29.t) \\
 Q_{Gg}^{(c)} &= Q_{Gg}^{(0)} & & g \in \Omega_{G-PQk} & (2-29.u) \\
 P_{ijk-\zeta}^{(c)} &= (V_i^{(c)})^2 G_{ij} - V_i^{(c)} V_j^{(c)} G_{ij} \cos \theta_{ij}^{(c)} - V_i^{(c)} V_j^{(c)} B_{ij} \sin \theta_{ij}^{(c)} & : \lambda_{P_c k-\zeta} & i \in \Omega_{k-\zeta}, j \in \Omega_{G-PVK'-\zeta} & (2-29.v) \\
 Q_{ijk-\zeta}^{(c)} &= -(V_i^{(c)})^2 \cdot (B_{ij} - (B_{sh}/2)) + V_i^{(c)} V_j^{(c)} B_{ij} \cos \theta_{ij}^{(c)} - V_i^{(c)} V_j^{(c)} G_{ij} \sin \theta_{ij}^{(c)} & : \lambda_{Q_c k-\zeta} & i \in \Omega_{k-\zeta}, j \in \Omega_{G-PVK'-\zeta} & (2-29.w) \\
 P_{ijk-\zeta}^{(c)} &= (V_i^{(c)})^2 G_{ij} - V_i^{(c)} V_j^* G_{ij} \cos \theta_{ij}^{(c)} - V_i^{(c)} V_j^* B_{ij} \sin \theta_{ij}^{(c)} & : \lambda_{P_c k-\zeta} & \begin{aligned} i &\in \Omega_{k-\zeta}, \\ j &\in \{\Omega_{k'-\zeta} - \Omega_{G-PVK'-\zeta}\} \end{aligned} & (2-29.x) \\
 Q_{ijk-\zeta}^{(c)} &= -(V_i^{(c)})^2 \cdot (B_{ij} - (B_{sh}/2)) + V_i^{(c)} V_j^* B_{ij} \cos \theta_{ij}^{(c)} - V_i^{(c)} V_j^* G_{ij} \sin \theta_{ij}^{(c)} & : \lambda_{Q_c k-\zeta} & \begin{aligned} i &\in \Omega_{k-\zeta}, \\ j &\in \{\Omega_{k'-\zeta} - \Omega_{G-PVK'-\zeta}\} \end{aligned} & (2-29.y) \\
 V_g^{(c)} &= V_g^* & & g \in \Omega_{G-PVK'-\zeta} & (2-29.z)
 \end{aligned}$$

This objective function (2-29.a) includes of three general parts. The first part is similar to (2-8.a) and maximizes the *ERPR* of generators within area k . The second part characterizes the cost of the added variables for obtaining the feasibility of reactive power balance in the optimization iterations. The third part includes five terms which they represent the effect of the optimizations of neighboring areas. The first two terms correspond to the current operating point and the third and fourth terms are for the collapse point. Note that the terms related to the current operating point are added to the objective function whereas the terms related to the collapse point are subtracted from the objective function, as the first term in the objective function. The fifth term takes into account the effect of the complementarity constraints of PV generators of neighboring areas at border buses.

The equations (2-29.b) – (2-29.g) and (2-29.l) – (2-29.u) represent the internal constraints of area k at the current operating point and the collapse point, respectively. It is worth to note that in equation (2-29.q) the Lagrangian multipliers are taken from the PV generators at the border buses ($\lambda_{PVk-\zeta}$).

The equations (2-29.j) – (2-29.k) (resp. (2-29.x) – (2-29.y)) represent the active and reactive power flows of the tie-lines at the current operating point (resp. at the collapse point). For the tie-lines connected to the PV generators of neighboring areas, these active and reactive power flow equations are replaced with equations (2-29.h) – (2-29.i) (resp. (2-29.v) – (2-29.w)). It must be noted that if several tie-lines are connected to a bus, $P_{ijk-\zeta}$ and $Q_{ijk-\zeta}$ are the sum of all tie-lines power flows connected to that bus. Note that the Lagrangian multipliers of power flows

$(\lambda_{P_0k-\zeta}, \lambda_{Q_0k-\zeta}, \lambda_{P_ck-\zeta}, \lambda_{Q_ck-\zeta})$ are calculated for the sum of all tie-lines power flows at that border bus.

In order to consider the effect of complementarity constraints modeling of a PV generator at a border bus, three additional variables are dedicated for the voltage of that PV generator at the border with the neighboring area. These variables represent the voltage of the current operating point, the collapse point and the over-excitation correction, respectively, given by $V_{gk'-\zeta}^{(0)}$, $V_{gk'-\zeta}^{(c)}$ and $V_{gk'-\zeta}^{oe(c)}$. The constraint (2-29.z) should be taken into consideration to guarantee the equality of the additional variable with its value obtained from the optimization of neighboring areas. However, for the decentralized optimization without complementarity constraints, the optimization of area k is solved while the voltage of neighboring border buses ($k' \neq k$) are assumed to be constant and equal to the obtained value in the last iteration. The effect of considering the complementarity constraints on the decentralized optimization is explained more in depth using illustrative examples in the following section.

2.6.3 Simulation Results

New England 39-bus system portioned into three areas is used to evaluate the effectiveness of the proposed centralized/decentralized optimizations for *max.ERPR*. The one line diagram of the system is represented in Figure 2.18 and its description and data can be found in [27]. The voltage deviation of all buses is acceptable within $\pm 10\%$ of the nominal voltage. The areas are selected such that at least one border bus (bus 4 and 14) is connected to more than one interconnection line and one border bus (bus 39) is connected to a generator with the complementarity constraints. This particular system allows verifying the proposed formulation when there are the complementarity constraints at the border buses as well as different number of the complicating variables and coupling constraints.

In order to obtain more general conclusions, simulations results provided in this section are carried out for high and low loading levels similar to the loading levels in the case study of section 2.4.4. Furthermore, the effect of the generators with the complementarity constraints at the border buses is investigated more in depth. The proposed OPF models are nonlinear optimization problems which they are solved using “fmincon” with interior-point algorithm in MATLAB R2011b. In the presented results the horizontal axis demonstrates the numbers of iterations since the decentralized approaches are iterative. Note that in the presented simulation results the abbreviation CC stands for the Complementarity Constraints.

In the first study case, the effect of the CC on the value of objective function is studied. For this purpose, the presented formulations for the centralized and decentralized *max.ERPR* are solved using equations (2-8) and (2-29), respectively. In order to deactivate the CCs, the value of v_g^{oe} is assumed equal to zero. Figure 2.24 demonstrates the simulation results at the high loading level for the centralized with CC and without CC and for the decentralized without CC. This figure shows that the centralized and decentralized optimizations without CC converge to the same objective value. Also the consideration of the CCs increases the value of the objective function

for the centralized optimization. Therefore, it is important to model these constraints to correctly represent the generators capability at the collapse point. It is expected that the CCs improves the results of the decentralized optimization similarly.

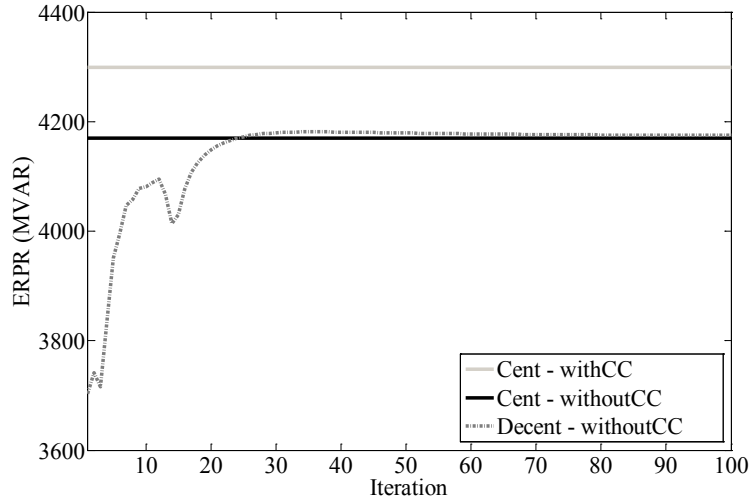


Figure 2.24. The $max.ERPR$ for New England 39-bus system: high loading level - centralized with CC and without CC - decentralized without CC.

Figure 2.25 shows the results at the high loading level for the centralized optimization with CC using equation (2-8) and also for the decentralized optimization using equation (2-29) while the proposed modification for the CC are disregarded. These modifications result mainly from the added variables for the voltage of PV generators at the border buses of neighboring areas. As a result, the modified formulation includes: (i) the fifth term of the third part of the objective function in (2-29.a), (ii) the power flow equations at the border buses with PV generators given by (2-29.v) – (2-29.w) and (2-29.h) – (2-29.i), (iii) the extra constraint given by (2-29.z) to guarantee the equality of the additional variable. Regardless of these proposed modifications, the objective function value becomes oscillatory as shown in Figure 2.25. It is due to the fact that in this case study, there is a PV generator {G10} at border bus 39.

In order to further investigate this issue, the generator {G10} is assumed as a PQ generator. The simulation results for the centralized and decentralized optimizations for the case with 9 PV generators and 1 PQ generator with CC and regardless to the proposed modifications in the formulation, is shown in Figure 2.26. In this case, the objective value of the decentralized optimization converges to the objective value of the centralized optimization since the PQ generator at the border bus does not have the CCs. This observation again confirms that the oscillatory behavior in Figure 2.25 is originated from the CCs of PV generator in the border bus. In addition, it is worth mentioning that the values of the objective function in the case of 9PV and 1PQ generators is lower than the case of 10PV generators because in the first case the number of voltage control generators is lower than the latter case.

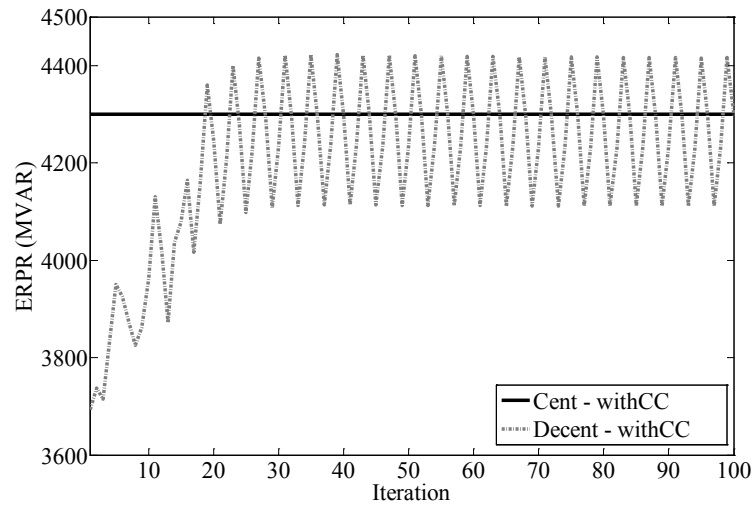


Figure 2.25. The $max.ERPR$ for New England 39-bus system: high loading level - centralized with CC - decentralized with CC regardless of the proposed modifications.

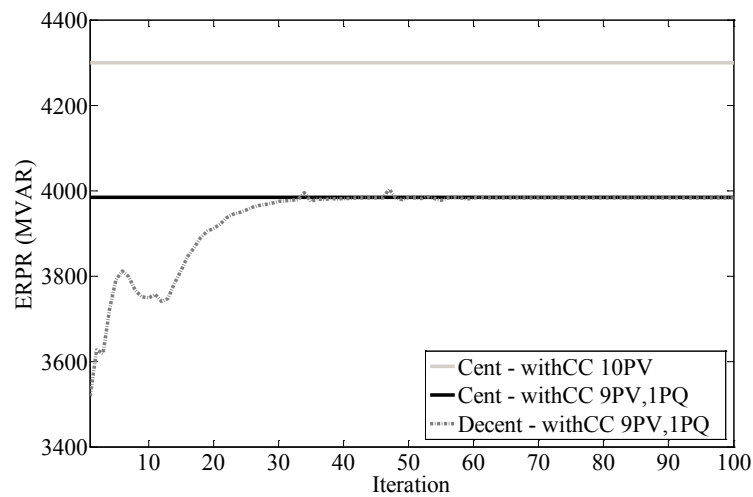


Figure 2.26. The $max.ERPR$ for New England 39-bus system: high loading level - centralized with CC -decentralized with CC regardless of the proposed modifications.

Here, the simulation results for the low loading level are not presented. The behaviors similar to the presented results in Figure 2.24, Figure 2.25 and Figure 2.26 are observed for the decentralized optimization at the low loading level. As a result, the formulation of the decentralized optimization needs additional consideration whenever there is a PV generator at a border bus. The required modifications are necessary due to the presence of the CCs at the border bus. The further coordination is proposed in the presented formulation in (2-29). These

further modifications can be scaped if the reactance of transformers that connects the generating units to the network has been added. In this way the generating units will not be directly connected to the border buses.

The simulation results for the centralized and decentralized optimizations with CC at the low/high loading levels are presented in Figure 2.27. The presented results for the decentralized optimization benefit from the proposed formulation in (2-29). Although a small sub-optimality (1.3%-1.4%) is observed in the results of the decentralized approach, the objective value is not oscillatory anymore, like Figure 2.25. Therefore, the proposed modifications in the formulation of the decentralized optimization according to equation (2-29) are quite effective whenever there is a PV generator with CC at the border bus. Finally, it is worth mentioning that the value of the objective function is higher in the case of the low loading level rather than the case of the high loading level since in the high loading level the system reaches its operating limits.

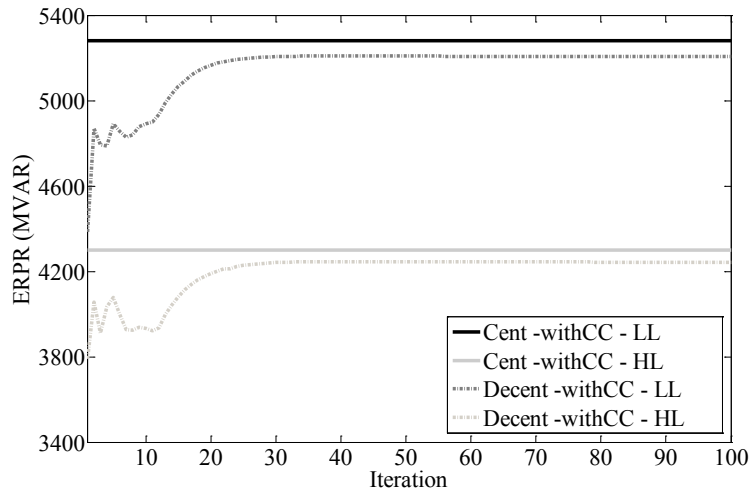


Figure 2.27. The *max.ERPR* for New England 39-bus system: high/low loading levels - centralized with CC - decentralized with CC using the proposed modifications.

The generators’ voltage set point and their reactive power output at the operating and collapse points for the low and high loading levels are reported in Table 2.23 and Table 2.24, respectively. In these tables, the obtained solutions for the control variables are given in bold. It is worth mentioning that in this study case the obtained control variables (here the voltage of generators) are generally similar for both centralized and decentralized approaches. The only exception is the voltage of G10 at high loading level which is a little bit different in the centralized and decentralized approaches (1.0912 pu in the centralized and 1.1000 pu in the decentralized). That is the reason for the higher sub-optimality observed in the case of the high loading level (73.89 MVAR) rather than in the case of the low loading level (56.19 MVAR).

Table 2.23. The value of control variables and generators reactive power output for New England 39-bus system in low loading level.

		Area A			Area B			Area C				Σ
		G1	G8	G9	G2	G3	G10	G4	G5	G6	G7	
Centralized	$V_o(pu)$	1.0932	1.1000	1.1000	1.1000	1.1000	1.0889	1.1000	1.1000	1.1000	1.1000	-
	$Q_o(MVAR)$	32.47	14.03	5.66	191.81	193.94	97.85	106.63	113.04	148.77	101.83	1006.01
	$Q_c(MVAR)$	315.52	644.67	791.74	574.47	723.91	572.32	646.15	650.09	638.25	729.45	6286.58
	$ERPR(MVAR)$	283.05	630.64	786.09	382.66	529.97	474.47	539.53	537.05	489.48	627.62	5280.56
Decentralized	$V_o(pu)$	1.0932	1.1000	1.1000	1.1000	1.1000	1.0889	1.1000	1.1000	1.1000	1.1000	-
	$Q_o(MVAR)$	28.97	14.03	5.36	184.94	188.70	158.79	105.74	112.64	147.76	101.26	1048.19
	$Q_c(MVAR)$	292.94	675.40	778.85	575.78	723.91	544.02	646.15	650.09	638.25	729.45	6254.86
	$ERPR(MVAR)$	263.97	661.38	773.49	390.83	535.21	385.23	540.42	537.46	490.49	628.19	5206.67

Table 2.24. The value of control variables and generators reactive power output for New England 39-bus system in high loading level.

		Area A			Area B			Area C				Σ
		G1	G8	G9	G2	G3	G10	G4	G5	G6	G7	
Centralized	$V_o(pu)$	1.1000	1.1000	1.1000	1.1000	1.1000	1.0912	1.1000	1.1000	1.1000	1.1000	-
	$Q_o(MVAR)$	93.54	34.18	55.28	252.18	255.67	173.45	152.43	146.32	210.13	143.80	1516.98
	$Q_c(MVAR)$	305.27	595.89	721.84	509.08	671.34	577.99	581.52	597.83	573.26	682.38	5816.42
	$ERPR(MVAR)$	211.74	561.71	666.56	256.90	415.67	404.54	429.09	451.51	363.13	538.58	4299.44
Decentralized	$V_o(pu)$	1.1000	1.1000	1.1000	1.1000	1.1000	1.1000	1.1000	1.1000	1.1000	1.1000	-
	$Q_o(MVAR)$	92.42	33.59	54.86	246.49	251.26	221.70	151.56	145.93	209.14	143.23	1550.18
	$Q_c(MVAR)$	283.69	636.50	721.84	506.15	664.39	556.05	575.72	597.83	568.89	682.38	5793.43
	$ERPR(MVAR)$	191.27	602.90	666.99	259.65	413.13	334.35	424.16	451.90	359.74	539.15	4243.25

It should be mentioned that in the proposed formulation for the decentralized optimization, every area exchange with its neighboring areas the voltage magnitude and angle at border buses as well as the Lagrangian multipliers related to the active and reactive power flows at the border buses. This information exchange should be carried out for both of the current operating and collapse points. In addition, for the areas whose border buses are connected to PV generators, the Lagrangian multipliers associated to the complementarity constraints of the generators, given by equation (2-29.q), should be exchanged with the neighboring areas.

2.7 Relation Between Voltage and Frequency Control

The voltage and frequency control reserves, introduced in chapter 1, are among the most important ancillary services. As mentioned in the introduction, the complex problems of power systems should be decomposed to several problems for which we will be able to investigate each problem relatively independent of the others. The time scale decomposition perspective, presented in Figure 1.1, decouples the short-term and long-term control schemes corresponding to the fast acting automatically and the slow acting manually controlled equipments. Furthermore, the active and reactive power decoupling is an assumption made in most of the

studies in the power systems. These kinds of assumptions are necessary for performing a specific study on the voltage and frequency control reserves. Although these assumptions cannot hold in all circumstances they provide a useful approach for the voltage and frequency control studies.

In chapter 2 several aspects of the voltage control in the SAPS and MAPS are investigated. Apart from the possible interaction between the voltage and frequency control reserves, the next chapter only focuses on the issue of the frequency control reserves. Several aspects of the frequency control reserves regarding the risk of cascading outages and blackouts will be studied in chapter 3.

3**Frequency Control vs. Blackouts Risk**

The study of the dynamics taking place during power system blackouts is a subject that receives continuous attention in view of its inherent complexity and relevant consequences. Within this context, this chapter aims at studying the role of the Frequency Control Reserves (FCRs) on the cascading outages and the relevant short-term dynamics associated with the blackout mechanisms. The relationship between the large and small blackout frequency with respect to the value of FCRs is assessed. More in particular, the main contribution is to study the influence of the power system interconnections on its pre- and post-blackout behavior. For this investigation, a statistical procedure, based on the Monte Carlo Simulation (MCS), is proposed. It performs a blackout risk analysis considering cascading outages as well as generators/loads response to the frequency deviation.

Power transmission networks are large and complex systems that have experienced wide blackouts in the recent two decades (i.e. the Northeast and Italy blackouts in 2003 and India 2012). Although large cascading blackouts are relatively rare events, the investigation of their mechanism calls for significant efforts in view of the relevant consequences. Understanding the dynamics of power system components through their interactions with different control methods are the main challenges in comprehending a blackout mechanism. In this respect, several investigations have been performed in the literatures [83], [84], [85], [86], [87], [88]. An additional aspect that increases the difficulty of the problem is the operation of single power systems within an interconnected continental-scale grid (e.g. ENTSOE and NERC). The areas

of an interconnected power system generally profit from (i) increased security and (ii) mutual economically efficient generation. The higher security margins are a consequence of shared active power reserves. However, the security of the resulting interconnected power system could decrease with the increase of the interconnection and, consequently, with the increase of the power systems operation-complexity due to propagation of events, inter-area oscillations, etc. Hence, the delivery of required control actions should be carefully evaluated due to the counter-intuitive effects of opposing driving forces in power systems.

This chapter of the thesis investigates the role of Frequency Control Reserves (FCRs) on cascading outages and short-term dynamic of blackout specifically in the interconnected systems. It should be noted that the study of power systems short-term dynamics assumes a system with a fixed topology. Therefore, the continuous evolution of the power system state and configuration under complex dynamics are, in general, neglected [89]. In this respect, this chapter firstly investigates the data of blackouts in ENTSOE using a detailed statistical analysis in section 3.1. Then, section 3.2 provides the problem definition and section 3.3 describes the blackout risk assessment methodology. The following section 3.4 illustrates and discusses the simulation results with reference to the IEEE 118-bus system considered as an interconnected network with three main areas. Finally section 3.5 discusses the possible approaches to solve the analyzed problem.

3.1 Investigation of Blackouts Data

The analysis of the times series of blackouts size measures, e.g. Energy Not Supplied (ENS) and Load Not Supplied (LNS), in North America, China, Sweden, Norway, New Zealand, and continental Europe has shown a power law region in their distributions [83]. In the distributions with the power law feature, the probability of occurrence of an event varies proportional to a power of some attribute of that event (e.g. its size). In this section, a detailed statistical analysis is performed on the blackouts data of the European transmission network for three reliability indicators considered by ENTSOE, which are ENS, LNS and Restoration Time (RT). The data are available for major fault events between January 2002 and June 2012 [90].

Several studies worldwide have shown a power law region in the distribution of the blackout size larger than a given size. Here, the maximum likelihood approach is used to estimate the power law function and the Kolmogorov-Smirnov (KS) statistic is used to test the goodness-of-fit [91]. The probability distributions of three measures and their maximum likelihood power law fit are shown in Figure 3.1. The generic statistical measures including the number of events (n), mean (\bar{x}), standard deviation (σ) and maximum observed occurrences (x_{max}) are given in the left side of Table 3.1. The right side of Table 3.1 shows the power law fits including the lower band to the power law behavior (x_{min}), exponent or scaling parameter (α), the number of occurrences in the power law region (n_{tail}) and p value (p).

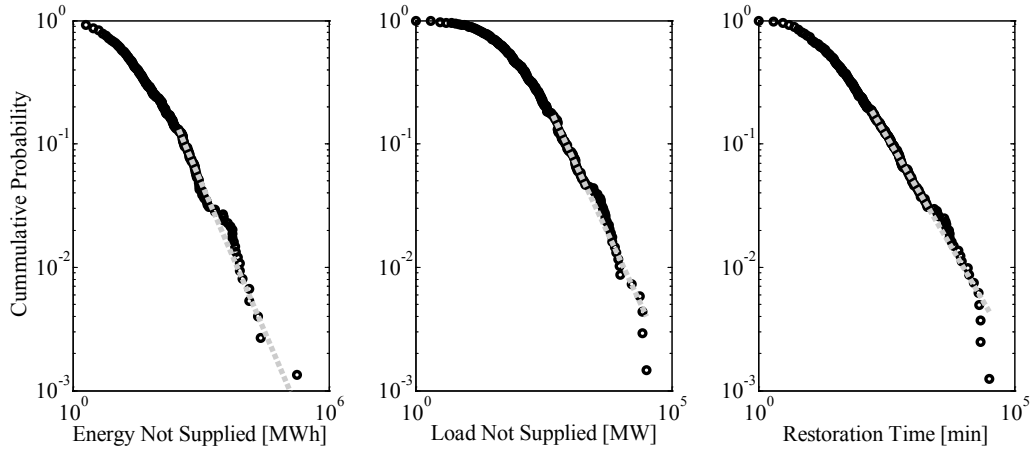


Figure 3.1. Cumulative distribution functions (black circles) and their maximum likelihood power law fit (gray dashed line) for ENTSOE reliability quantities from January 2002 to June 2012.

Table 3.1. Statistics of major events in ENTSOE from January 2002 to June 2012.

Data Set	n	\bar{x}	σ	x_{max}	x_{min}	A	n_{tail}	p
ENS	747	559.71	6773.6	180000	300±154	1.81±0.11	94±116	0.495
LNS	686	584.84	2438.4	31990	478±141	1.89±0.10	115±80	0.372
RT	807	407.99	2178.2	32126	163±52	1.71±0.06	148±92	0.935

A similar approach is applied in [92] to the ENTSOE major event data from 2002 to 2008. The obtained statistical results in Figure 3.1 and Table 3.1 are consistent with the presented results in [92] whereas our results profit from the longer time series of blackouts data until July 2012. It is worth mentioning that these statistical properties are obtained for a power grid whose topology continuously evolves over time. However, a power system with a fixed topology (that is sufficiently large) is also expected to have an approximate power law over some range of values.

This peculiarity demonstrates that the dynamics of blackouts can be associated with complex systems with Self-Organized Criticality (SOC) feature [83]. In the system with the SOC characteristic, there are different types of variables with opposing driving forces that, in certain conditions, could drive the system into a critical operation state. In this case, after the occurrence of an initial fault or disturbance, cascading outages could cause a blackout (e.g. [84]). Furthermore, the power law region in the distributions implies that the blackouts of different scales may take place and the extreme events cannot be overlooked. The system may experience large blackouts with certain probabilities and the occurrences of small/large blackouts are not independent but correlated to each other (e.g. [85], [93]). Therefore, a proposed blackout risk assessment method should quantify the power law region with reference to different quantities of blackout size [85].

3.2 Problem Definition

The different aspects of the cascading dynamics could be investigated in different time scales, namely, long-term, short-term, and transient dynamics [84]. The long-term dynamic investigates the role of load growth and engineering responses as external opposing forces to evaluate the system margins from critical loading in monthly or yearly time scales. The short-term dynamic in the range between several minutes to an hour represents the internal system driving forces, while the external forces have approximately remained constant. It is associated with the redistribution of power flows after the event and the response of controllers designed beforehand. The transient dynamics from milliseconds to seconds represents the inductive factor initiated by transient instability subsequent to large disturbances. The successive transient dynamics may cause abrupt outages.

The understanding of these dynamics can help to analyze characteristics of disasters and catastrophes, to evaluate the distance between the system's current state and its critical state and then to design preventive control strategies. In this respect, the blackout dynamics of the power grid should be appropriately modeled. Various methods have been proposed to model and analyze different aspects of blackouts in long-term, short-term and transient dynamics [94], such as, hidden failure model, OPA (ORNL-PSerc-Alaska) model, Manchester model, Optimal Power Flow (OPF) based model and OPF Transient Stability (OTS) model. Besides these research models, several commercial tools have been developed in the industry, for instance, ASSESS, CAT, POM-PCM, TRELSS [94].

In this thesis we focus specifically on the short-term dynamics of blackouts concerning the FCRs. The main idea is to study the dynamics of blackouts regarding the counteraction of the FCRs and the load shedding (including load curtailment and under-frequency load shedding) and their impacts on cascading outages. In traditional approaches, regardless cascading outages, it is considered that the higher amount of the FCRs leads to higher system security. Whereas, on one hand, a smaller amount of the FCRs may cause successive actions of under-frequency load shedding which increase the number of small blackouts. On the other hand, an excessive amount of the FCRs avoids the operation of the under-frequency load shedding and decreases the probability of small blackouts. However, it can increase the probability of line overloads that produces a triggering of cascading outages and consequent large blackouts. One may state that, within the context of the real operation of a given power system, the operator should ensure, for the different time frames, the transferability of FCRs avoiding transmission lines overloading. However, in the provision of control actions of interconnected power systems operated by several operators with limited coordination, it is practically impossible to take into account all possible contingency scenarios $N-k$ ($k=1, \dots, N$) together with cascading failures. Therefore, the response of the control actions to the extreme perturbations is not studied.

In order to study the aforementioned phenomena, a blackout risk analysis method based on Monte Carlo Simulation (MCS) is proposed. It takes into account different aspects such as the effects of cascading outages and the response of generating units/loads to the power imbalance. As a result, appropriate modeling of the fast and slow progress events, and the corresponding response of controllers, are necessary to study the blackout dynamics in power systems [95].

In blackout dynamics, cascading outages of overloaded components can progress either quickly or slowly. Fast progress events, initiated by large outages, involve different types of instability phenomena in time scales of seconds to several tens of seconds. Slow progress events are, typically, line tripping due to overloading in minutes time scales [96].

Concerning what FCRs entail, across different systems there are many different terms, definitions, and rules [10]. In this thesis, the frequency reserve services are classified into automatically and manually activated FCRs given by P_{g_A} and P_{g_M} , respectively. According to the hierarchical FCR classification (with primary, secondary and tertiary), the automatic FCR can be considered, in general, as primary and part of the secondary whereas the manual FCR is composed of the remaining part of the secondary and the tertiary. After a contingency occurrence, it is assumed that the automatic FCRs are decentrally activated in proportion to the frequency deviation to restore the equilibrium between generation and consumption in the operating time frame. Note that for the automatic frequency regulation intervals the transmission elements flow limits are not enforced [97]. Moreover, the automatic under-frequency load shedding scheme is considered whenever there is not enough automatic FCRs to meet the generation and demand balance. Then, cascading outages progress in the system according to the re-established balance and the new power flows resulted from the activation of reserves. After a certain time, the system operator optimally deploys the automatic and manual FCRs to avoid the overloading and minimize the load curtailment in a centralized manner. Other control means, such as modification of line topology or adjustment of phase shifters, could also be used by the system operator. However they have been disregarded in the development of this thesis for the sake of simplicity. In this respect, further investigations are needed.

In view of the above, the proposed model aims to effectively show the interaction between FCRs and load shedding as opposing forces in the short-term dynamics. The set points of the controllers designed beforehand, as external driving forces, are assumed to be fixed during fast dynamics. The general structure of this model is shown in Figure 3.2.

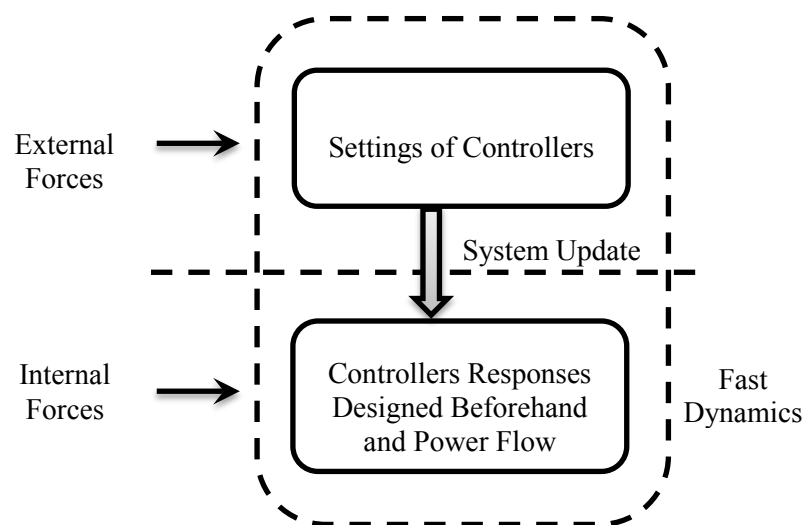


Figure 3.2. Fast dynamics and external/internal forces.

From the practical point of view, the ENTSOE allows exchange, sharing and distribution of reserves between synchronous areas so that the activation of these reserves does not jeopardize the system security [98]. A survey study has been published in [88] concerning the assessment of inter-area FCR by means of different approaches that accounts for the system security. However, none of these approaches captures the dynamics of the cascading events and blackouts. Consequently the risk of large blackouts is not taken into consideration effectively.

3.3 Proposed Risk Assessment Approach

This section describes a statistical method which aims to numerically evaluate the risk of cascading blackouts regarding the FCRs. The method considers the following elements: (i) the effects of cascading outages due to overloads and hidden failure of protection systems, (ii) the response of the FCRs of the generating units and the self-regulation of loads to power imbalance (i.e. frequency deviation) in each step of cascading outages. It must be noted that this model represents only some of the main important mechanisms associated to blackout dynamics. The other concomitant mechanisms, such as voltage excursions and collapse and transient instability, are not taken into consideration. Generally, the impact of these mechanisms on the frequency control reserve and the frequency control procedure are not considered. That is due to the commonly acceptable assumptions to decouple the power systems analyses into (i) transient and steady state studies and (ii) voltage and frequency studies [6].

For the blackout risk assessment purpose, the MCS is applied to provide contingency scenarios including both generation and transmission outages. The system states are derived by sampling the state of each component based on its own availability. One of the merits of the MCS method is that it has the ability to look beyond the probable contingencies, taking into account rare, but significant, events. Moreover, the dagger sampling is used as a variance reduction technique to simulate the rare event cases and to improve the performance of the MCS [99]. This method is appropriate for two state variables and small probability events. In this sampling method, for each component with failure probability p , a single failure is randomly selected within each $1/p$ trials. Hence, only one random number determines the state of the component for $1/p$ trials [100]. Moreover, a random variation in the loading pattern is considered while the total load is kept constant. The reason for this is that the distribution of loads changes during the day and between days and cascading blackouts could start at different random loading patterns. The random loading pattern is modeled with a normal distribution whereas the mean is equal to the amounts of the loads. A 5% of the variance is also considered in the loading pattern distribution.

The contingency scenarios construct the system states and model the initial event. In the simulation procedure, after the initial event or after each step of cascading outages, there may be a power imbalance and, consequently, a frequency deviation in the system. It is assumed that the frequency deviation spreads uniformly in the system and all the generators with their automatic frequency control respond to this power imbalance. A distributed slack bus model is employed in such a way that all of the remaining dispatched generating units share the power imbalance according to their droop frequency-control characteristics with respect to their

capacity limit ($\bar{P}_g = P_{g_0} + P_{g_A}$) where $P_{g_0}(\bar{P}_g)$ is the initial (maximum) power output of generators and P_{g_A} is the automatic FCR of generators. The self-regulation effect of loads is also taken into account. So, the frequency deviation (Δf) of the system in each step of cascading outages is calculated according to the following equation [6]:

$$\Delta f = \frac{-\Delta P}{\sum_{\Omega_D} D_d + \sum_{\Omega_G} \frac{1}{R_g}} \quad (3-1)$$

where ΔP is the power imbalance in *MW*, D_d and R_g are the frequency characteristics of d -th load and g -th generator (droop) in *MW/Hz* and *Hz/MW*, respectively. Ω_D and Ω_G indicate the set of demands and generators, respectively.

It is assumed that, if the frequency deviation in the system exceeds or drops 5% of the nominal frequency, all the generators in this area trip and the system collapses [95]. Moreover, if the total minimum output of generators ($\sum P_g^{min}$) is higher than the total amount of load ($\sum P_d$), the system is not any more controllable and it collapses.

Whenever the frequency deviation is in the allowed range, but the available capacities of the synchronized generating units are unable to satisfy the load, a frequency load shedding scheme uniformly disconnects the amount of the load to reach a new power balance. In the case of overfrequency in the allowed range, the generating units decrease their surplus output according to their frequency-control characteristics while accounting for their output lower bounds. After the generation and load balance is restored, a linearized load flow (DCLF) is applied to calculate the power flow and the transmission loading in each step of the cascading outages.

The outage of overloaded lines is one of the most important mechanisms in power system blackouts. Moreover, the protection system has an undetected defect that remains dormant until an abnormal operating condition is reached. This state is often referred to as ‘hidden failure’. In order to consider the effect of hidden failure in cascading outages, it is assumed that each transmission line has a different flow-dependent probability of incorrect trip. This characteristic is modeled as an increasing function of the line flow which is seen by the line protective relay [86]. As shown in Figure 3.3, the probability of failure is small and equal to 0.01 for line flow lower than the line limit. This probability increases in proportion to the line flow between 1 and 1.4 times of the line limit. The lines that loaded more than 1.4 times of the line limit (overloaded lines) trips. It is worth to mention that in this model, in a given step of the cascading outages, the hidden failures can occur if none of the lines is loaded more than 1.4 times the capacity limit. Also, the lines which are connected to the last tripped lines are exposed to the hidden failure of protection system according to the obtained probability from Figure 3.3.

As above-mentioned, after each step of cascading outage, power generation and consumption balance would be restored mainly through the generator’s automatic frequency response. These generating units reach their new operating points typically in tens of seconds. Therefore, the operator has the opportunity to implement some remedial (corrective) actions and minimize the amount of lost load, after several steps of cascading outages. The model of operators’ response to contingencies is considered as a linearized Optimal Power Flow (DC OPF) [95]. This control decision is calculated centrally for the interconnected system. Five steps of cascades are allowed before the operator intervention using DC OPF, which is an appropriate delay to model this

3.3 Proposed Risk Assessment Approach

action according to [6]. The aim of the DC OPF is the minimization of the lost load through re-dispatching the generating units and shedding some loads. It is assumed that in this step the operator can utilize both automatic and manual FCRs ($\bar{P}_g = P_{g_0} + P_{g_A} + P_{g_M}$). Here, the generating unit shut down is also considered as a control action, whenever the total load ($\sum P_d$) is less than the minimum generation output ($\sum P_g^{min}$).

In each step of the cascading outages, if the system is divided into multiple segments, the simulation would be separately performed for each segment. It is assumed that each segment continues its operation under this condition considering its own constraints.

For a given scenario s , the flowchart and models of the proposed blackout risk assessment procedure are given in Figure 3.3. The step-by-step procedure to simulate the system for the s -th scenario is as follows.

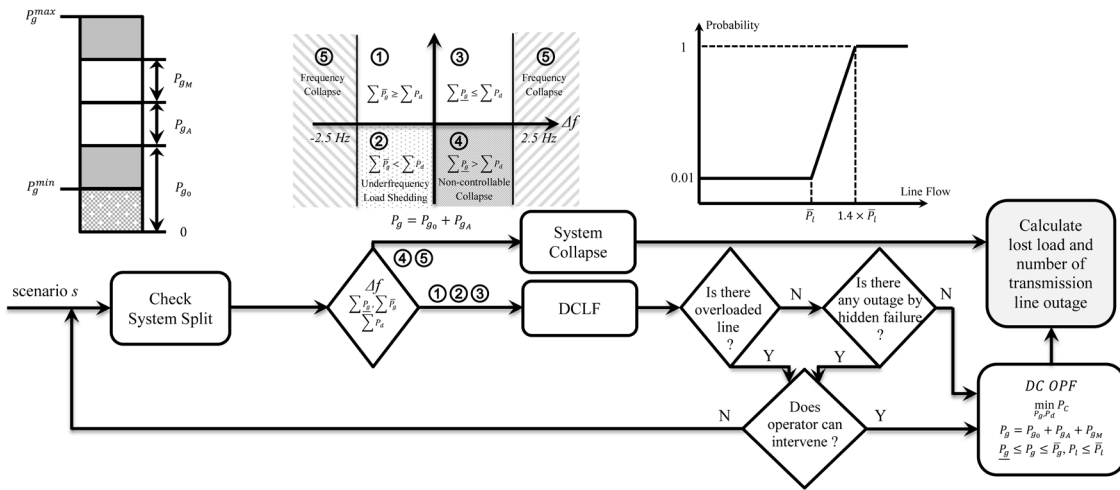


Figure 3.3. Flowchart and models of the proposed simulation procedure for a given scenario s .

- (1) Check the system split and perform the simulation for each segment.
- (2) Calculate the frequency deviation due to contingency according to the generators automatic frequency control response and the load frequency characteristics in (3-1).
- (3) According to the computed frequency deviation, demand, upper and lower limits of generators (\bar{P}_g and \underline{P}_g), if the frequency deviation is higher than the frequency protection of the generating units (⑤) or the system is not controllable (③), the system collapses; otherwise (②④) restore the generation and load balance and use a DCLF to find the transmission flows.
- (4) If there is any overloading in the transmission system, trip the overloaded elements and then go to step (6); otherwise check the hidden failure of the protection system and go to step (5).
- (5) Check if there is any outage due to hidden failure and then go to step (6).

- (6) Check if the operator can intervene and perform remedial (corrective) action; otherwise go to step (1). It is considered that the operator would have time to perform the remedial actions after five steps of cascading outages. This corrective action is a DC OPF for the minimization of lost load ($\min P_C$) concerning the constraints of generators ($\overline{P}_g \leq P_g \leq \underline{P}_g$) and transmission elements ($P_l \leq \overline{P}_l$).
- (7) Save the number of transmission line outage and the amount of lost load.

After simulating each scenario, the obtained amount of lost loads and the number of transmission component outages are used to evaluate the risk of blackout. For this purpose, the Complementary Cumulative Distribution Function (CCDF) of continuous random variables (lost load) is calculated by simply ranking the data and then scaling the ranked data. Also, the Probability Distribution Function (PDF) of discrete random variables (number of transmission component outages) is calculated simply by assigning a probability to each possible value such that the total probability for all random variables is equal to 1. In general, for the cumulative probability associated with a particular quantity (e.g. lost load), a sufficient number of the MCS samples should be calculated to ensure a specific level of accuracy ($\pm\delta$) associated with a confidence level (σ). The accuracy level is used as the stopping criteria for the MCS. For an output distribution, the regions closer to small size quantities will reach higher accuracy levels relatively faster compared to regions towards the heavy tail. The proposed method ensures the required level of accuracy associated with a value x_m by determining what fraction of the samples fell at or above x_m . If so far we have had n samples of MCS and m have fallen at or above x_m , the cumulative percentile (p_m) can be estimated as $p_m = m/n$. Then, by using (3-2) and monitoring m and n we can determine whether the required level of accuracy is obtained [99]. Here, the variable x_m could be considered for the lost load as well as the number of outages.

$$\delta = z \cdot \sqrt{\frac{p_m \cdot (1 - p_m)}{n}} \quad (3-2)$$

where z is 1.96, 2.56 and 3.29 for 95%, 99% and 99.9% of the confidence level, respectively. Here, all the simulations come with 99% of the confidence level. In order to provide the stopping criteria for the MCS using (3-2), the value x_m should be defined for any output quantity. Since in this thesis we derive the CCDF of the lost load and the PDF of the outages number, two different values x_c and x_p are specified. In order to tune the process, x_c and x_p have been chosen according to a sensitivity analysis that accounts for the ratio of the lost load to the total load and the ratio of the number of outages to the total number of lines, respectively. With regard to x_c and x_p , the distributions could be effectively demonstrated by obtaining an accuracy levels (δ) lower than 0.001 [101]. This value is selected by qualitatively analyzing the smoothness of distributions particularly in their tail behaviors. At the end of the MCS trials, the Expected Load Not Supplied (*ELNS*) is calculated as follows [100].

$$ELNS = \frac{\sum_n P_C^{(n)}}{n} \quad (3-3)$$

where $P_C^{(n)}$ is the lost load in n -th trial of the MCS. It should be noted that the coefficient of variance (c_v) of an expected value (e.g. *ELNS*) can be obtained according to

$$c_v = \frac{\sqrt{\text{var}(x)}}{E(x)} \quad (3-4)$$

where $\text{var}(\cdot)$ and $E(\cdot)$ are the variance and the expected value of the random variable x , respectively. When the MCS is employed to estimate an expected or a mean value, c_v can be used as the stopping criteria [95]. Generally, fewer of the MCS trials are required to estimate an expected value (with a certain coefficient of variance) rather than a distribution function (with a certain accuracy level). The reason is that the stability of the expected values is not affected by the number of MCS trials as much as the smoothness of the tail behavior in the probability distributions.

It is worth to mention that in [95] it is demonstrated that the convergence of the MCS in the case regarding cascading outages is slower than the case regardless cascading outages. The main reason is that the obtained random variable of the case regarding cascading outages has greater values and also it is dispersed over a wider range of the values. Therefore, more trials of the MCS are required to obtain the same degree of confidence when the cascading outage has been considered.

3.4 Simulation Results

The aforementioned dynamics of blackouts in the FCRs is investigated with reference to the IEEE 118-bus system. As shown in Figure 3.4, such a system is considered as an interconnected one with three main areas. The detailed data of generation, load, and transmission system are given in [56]. The unavailability of transmission lines (U_l) and generation units (U_g) are assumed equal to 0.01. The response of generator (r_g) and loads (d_n) to the frequency deviation are considered equal to 0.05 and 1.00, respectively. Note that r_g and d_n are in per-unit and they are converted to R_g and D_n for each generator and load by using (3-1).

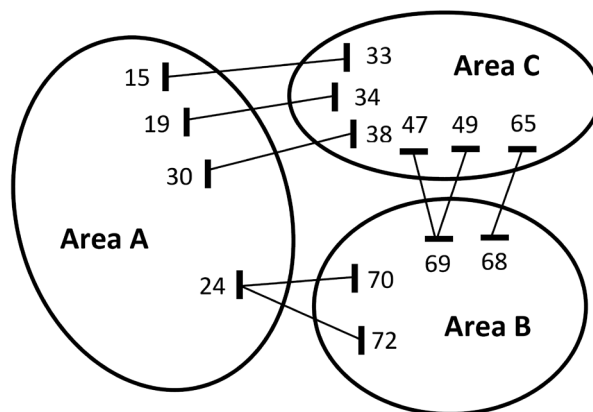


Figure 3.4. IEEE 118-bus system with three areas.

The proposed blackout risk analysis method is applied for each area separately as well as for the interconnected system. Different amounts of the automatic reserve are specified for each one of the four study cases while the manual reserve is retained fixed. Then, the risks of blackout in each area and in the interconnected system are compared using the distribution of the lost load and the number of transmission component outages as the measures of the blackout size. For this purpose, the CCDF of the lost load and the PDF of the number of transmission outages are calculated. The CCDF of the lost load and the PDF of the outage numbers are plotted in the log-log and log-linear axes, respectively, to effectively illustrate the distributions characteristics. For the convenience of comparing different systems, the amount of disconnected load divided by the total load, as a normalized blackout indicator, is used in this study.

The amount of generation and the maximum available reserve ($P_g^{max} - P_{g_0}$) for each area is given in Table 3.2. In reality, different deterministic and probabilistic approaches can be used for the provision of the FCRs with respect to the security and economy criterion. At the end, the total amount of FCRs could be represented as a percentage of the total capacity of generators. Moreover, it is assumed that the FCRs are evenly distributed based on the net generation and consumption and the remaining capacity of each generator. This simplifying assumption is somewhat conservative regarding the aim of this analysis because a given generator response to a frequency deviation will be provided, in reality, by different generators connected to the system. It reduces the risk of further overloads comparing to the case when a certain limited number of generators respond to the frequency deviation. Here, the simulations are performed for the four study cases with different amounts of automatic FCR (which are 5%, 15% and 25%) and with the same value of the manual FCR (which is 15%). Since the manual reserve remains unchanged, from now whenever the term reserve is used, it refers to the automatic reserve.

Table 3.2. Generation and reserve of each area.

	Generation (MW)	Maximum Available Reserve (MW)
Area A	1076.00	500.00
Area B	1866.53	1024.20
Area C	1547.84	700.00

It should be noted that, for each area, the neighboring ones beyond the interconnections, are modeled by a simple active power injection. In this way, each interconnection line is modeled by a consumption or generation.

As mentioned earlier, the obtained distributions from the MCS always come with a confidence interval which ensures the specified accuracy level. As an example, in the interconnected system case study with $P_{g_A} = 25\%$, for the corresponding CCDF of the lost load, the confidence interval associated with the accuracy level is shown in Figure 3.5. Another interesting point of the obtained results is that the maximum blackout size is 0.76 of the total load. This value is

consistent with the reality, because no blackout has been recorded in which all the interconnected system demands have been interrupted. Additionally, since this work studies the short-term dynamics of a power system with a fixed topology, it is expected to have an approximated power law region that covers a specific range of values. This region is much more limited in the distributions of each area because the system size is not sufficiently large.

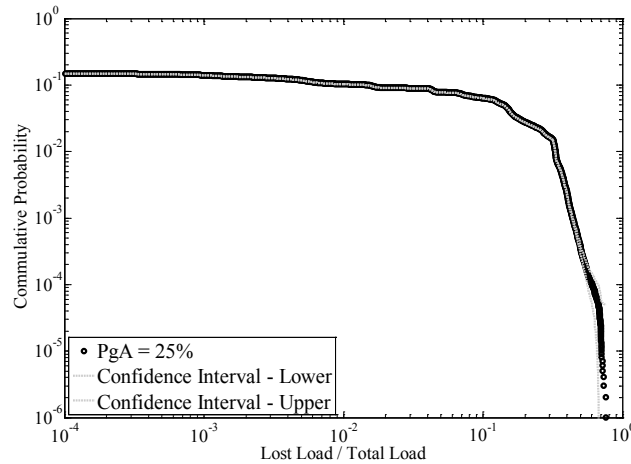


Figure 3.5. CCDF of lost load for interconnected system for $P_{gA} = 25\%$ with its confidence interval.

The obtained results of the PDF of the number of outages for Area A, B, C and the interconnected system are given in Figure 3.6-a, b, c and d, respectively. These figures effectively demonstrate that the occurrences of small and large number of outages are dependent. Generally, as the amount of reserves increases, the probability of a higher number of outages increases. This behavior is more explicit in Area B in comparison with the other ones. The reason is the higher amount of the reserve in Area B. However, the interconnection of the areas intensifies this behavior as depicted in Figure 3.6-d. Thus, in the interconnected system the provision of FCRs should receive more consideration.

Furthermore, the different regions in the CCDFs of the number of outages for different amounts of reserves concerning areas A, B, C and the interconnected system, are presented in Figure 3.7-a, b, c and d, respectively. They indicate two regions for the small and large number of outages. The distribution curve with the lower values of reserve corresponds to the lower probability of a specified blackout size. According to Figure 3.7, the increase of the reserve starting from 5% decreases (resp. increases) the probability of small (resp. large) number of outages. It means that the number of events with small (resp. large) number of outages decreases (resp. increases). This behavior becomes more significant in the interconnected system as illustrated in Figure 3.6-d. These results confirm the obtained results from the PDF of the number of outages. It seems surprising but the detailed explanations are given at the end of this section.

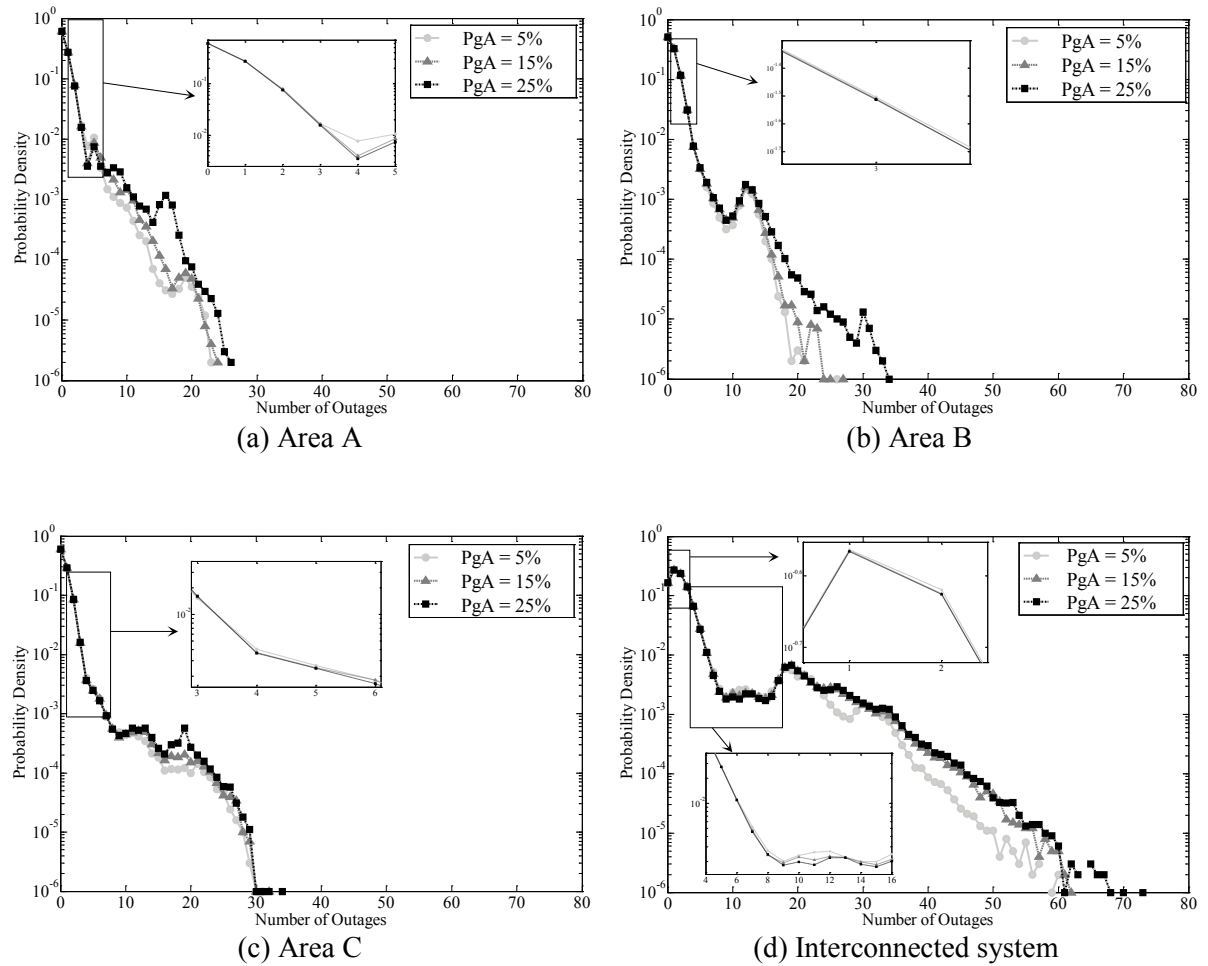


Figure 3.6. PDF of number of transmission outages

3.4 Simulation Results

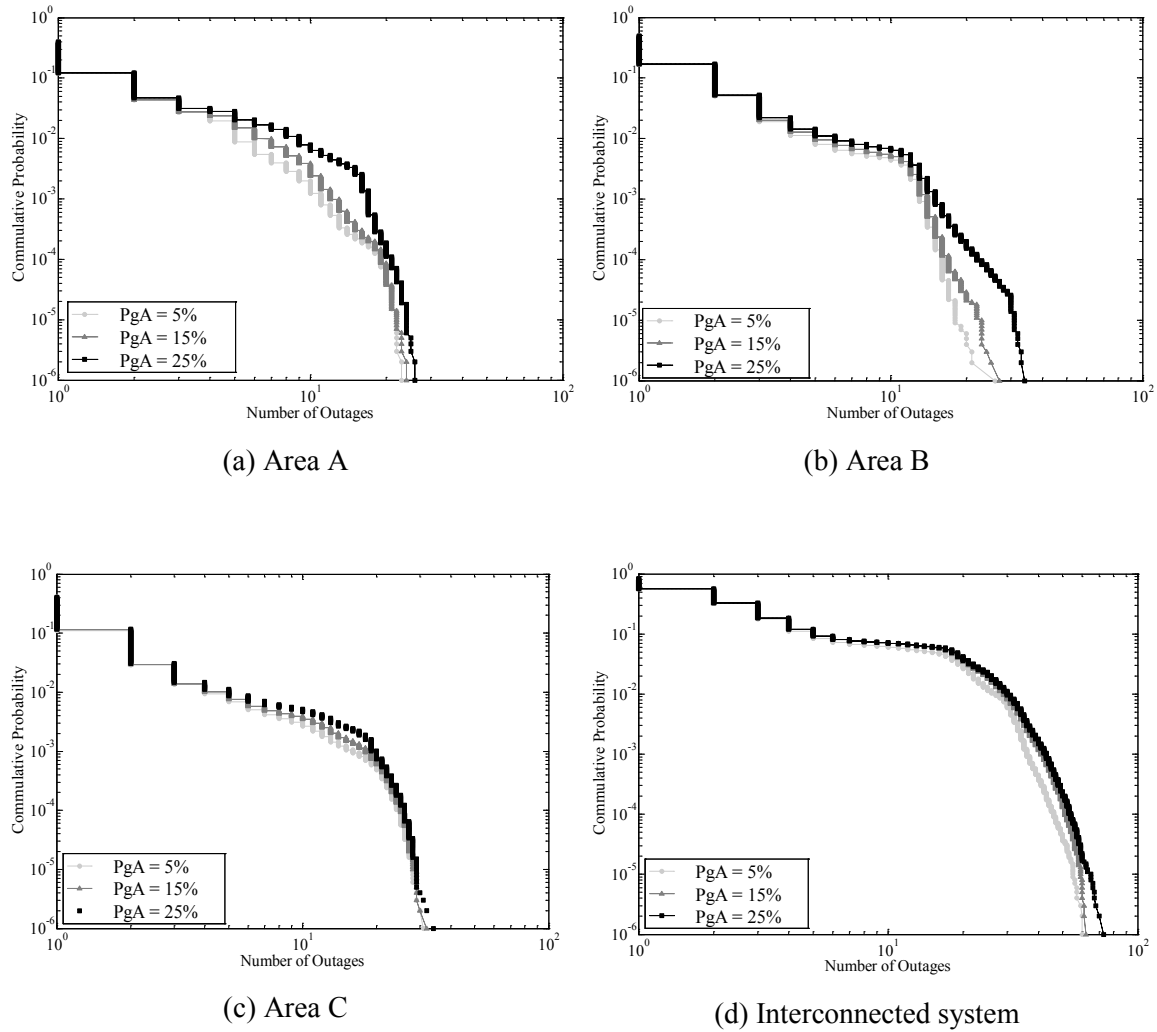


Figure 3.7. CCDF of number of transmission outages

The expected number of outages (ENO) is calculated analogous to (3-3) for the result of different study cases. Then, an unbiased expected number of outage (UENO) is defined as the ratio of the ENO to the total number of transmission lines in each study case. The value of UENO for every study case is given in Table 3.3. This table effectively demonstrates the increase of the UENO with the increase of the reserve. Also, for each amount of reserve, the value of UENO is higher in the interconnected system which demonstrates a higher level of risk.

Table 3.3. Unbiased expected number of outages for all study cases for various amounts of reserve

P_{gA} (%)	Area A	Area B	Area C	Interconnected System
5	0.0129	0.0113	0.0114	0.0168
15	0.0135	0.0115	0.0118	0.0181
25	0.0147	0.0118	0.0121	0.0184

The CCDF of the lost load for Area A, B, C and the interconnected system are given in Figure 3.8-a, b, c and d, respectively. The CCDF of the lost load starts at different values. This value shows the total number of scenarios with lost load per total number of scenarios (probability of scenarios with lost load). For instance in Figure 3.8-d, the probability of scenarios with lost load considering the reserve 5%, 15% and 25% are 0.2291, 0.1619 and 0.1494, respectively. These values for different cases are given in Table 3.4. In all the study cases, as illustrated in Figure 3.8 and in Table 3.4, the higher amount of the reserve decreases the number of scenarios with lost load. It means that the higher reserve decreases the number of small blackouts. This specific aspect has been previously shown by the fact that a higher reserve increases the number of large blackouts.

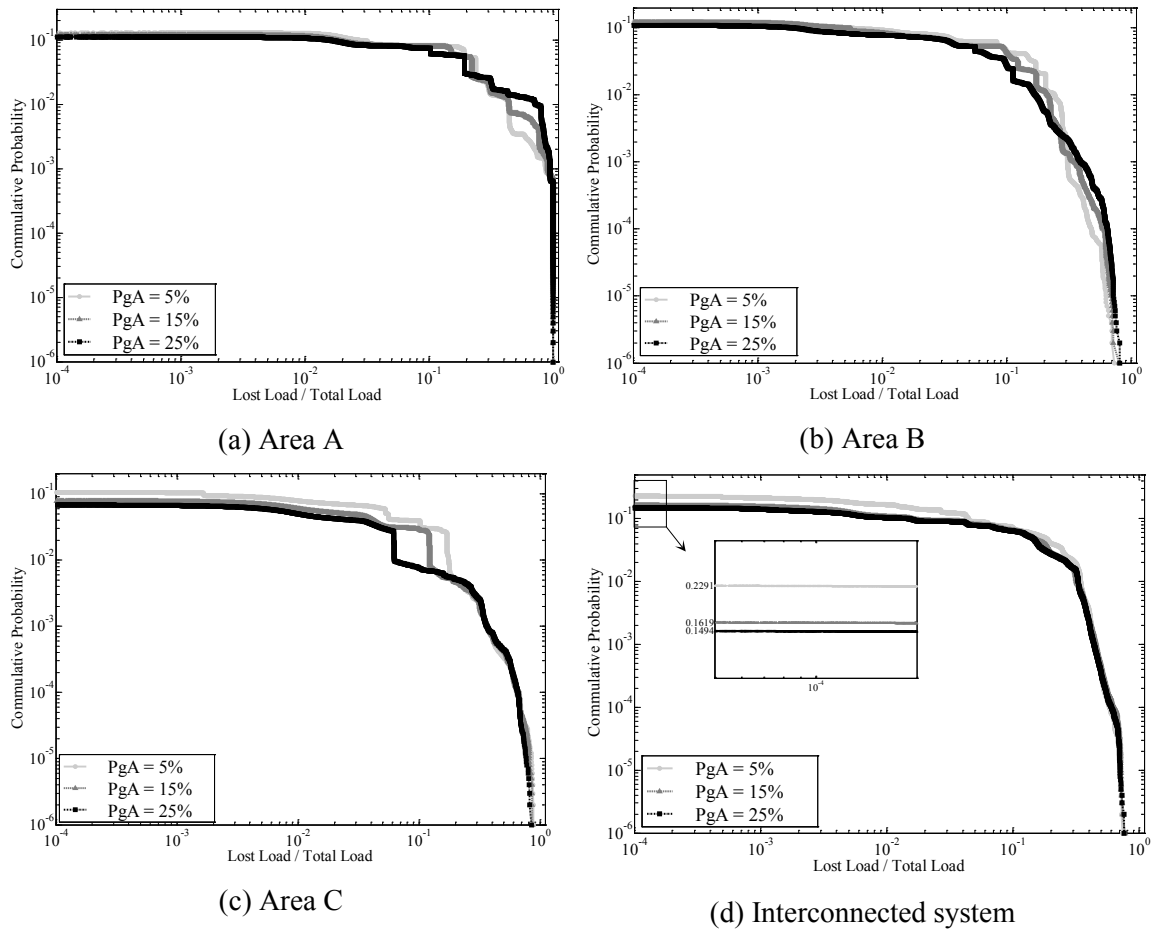


Figure 3.8. CCDF of lost load

Table 3.4. Probability of Scenario with lost load for all study cases for various amounts of reserve

P_{gA} (%)	Area A	Area B	Area C	Interconnected System
5	0.1299	0.1227	0.1056	0.2291
15	0.1196	0.1217	0.0784	0.1619
25	0.1113	0.1103	0.0681	0.1494

In addition to studying the distributions of the blackout size, the expected measures (e.g. *ELNS*) could also be investigated. Hence, the *ELNS* for each case obtained from (3-3) is given in Table 3.5. The results show that the *ELNS* decreases by the increase of the reserve in all the cases as consistent to traditional findings. The expected values like *ELNS* cannot effectively reveal the impact of large blackouts since these events occur with small probabilities. As a matter of fact, this measure cannot show the impact of the aforementioned cascading dynamics with respect to the FCR.

Table 3.5. *ELNS* in every area and interconnected system for various amounts of reserves

P_{gA} (%)	Area A	Area B	Area C	Interconnected System
5	0.2550	0.2100	0.1322	0.8859
15	0.2488	0.1719	0.0894	0.7048
25	0.2600	0.1384	0.0637	0.6730

In order to evaluate the overall risk for blackouts of all possible scales, the unserved energy and its frequency should be known. The unserved energy can be derived as the product of the lost load and the duration of the blackout to obtain the direct cost. On one hand, the cost of small power interruptions, which are more frequent, have a strong impact on the total cost of power outages. On the other hand, if the costs of the large blackouts are considered, the risk of the large blackouts may exceed the risk of more frequent small blackouts [85]. Value at Risk (VaR) and Conditional Value at Risk (CVaR) are introduced to evaluate the blackout risk quantitatively with more focus on the large scale blackouts [79]. Non-linear indications are utilized to define a cost function in [85]. The discussions on the *ELNS* and the blackout cost are presented as general remarks and further details on these issues are out of the scope of this thesis.

In order to further investigate the above discussed dynamics of FCRs in the interconnected system, the frequency deviation (Δf) and the average tie line loading after the occurrence of any initial contingency have been preserved for every scenario. Figure 3.9 (resp. Figure 3.11) and Figure 3.10 (resp. Figure 3.12) show the simulation results for the interconnected system with $P_{gA} = 5\%$ and $P_{gA} = 25\%$, respectively. In these figures each simulated scenario is represented by a point. The position of every point according to the horizontal axis in Figure 3.9 and Figure 3.10 (resp. Figure 3.11 and Figure 3.12) indicates the frequency deviation in Hz (resp. the average tie line loading in percentage). The position of every point according to the vertical

axis indicates the total number of outages. The color of each point indicates the amount of lost load in MW according to the given color bar in the right side of the figures. It should be reminded that the total system load is equal to 4242 MW. The presented results illustrate that the increase of reserve from 5% up to 25%, effectively increases the number of scenarios with large number of outages (larger than 60). Note that these scenarios generally have a high amount of lost load. Additionally, scenarios with the same amount of lost load, shown with the same color, appear with larger number of outages in the case of $P_{gA} = 25\%$ than in the case of $P_{gA} = 5\%$. In other words, these scenarios representative points are spreading in the direction of the vertical axis with the increase of the amount of reserve. These observations once more confirm the conclusions presented earlier.

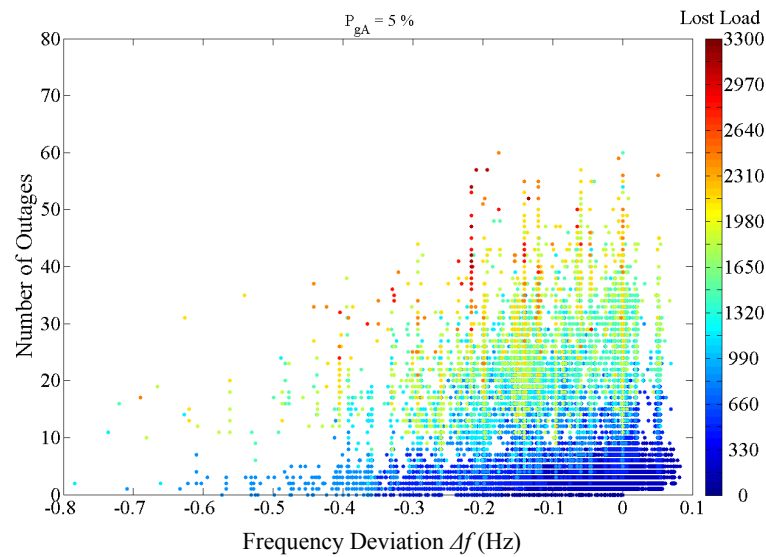


Figure 3.9. The simulation results of all the scenarios for the interconnected system based on frequency deviation and for $P_{gA} = 5\%$.

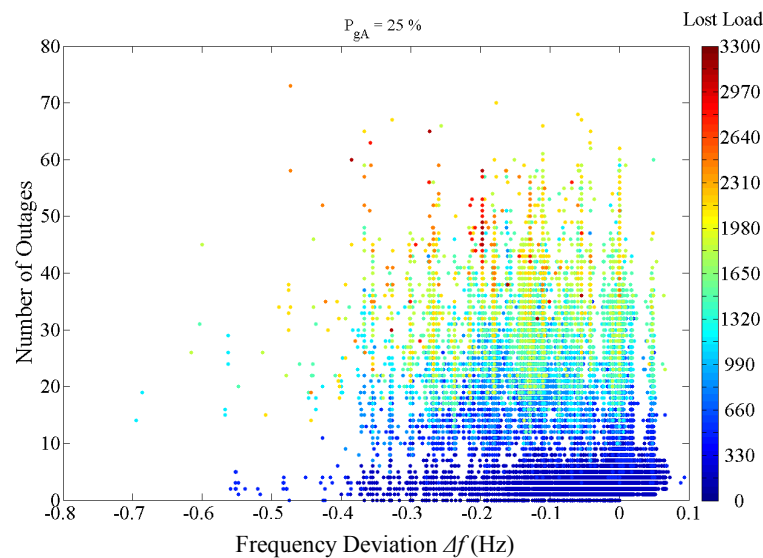


Figure 3.10. The simulation results of all the scenarios for the interconnected system based on frequency deviation and for $P_{gA} = 25\%$.

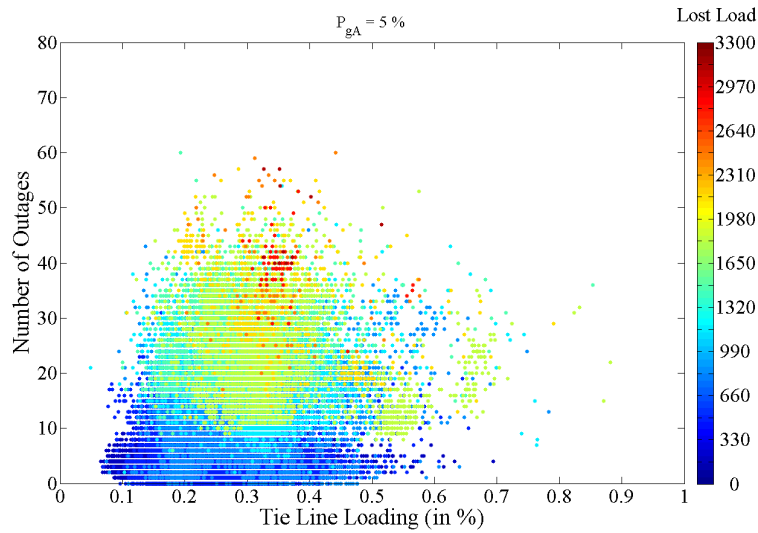


Figure 3.11. The simulation results of all the scenarios for the interconnected system based on tie line loading and for $P_{gA} = 5\%$.

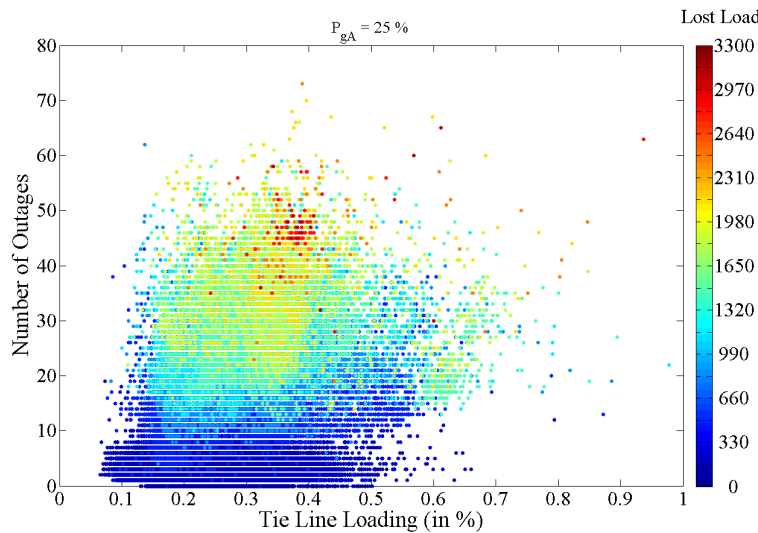


Figure 3.12. The simulation results of all the scenario for the interconnected system based on tie line loading and for $P_{gA} = 25\%$.

According to the results and discussions above, a system dynamics model for the FCRs considering the cascading outages is represented in Figure 3.13-a. As a complement, the effect of different forces on the PDF of the blackout size is given in Figure 3.13-b. As it is illustrated in Figure 3.13-b, the high (resp. low) amount of FCRs decreases (resp. increases) the probability of partial under-frequency load shedding and frequency collapse whereas it increases (resp. decreases) the probability of cascading outages. As a result, the control of the system with such a sophisticated dynamic should be enhanced with sophisticated control or optimization approaches, specifically in the interconnected systems.

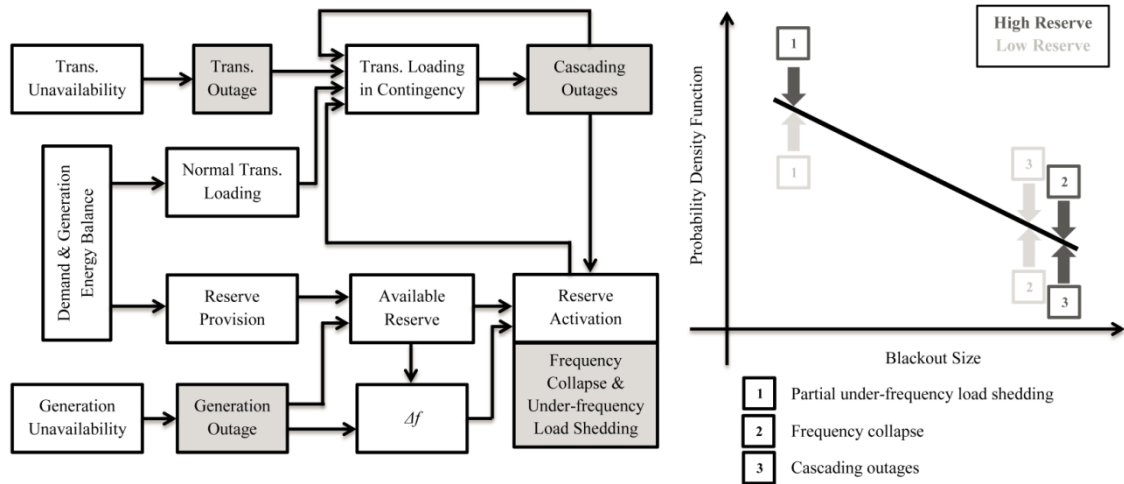


Figure 3.13. a) The system dynamics model for FCRs regarding cascading outages, b) The effect of different forces on PDF of blackout size measure.

3.5 Discussion for Further Investigations

The effects of different policies of FCRs on cascading outages, and the consequent risk of small and large blackouts, have been studied in this thesis. As a result, a tradeoff should be assessed between large and small blackout frequency with respect to the value of FCRs, specifically in interconnected power systems. This new solution might affect both economical and reserve dispatching that would impose additional cost to the system operation. It should be noted that this chapter faces the modeling, simulation and analysis of complex power grids; however, there are mathematical research challenges for the optimization of complex systems [102].

So far the proposed optimization approaches in literatures for the management of uncertainties, including deterministic (e.g. $N-1$ criteria) and probabilistic (e.g. stochastic and robust) optimizations, do not consider the cascading outages and large blackouts. Therefore, the risk of high impact / low probability scenarios is generally neglected. Actually the consideration of extreme scenarios and cascading effects in the optimizations may not be a plausible approach since the obtained solution becomes more expensive from the economical point of view and also its computational complexity increases. However, the robustness and resilience of the solution of an optimization can be evaluated using the proposed MCS in section 3.3 for which the model of dependent and cascading outages are taken into consideration [103].

Alternatively, the Qualitative Indices (QI) method presented in [104] can also be proposed to manage the difficulties through a multimodal approach by introducing a threshold. As far as the QI indicates the normal condition, the current hierarchical control is effective. Whenever the QI indicates the system is departed from the normal condition, it informs the primary controllers whose logic has been changed to effectively act as conditions change. In this case, the resources should be adjusted to keep the interconnections operation as close as possible to the normal condition by means of hierarchical control, while critical desynchronization with the system

islanding and load shedding could also be included. This approach is an online control that acts as a corrective action and it does not impose additional constraints on energy and reserve provision markets. This method could be implemented in a fully decentralized way or in the security control centers like Coreso. However, the main issues are the definition of the QI and the value of the threshold to characterize the “extreme outlier events”.

Furthermore, the fast power electronic controllers of HVDC links, installed on the interconnections, could be employed to control the flows between utilities during emergencies. They could act like firewalls against the spread of the cascading outages. [105] deals with a DC-segmentation of interconnected power systems which is a relatively new and interesting approach that could be a potential solution for mitigation of the cascading outages effects. In this reference the effectiveness of the DC-segmentation for reducing the risk of large blackouts is assessed using the proposed risk assessment method in section 3.3.

This chapter has investigated the dependency of the probability of different blackouts scales with respect to the FCRs. Within the context of the blackouts scales assessment, the first aim has referred to investigating the counter-intuitive effect of the under-frequency load shedding and the FCR in the short-term dynamics. Secondly, it is shown that this issue becomes more significant in interconnected power systems. Moreover, it is illustrated that the decrease of the amount of reserve increases the number of under-frequency load shedding and consequently increases the number of small blackouts. As a counter effect, the higher amounts of reserve increase the probability of overloading and cascading outages and consequently large blackouts.

The main conclusion of the work is that this specific behavior should be considered in the reserve assessment of interconnected systems to prevent the risk of large blackouts. In particular, additional constraints should be taken into account in the operation of interconnected power systems in order to control the participation of each area in the reserve provision.

As the last remark, this work only considers the provided reserve of the generators and the self-regulating effect of the loads; however, the required reserves could also be provided from the demand side. The fast demand side reserves contribute by curtailing a portion of the load. It effectively decreases the level of the illustrated complications, since it does not inject additional power into the grid after a disturbance. As a result, the probability of cascading outages and eventually large blackouts could decrease.

4**Conclusions**

The aim of this thesis is to study the effects of the voltage and frequency control on the security of multi-area power systems. These studies have become more and more important due to power systems evolutions toward (i) the increase of the interconnections of networks with independent system operators, (ii) the intention for economic utilization of resources under liberalized electricity market, (iii) the increase of uncertainty in the operation of the system due to large penetration of renewable energies and load forecast deviation. These issues highlight the requirements for additional coordination and revision of security studies in interconnected power systems.

4.1 Highlights

This thesis starts with a review of fundamental preliminaries of voltage and reactive power control. Then, the current practices of several TSOs in the field of voltage and reactive power control are investigated. The proposed classification is based on the centralized and the hierarchical controls schemes. Moreover, the analysis and optimization of the voltage stability margin is investigated based on PV and VQ curves. Regarding these two approaches, two optimizations are developed for the maximization of loading factor and the maximization of effective reactive power reserve. These formulations are considered as preventive actions for improving voltage stability margins. Other formulations are proposed for contingency analysis and evaluation of required corrective actions. The simulation results demonstrate that the detailed modeling of generators reactive power limits is quite important for realistic optimizations, although they increase the nonlinearities of the optimization problems. The modeling of generators' switch between constant terminal voltage and constant reactive power output with complementarity constraints also play an important role in the optimization results. The consideration of complementarity constraints is another cause of nonlinearity in the formulations of the optimization. Nevertheless, the developed solution approaches are effective for dealing with the abovementioned nonlinearities.

Afterwards, the proposed methodologies in the literature for the multi-area voltage and reactive power optimization are investigated. These optimization methods are classified based on collaborative/non-collaborative behavior of TSOs and centralized/decentralized implementation approaches. A unified mathematical formulation is proposed for various approaches of the multi-area voltage and reactive power optimization. Several aspects of the mathematical formulation of the optimization problem in the interconnected power system are investigated. These optimizations benefit from the distributed slack bus model, that helps to fix the reference bus selection, and the limitation of the voltage and reactive power in the interconnection links, that is effective against strategic behaviors of TSOs.

The effective reactive power reserve is introduced as an effective objective criterion for the management of the voltage and reactive power resources that takes into account the voltage stability margin. This particular objective function requires appropriate selection of pilot nodes. For this purpose, additional optimization is developed for the optimal selection of the pilot nodes.

Furthermore, the optimization model for the maximization of reactive power reserves is extended to MAPS using centralized/decentralized implementations. The simulation results demonstrated that the well-known decentralized implementation does not converge whenever there are PV generators at border buses. It is illustrated that this problem occurs when the complementarity constraints at border buses are considered. Appropriate modifications are proposed for the formulation of the decentralized optimization implementation in order to consider the effect of the complementarity constraints at border buses. The proposed coordinated voltage and reactive power optimization takes into account the security of MAPS.

Regarding the investigations on the frequency control, the power law pattern in the distributions of the blackouts data of continental Europe as well as its consequences on the short- and long-term dynamics of cascading outages and blackouts are investigated. In the context of short-term dynamics, a Monte Carlo simulation based approach is proposed to evaluate the effect of the frequency control reserves on the risk of cascading outages and blackouts. The main issue of the proposed risk assessment method is that the evaluation of the risk of low probable scenarios, with a certain accuracy level, requires a large number of iterations of Monte Carlo simulation, even though the variance reduction methods are used. The proposed risk evaluation method takes into consideration the cascading outages due to the transmission overloading and the hidden failure of protection systems as well as automatic and manual response of frequency control reserves and under-frequency load shedding. It is demonstrated that there is a trade-off between the probability of small and large blackouts with respect to the value of frequency control reserves, particularly for interconnected power systems.

4.2 Perspectives

The work of this thesis has contributed in the optimization of the voltage and reactive power control and in the simulation of the frequency controls and their impacts on the security of multi-area power systems.

The maximization of the effective reactive power reserve is proposed as an original contribution for the management of the voltage and reactive power resources. This optimization problem takes into account several detailed modeling aspects for the generators. Moreover, this optimization problem is extended for MAPS using centralized/decentralized implementations. In spite of lots of researches accomplished for the mathematical formulation of the voltage and reactive power management using various implementation methods, still there is not any real implementation of these optimization methods in practice for MAPS. Therefore, the performance of different optimization formulations for the voltage and reactive power management can be evaluated in practice for large scale power systems, particularly using decentralized approaches.

Additional optimization problem is developed for the optimal pilot node selection in the SAPS using genetic algorithm. This optimization is also studied for MAPS using centralized/decentralized approaches. Nevertheless, in the case of decentralized optimization the results were not enough satisfactory. Therefore, the solution of the optimization problem for pilot node selection for MAPS using decentralized approaches can be further enhanced.

Although, in this thesis the voltage and frequency control reserves are studied separately, their interactions with each other can be further investigated. In this way, one can consider the circumstances for which a contingency occurs and the dependence between the active and reactive power reserves may lead to insecure operation of systems. This condition may happen since both of the active and reactive power reserves are provided by generating units that are limited by their maximum power outputs.

A sophisticated risk assessment method is developed in this thesis to effectively evaluate the impact of FCRs on the risk of cascading outages and blackouts. The proposed method is quite effective for the simulation and analysis of the effects of FCRs on the short-term dynamics of power grids. The incorporation of the risk of low probability events with severe consequences, like cascading events and blackouts, in the management of FCRs might affect the optimal dispatch of energy and reserves. Therefore, novel optimization algorithms should be developed to account for complex perturbations and dependent events like cascading outages as well as the effects of different source of uncertainties. This issue is an open question which can be a direction for further investigations.

As final remark, the proposed risk assessment method considers a linearized model of power systems and the steady state frequency stability. The other concomitant mechanisms like voltage and transient instabilities are not taken into consideration. However, in certain situations these decoupling assumptions cannot be hold anymore and these complex mechanisms altogether increase the cascading outages and the size of blackouts. In this respect, a comprehensive risk assessment method can be explored by taking into account the frequency, voltage and transient stability issues as well as their interactions with each other. On one hand, the utilized models should be precise enough to demonstrate the abovementioned dynamics and on the other hand, they should be computationally efficient.



Bibliography

- [1] O. Mäkelä and G. Andersson, "On Pitfalls of Current Security Assessment Practice in Multi-Area Power Systems," in *ENERGYCON*, Florence, 2012.
- [2] "Coreso: Coordination of Electricity System Operators," [Online]. Available: <http://www.coreso.eu>.
- [3] "TSC: TSO Security Cooperation," [Online]. Available: <http://www.tso-security-cooperation.eu>.
- [4] "SSC: Security Service Centre," [Online]. Available: <http://www.securityservicecentre.eu>.
- [5] A. Gómez-Expósito, A. Conejo and C. Cañizares, *Electric Energy Systems: Analysis and Operation*, Taylor & Francis, 2008.
- [6] P. Kundur, *Power system stability and control*, McGraw-Hill, 1994.
- [7] X. Chen, *Preventive/corrective Actions for Power Systems in the Context of Risk Based Security Assessment*, Iowa State University, 2001.
- [8] T. Van Cutsem and C. Vournas, *Voltage Stability of Electric Power Systems*, Kluwer Academic Publisher, 1998.
- [9] O. Alizadeh Mousavi and R. Cherkaoui, "On the inter-area optimal voltage and reactive power control," *International Journal of Electrical Power & Energy Systems*, vol. 52, pp. 1-13, 2013.
- [10] M. Milligan, "Operating reserves and wind power integration: an international comparison," Golden, CO: National Renewable Energy Laboratory, 2010.

- [11] Y. Rebours and D. Kirschen, "A survey of definitions and specifications of reserve services - Release 2," The University of Manchester, 2005.
- [12] "ACER draft framework guidelines on electricity balancing," ENTSO-E Response, Brussels, 2012.
- [13] "Principles for Efficient and Reliable Reactive Power Supply and Consumption," Federal Energy Regulatory Commission Staff Report, 2005.
- [14] W. Lu, Y. Bésanger, E. Zamaï and D. Radu, "Blackouts: Description, Analysis and Classification," in *6th WSEAS International Conference on Power Systems*, Lisbon, 2006.
- [15] O. Alizadeh Mousavi and R. Cherkaoui, "Literature Survey on Fundamental Issues of Voltage and Reactive Power Control," Technical Report, 2011.
- [16] G.-Y. Cao and D. Hill, "Power system voltage small-disturbance stability studies based on the power flow equation," *IET Generation, Transmission & Distribution*, vol. 4, no. 7, pp. 873 - 882, 2010.
- [17] C. W. Taylor, *Power system voltage stability*, McGraw-Hill Ryerson, 1994.
- [18] T. Van Cutsem, "Voltage instability: Phenomena, Contermeasures, and Analysis Methods," *Proceedings of the IEEE*, vol. 88, no. 2, pp. 208 - 227, 2000.
- [19] "Guide to WECC/NERC Planning Standards I.D: Voltage Support and Reactive Power," Western Electricity Coordination Council - Reactive Reserve Working Group (RRWG), 2006.
- [20] D. Feng, B. H. Chowdhury, M. L. Crow and L. Acar, "Improving voltage stability by reactive power reserve management," *IEEE Transactions on Power Systems*, vol. 20, no. 1, pp. 338-345, 2005.
- [21] F. Capitanescu, "Assessing reactive power reserves with respect to operating constraints and voltage stability," *IEEE Transactions on Power Systems*, vol. 26, no. 4, pp. 2224 - 2234, 2011.
- [22] B. Lee, Y. Moon and H. Song, "Reactive Optimal Power Flow incorporating margin enhancement constraints with nonlinear interior point method," *IEE Proceedings on Generation Transmission and Distribution*, vol. 152, no. 6, pp. 961-968, 2005.
- [23] H. Song, B. Lee , S.-h. Kwon and V. Ajjarapu, "Reactive Reserve-Based Contingency Constrained Optimal Power Flow (RCCOPF) for Enhancement of Voltage Stability

- Margins," *IEEE Transactions on Power Systems*, vol. 18, no. 4, pp. 1538-1546, 2003.
- [24] C. Canizares, I. Dobson, N. Miller, V. Ajjarapu and H. Hamadanizadeh, Voltage Stability Assessment: Concepts, Practices and Tools, IEEE Power Engineering Society, Power System Stability Subcommittee, Tech. Rep. SP101PSS, 2002.
- [25] I. El-Samahy, K. Bhattacharya, C. Canizares, M. Anjos and P. Jiuping, "A Procurement Market Model for Reactive Power Services Considering System Security," *IEEE Transactions on Power Systems*, vol. 23, no. 1, pp. 137-149, 2008.
- [26] B. Tamimi, C. Canizares and S. Vaez-Zadeh, "Effect of Reactive Power Limit Modeling on Maximum System Loading and Active and Reactive Power Markets," *IEEE Transactions on Power Systems*, vol. 25, no. 2, pp. 1106-1116, 2010.
- [27] O. Alizadeh Mousavi, M. Bozorg and R. Cherkaoui, "Preventive reactive power management for improving voltage stability margin," *Electric Power Systems Research*, vol. 96, pp. 36-46, 2013.
- [28] B. Chowdhury and C. W. Taylor, "Voltage stability analysis: V-Q power flow simulation versus dynamic simulation," *IEEE Transactions on Power Systems*, vol. 15, no. 4, pp. 1354-1359, 2000..
- [29] "Ancillary Services Measurement Handbook," EPRI, 2001.
- [30] T. Van Cutsem, "An approach to corrective control of voltage instability using simulation and sensitivity," *IEEE Transactions on Power Systems*, vol. 10, no. 2, pp. 616 - 622, 1995.
- [31] F. Capitanescu and L. Wehenkel, "Improving the Statement of the Corrective Security-Constrained Optimal Power-Flow Problem," *IEEE Transactions on Power Systems*, vol. 22, no. 2, pp. 887-889, 2007.
- [32] F. Capitanescu and L. Wehenkel, "A New Iterative Approach to the Corrective Security-Constrained Optimal Power Flow Problem," *IEEE Transactions on Power Systems*, vol. 23, no. 4, pp. 1533 - 1541, 2008.
- [33] F. Capitanescu, T. Van Cutsem and L. Wehenkel, "Coupling Optimization and Dynamic Simulation for Preventive-Corrective Control of Voltage Instability," *IEEE Transactions on Power Systems*, vol. 24, no. 2, pp. 796 - 805, 2009.
- [34] H. Vu, P. Pruvot, C. Launay and Y. Harmand, "An improved voltage control large-scale power system," *IEEE Transactions on Power Systems*, vol. 11, no. 3, pp. 1295-1303, 1996.

- [35] "ENTSO-E operation hand book," March 2009. [Online]. Available: <https://www.entsoe.eu>.
- [36] S. Corsi, "Wide Area Voltage Regulation & Protection," in *PowerTech*, Bucharest, 2009.
- [37] Y. Phulpin, M. Begovic and D. Ernst, "Coordination of voltage control in a power system operated by multiple transmission utilities," in *IREP Symposium - Bulk Power System Dynamics and Control IIX (IREP)*, Buzios, 2010.
- [38] Y. Phulpin, "Coordination of Reactive Power Scheduling in a Multi-Area Power System Operated by Independent Utilities," PhD Thesis in Georgia Institute of Technology, 2009.
- [39] A. Rabiee, "MVAR management using generator participation factors for improving voltage stability margin," *Journal of Applied Science*, vol. 9, no. 11, pp. 2123-2129, 2009.
- [40] T. V. Menezes, L. C. P. da Silva and V. F. da Costa, "Dynamic VAR Sources Scheduling for Improving Voltage Stability Margin," *IEEE Transactions on Power Systems*, vol. 18, no. 2, p. 969-971, 2003.
- [41] T. V. Menezes, L. C. P. da Silva, C. M. Affonso and V. F. da Costa, "MVAR management on the pre-dispatch problem for improving voltage stability margin," *IEE Proceeding Generation, Transmission and Distribution*, vol. 151, no. 6, pp. 665-672, 2004.
- [42] F. Capitanescu and T. Van Cutsem, "Preventive control of voltage security margins: a multi-contingency sensitivity-based approach," *IEEE Transactions on Power Systems*, vol. 17, no. 2, pp. 358-364, 2002.
- [43] R. A. Schlueter, "A Voltage Stability Security Assessment Method," *IEEE Transactions on Power Systems*, vol. 13, no. 4, pp. 1423-1438, 1998.
- [44] M. Zima and D. Ernst, "On Multi-Area Control in Electric Power Systems," in *15th Power Systems Computation Conference (PSCC)*, Liège, 2005.
- [45] Y. Phulpin, M. Begovic, M. Petit and J. Heyberger, "Evaluation of network equivalents for voltage optimization in multi-area power systems," *IEEE Transactions on Power Systems*, vol. 24, no. 2, pp. 729-743, 2009.
- [46] P. R. Ruiz and P. W. Sauer, "Reactive Power Reserve Issues," in *Proceeding of North American Power Symposium*, Carbondale, 2006.
- [47] O. Alizadeh Mousavi, M. Bozorg and R. Cherkaoui, "Reactive Power Reserve Management: Preventive Countermeasure for Improving Voltage Stability Margin," in

IEEE Power Engineering Society General Meeting, San Diego, 2012.

- [48] R. Ramanathan and C. Taylor, "BPA Reactive Power Monitoring and Control following the August 10, 1996 Power Failure," in *VI Symposium of Specialists in Electric Operational and Expansion Planning*, Salvador, 1998.
- [49] F. Capitanescu and T. Van Cutsem, "Evaluation of reactive power reserves with respect to contingencies," in *IREP Symposium - Bulk Power System Dynamics and Control V (IREP)*, 2001.
- [50] L. Bao, Z. Huang and W. Xu, "On-line Voltage Stability Monitoring Using Var Reserves," *IEEE Transactions on Power Systems*, vol. 18, no. 4, pp. 1461-1469, 2003.
- [51] B. Leonardi and V. Ajjarapu, "Investigation of Various Generator Reactive Power Reserve (GRPR) Definitions for Online Voltage Stability/Security Assessment," in *IEEE Power and Energy Society General Meeting*, 2008.
- [52] W. Rosehart, C. Roman and A. Schellenberg, "Optimal Power Flow with Complementarity Constraints," *IEEE Transactions on Power Systems*, vol. 20, no. 2, pp. 843-822, 2005.
- [53] A. Expósito, J. Ramos and J. Santos, "Slack Bus Selection to Minimize the System Power Imbalance in Load-Flow Studies," *IEEE Transactions on Power Systems*, vol. 19, no. 2, pp. 987-995, 2004.
- [54] R. Natarajan, *Computer-Aided Power System Analysis*, New York - Basel: Marcel Dekke Inc., 2002.
- [55] A. Efthymiadis and Y. Guo, "Generator Reactive Power Limits and Voltage Stability," in *Fourth International Conference on Power System Control and Management*, London, 1996.
- [56] "Power systems test case archive," University of Washington, [Online]. Available: <http://www.ee.washington.edu/research/pstca/>.
- [57] "Symbolic Math Toolbox Calculates Gradients and Hessians," MathWorks, 2013. [Online]. Available: <http://www.mathworks.ch/ch/help/optim/ug/symbolic-math-toolbox-calculates-gradients-and-hessians.html>.
- [58] "How GlobalSearch and MultiStart Work," MathWorks, 2013. [Online]. Available: <http://www.mathworks.ch/ch/help/gads/how-globalsearch-and-multistart-work.html>.
- [59] A. Zhang, H. Li, F. Liu and H. Yang, "A coordinated voltage/reactive power control

- method for multi-TSO power systems," *International Journal of Electrical Power & Energy Systems*, vol. 43, pp. 20-28, 2012.
- [60] M. Arnold and S. Knöpfli, "Multi-Area Control in Electric Power Systems," Master's Thesis, ETH Zürich, 2006.
- [61] Y. Phulpin, M. Begovic, M. Petit and D. Ernst, "A fair method for centralized optimization of multi TSO power system," *International Journal of Electric Power Energy Systems*, vol. 31, p. 482-488, 2009.
- [62] Y. Phulpin, M. Begovic, M. Petit and D. Ernst, "On the fairness of centralized decision making strategies in multi TSO power systems," in *16th Power Systems Computation Conference (PSCC)*, Glasgow, 2008.
- [63] Y. Phulpin, M. Begovic and M. Petit, "External Network Modeling for MVar Scheduling in Multi Area Power Systems," in *PowerTech*, Lausanne, 2007.
- [64] Y. Phulpin, M. Begovic, M. Petit and D. Ernst, "Decentralized reactive power dispatch for a time varying multi TSO system," in *Hawaii International Conference on Systems Science*, 2009.
- [65] G. Hug-Glanzmann and G. Andersson, "Decentralized Optimal Power Flow Control for Overlapping Areas in Power Systems," *IEEE Transactions on Power Systems*, vol. 24, no. 1, pp. 327-336, 2009.
- [66] Y. Phulpin, M. Begovic and M. Petit, "Impact of non-Coordinated MVar Scheduling Strategies in Multi Area Power Systems," in *IEEE Power Engineering Society General Meeting*, Florida, 2007.
- [67] M. Arnold, S. Knöpfli and G. Andersson, "Improvement of OPF Decomposition Methods Applied to Multi-Area Power Systems," in *PowerTech*, Lausanne, 2007.
- [68] M. Granada, M. Rider, J. Mantovani and M. Shahidehpour, "A decentralized approach for optimal reactive power dispatch using a Lagrangian decomposition method," *Electric Power Systems Research*, vol. 89, pp. 148-156, 2012.
- [69] W. Yan, L. Wen, W. Li, C. Chung and K. Wong, "Decomposition-coordination interior point method and its application to multi-area optimal reactive power flow," *International Journal of Electric Power Energy Systems*, vol. 33, pp. 55-60, 2011.
- [70] P. Biskas and A. Bakirtzis, "Decentralised OPF of large multiarea power systems," *IEE Proceeding Generation, Transmission and Distribution*, vol. 153, pp. 99-105, 2006.

-
- [71] A. Marinakis, M. Glavic and T. Van Cutsem, "Control of Phase Shifting Transformers by Multiple Transmission System Operators," in *PowerTech*, Lausanne, 2007.
- [72] T. Amraee, A. Soroudi and A. Ranjbar, "Probabilistic determination of pilot points for zonal voltage control," *IET Generation, Transmission & Distribution*, vol. 6, no. 1, pp. 1-10, 2012.
- [73] J. Paul, J. Leost and J. Tesseron, "Survey of the Secondary Voltage Control in France: Present Realization and Investigations," *IEEE Transactions on Power Systems*, vol. 2, no. 2, pp. 505-511, 1987.
- [74] T. Amraee, A. Ranjbar and R. Feuillet, "Immune-based selection of pilot nodes for secondary voltage control," *European Transactions on Electric Power*, vol. 20, no. 7, pp. 938-951, 2010.
- [75] M. Spong, J. Christensen and K. Eichorn, "Secondary Voltage Control Using Pilot Point Information," *IEEE Transactions on Power Systems*, vol. 3, no. 2, pp. 660-668, 1988.
- [76] A. Conejo and M. Aguilar, "A Non-Linear Approach to the Selection of Pilot Buses for Secondary Voltage Control," in *Power System Control and Management*, 1996.
- [77] A. P. L. André, "Using the Bifurcation Theory to Select Pilot Busbars in a Secondary Voltage Regulation Scheme," in *IEEE Power Systems Conference and Exposition*, 2006.
- [78] X. Wang and Z. Cai, "Network Partition and Pilot Nodes Selection for Reactive Power/Voltage control Based on the Complex Network Theory," *Applied Mechanics and Materials*, pp. 291-294, 2013.
- [79] S. Mei, X. Zhang and M. Cao, *Power Grid Complexity*, Beijing: Springer, 2011.
- [80] U. Javaid, "Pilot Bus Selection for Tertiary Level Control of Voltage Regulation," Master Thesis EPFL, 2013.
- [81] A. Conejo, J. Fuente and S. Göransson, "Comparison of Alternative Algorithms to Select Pilot Buses for Secondary Voltage Control in Electrical Power Networks," in *7th Mediterranean Electrotechnical Conference*, 1994.
- [82] "The MathWorks, Inc. Genetic Algorithm.," [Online]. Available: [Online]. <http://www.mathworks.com/discovery/genetic-algorithm.html>.
- [83] B. Carreras, D. Newman, I. Dobson and A. Poole, "Evidence for self-organized criticality in a time series of electric power system blackouts," *IEEE Transactions on Circuits and*

- Systems*, vol. 51, no. 9, pp. 1733-1740, 2004.
- [84] M. ShengWei, X. AnCheng and Z. XueMin, "On power system blackout modeling and analysis based on self-organized criticality," *Science in China Series E: Technological Sciences*, vol. 51, no. 2, pp. 209-219, 2008.
- [85] D. Newman, B. Carreras, V. Lynch and I. Dobson, "Exploring complex systems aspects of blackout risk and mitigation," *IEEE Transactions on Reliability*, vol. 60, no. 1, pp. 134-143, 2011.
- [86] J. Chen, J. Thorp and I. Dobson, "Cascading Dynamics and Mitigation Assessment in Power System Disturbances via a Hidden Failure Model," *Electric Power Energy Systems*, vol. 27, no. 4, pp. 318-326, 2005.
- [87] I. Dobson, B. Carreras and D. Newman, "A loading dependent model of probabilistic cascading failure," *Probability in the Engineering and Informational Sciences*, vol. 19, no. 1, pp. 15-32, 2005.
- [88] M. Schilling, R. Billinton and M. Dos Santos, "Bibliography on power systems probabilistic security analysis 1968-2008," *International Journal of Emerging Electric Power Systems*, vol. 10, no. 3, pp. 1-48, 2009.
- [89] H. Ren, I. Dobson and B. Carreras, "Long-Term Effect of the n-1 Criterion on Cascading Line Outages in an Evolving Power Transmission Grid," *IEEE Transactions on Power Systems*, vol. 23, no. 3, pp. 1217-1225, 2008.
- [90] "European Network of Transmission System Operators for Electricity, Monthly Statistics 2002-2012," ENTSOE, July 2012. [Online]. Available: <https://www.entsoe.eu/resources/publications/general-reports/monthly-statistics/>.
- [91] A. Clauset, C. Shalizi and M. Newman, "Power-law distributions in empirical data," *SIAM Review*, vol. 51, no. 4, pp. 661-703, 2009.
- [92] M. Rosas-Casals and R. Solé, "Analysis of major failures in Europe's power grid," *Electrical Power & Energy Systems*, vol. 33, no. 3, pp. 805-808, 2011.
- [93] "Initial review of methods for cascading failure analysis in electric power transmission systems," in *IEEE Power Engineering Society General Meeting*, Pittsburgh, 2008.
- [94] M. Papic, K. Bell, Y. Chen, I. Dobson, L. Fonte, E. Haq, P. Hines, D. Kirschen, X. Luo, S. Miller, N. Samaan, M. Vaiman, M. Varghese and P. Zhang, "Survey of Tools for Risk Assessment of Cascading Outages," in *IEEE Power & Energy Society General Meeting*, San Diego, 2011.

- [95] O. Alizadeh Mousavi, R. Cherkaoui and M. Bozorg, "Blackouts risk evaluation by Monte Carlo Simulation regarding cascading outages and system frequency deviation," *Electric Power Systems Research*, vol. 89, no. 1, pp. 157-164, 2012.
- [96] M. Zima and G. Andersson, "Wide area monitoring and control as a tool for mitigation of cascading failures," in *8th International Conference on Probabilistic Methods Applied to Power Systems (PMAPS)*, Iowa, 2004.
- [97] F. Galiana, F. Bouffard, J. Arroyo and J. Restrepo, "Scheduling and Pricing of Coupled Energy and Primary, Secondary, and Tertiary Reserves," *Proceedings of the IEEE*, vol. 93, no. 11, pp. 1970 - 1983, 2005.
- [98] "ENTSO-E Response, ACER draft framework guidelines on electricity balancing," ENTSOE, Brussels, 2012.
- [99] G. Rubino and B. Tuffin, *Rare event simulation using Monte Carlo methods*, John Wiley & Sons, 2009.
- [100] W. Li, *Risk Assessment of Power Systems, Models, Methods, and Applications*, IEEE Press, John Wiley & Sons Inc., 2005.
- [101] O. Alizadeh Mousavi, M. Bozorg, R. Charkaoui and M. Paolone, "Investigation of the blackouts complexity regarding spinning reserve and frequency control in interconnected power systems," in *12th International Conference on Probabilistic Methods Applied to Power Systems (PMAPS)*, Istanbul, 2012.
- [102] "A Multifaceted Mathematical Approach for Complex Systems," Department of Energy Workshop, 2011.
- [103] O. Alizadeh Mousavi and R. Cherkaoui, "Discussion on uncertainty management in power systems," in *IREP Symposium - Bulk Power System Dynamics and Control IX (IREP)*, Rethymnon, 2013.
- [104] M. Ilic, H. Allen, W. Chapman, C. King, J. H. Lang and E. Litvinov, "Preventing future blackouts by means of enhanced electric power systems control: From complexity to order," *Proceeding of IEEE*, vol. 93, no. 11, pp. 1920-1941, 2005.
- [105] O. Alizadeh Mousavi, L. Bizumic and R. Cherkaoui, "Assessment of HVDC Grid Segmentation for Reducing the Risk of Cascading Outages and Blackouts," in *IREP Symposium - Bulk Power System Dynamics and Control IX (IREP)*, Rethymnon, 2013.

Curriculum Vitae

Omid Alizadeh Mousavi

Date of Birth : 26th February 1984
Nationality : Iranian
Tel: (+41) 21-69-34661
Email: omid.alizadeh@epfl.ch

Education

2010–2013 **Ph.D. in electrical power engineering,**
École Polytechnique Fédérale de Lausanne (EPFL), Lausanne, Switzerland.

2006–2009 **Master of Science in electrical power engineering,**
Amirkabir University of Technology (Tehran Polytechnic), Tehran, Iran.

2002–2006 **Bachelor of Science in electrical power engineering,**
Ferdowsi University of Mashhad, Mashhad, Iran.

Professional Experiences

2009-2010 **IWPC:** Iran Water and Power Resources Developments Co., Tehran and Siahbishe (in site), Iran.

2008-2009 **IGSORC:** Iran Grid Secure Operation Research Center, Tehran, Iran.

2007-2010 **NRI:** Niroo Research Institute, Tehran, Iran.

Distinctions

2012 Nomination for «Best Student Paper Award» in the conference « Probabilistic Methods Applied to the Power Systems (PAMPS 2012) ».

Languages

Persian : Mother tongue
English : Fluent
French : Good knowledge

Related Publications

Journal Papers

- 1- **O. Alizadeh Mousavi**, R. Cherkaoui, M. Bozorg, “Blackouts Risk Evaluation by Monte Carlo Simulation Regarding Cascading Outages and System Frequency Deviation”, *Electric Power Systems Research (EPSR)*, vol. 89, pp. 157-164, 2012.
- 2- **O. Alizadeh Mousavi**, M. Bozorg, R. Cherkaoui, “Preventive Reactive Power Management for Improving Voltage Stability Margin”, *Electric Power Systems Research (EPSR)*, vol. 96, pp. 36-46, 2013.
- 3- **O. Alizadeh Mousavi**, R. Cherkaoui, “On the Inter-area Voltage and Reactive Power Optimization”, *International Journal of Electrical Power & Energy Systems (IJEPES)*, vol. 52, pp. 1-13, 2013.
- 4- **O. Alizadeh Mousavi**, M. Bozorg, R. Cherkaoui, M. Paolone, “Inter-Area Frequency Control Reserve Assessment Regarding Dynamics of Cascading Outages and Blackouts”, *Electric Power Systems Research (EPSR)*, vol. 107, pp. 144-152, 2014.
- 5- **O. Alizadeh Mousavi**, R. Cherkaoui, “Investigation of P-V and V-Q based Methods for Voltage and Reactive Power Analysis”, submitted to *International Journal of Electrical Power & Energy Systems (IJEPES)*.
- 6- **O. Alizadeh Mousavi**, R. Cherkaoui, “Multi-Area Voltage and Reactive Power Management for Maximizing Stability Margin with Complementarity Constraints” submitted to *IEEE Transactions on Power Systems*.

Conference Papers

- 1- **O. Alizadeh Mousavi**, M. Bozorg, R. Cherkaoui, “Reactive Power Reserve Management: Preventive Countermeasure for Improving Voltage Stability Margin”, *IEEE Power Engineering Society General Meeting*, 22-26 July, 2012, San Diego, California USA.
- 2- **O. Alizadeh Mousavi**, M. Bozorg, R. Cherkaoui, M. Paolone, “Investigation of the Blackouts Complexity Regarding Spinning Reserve and Frequency Control in Interconnected Power Systems”, *12th International Conference on Probabilistic Methods Applied to Power Systems (PMAPS)*, 10-14 June, 2012. Istanbul, Turkey.
- 3- **O. Alizadeh Mousavi**, L. Bizumic, R. Cherkaoui, “Assessment of HVDC Grid Segmentation for Reducing the Risk of Cascading Outages and Blackouts”, *IREP Symposium - Bulk Power System Dynamics and Control IX (IREP)*, 25-30 August, 2013, Rethymnon, Greece.
- 4- **O. Alizadeh Mousavi**, R. Cherkaoui, “Discussion on Uncertainty Management in Power Systems”, *IREP Symposium - Bulk Power System Dynamics and Control IX (IREP)*, 25-30 August, 2013, Rethymnon, Greece.
- 5- U. Javaid, **O. Alizadeh Mousavi**, R. Cherkaoui, “On Pilot Bus Selection for Voltage Control of Single- and Multi-Area Power Systems”, submitted to *IEEE Power Engineering Society General Meeting*, 27-31 July, 2014, Maryland, Washington DC, USA.